NOTE TO USERS

Hybrid Silicon-Organic Ring Resonator Photonic Devices

Llewellyn Rhys Lawson

A dissertation submitted in partial fulfillment of the
requirements for the degree of:

Doctor of Philosophy

University of Washington

2006

Program Authorized to Offer Degree: Department of Chemistry

INFORMATION TO USERS

The quality of this reproduction is dependent upon the quality of the copy submitted. Broken or indistinct print, colored or poor quality illustrations and photographs, print bleed-through, substandard margins, and improper alignment can adversely affect reproduction.

In the unlikely event that the author did not send a complete manuscript and there are missing pages, these will be noted. Also, if unauthorized copyright material had to be removed, a note will indicate the deletion.

ProQuest Information and Learning Company
300 North Zeeb Road
P.O. Box 1346
Ann Arbor, MI 48106-1346

University of Washington
Graduate School

This is to certify that I have examined this copy of a doctoral dissertation by

Llewellyn Rhys Lawson

and have found that it is complete and satisfactory in all respects,
and that any and all revisions required by the final
examining committee have been made.

Chair of the Supervisory Committee:

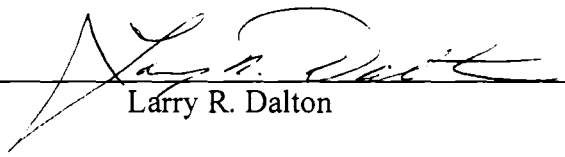

Larry R. Dalton

Reading Committee:

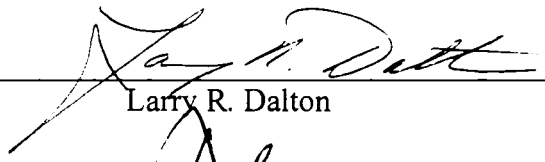

Larry R. Dalton

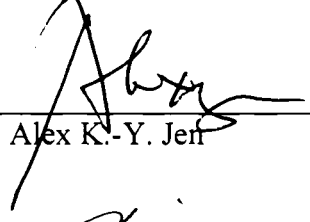

Alex K.-Y. Jen

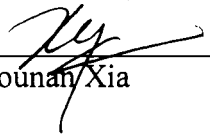

Younan Xia

Date: 3.9.06

In presenting this dissertation in partial fulfillment of the requirements for the doctoral degree at the University of Washington, I agree that the Library shall make its copies freely available for inspection. I further agree that extensive copying of the dissertation is allowable only for scholarly purposes, consistent with "fair use" as prescribed in the U.S. Copyright Law. Requests for copying or reproduction of this dissertation may be referred to Proquest Information and Learning, 300 North Zeeb Road, Ann Arbor, MI 48106-1346, 1-800-521-0600, to whom the author has granted "the right to reproduce and sell (a) copies of the manuscript in microform and/or (b) printed copies of the manuscript made from microform."

Signature C. Rhys Lawson

Date 3.9.06

University of Washington

Abstract

Hybrid Silicon-Organic Ring Resonator Photonic Devices

Llewellyn Rhys Lawson

Chairperson of the Supervisory Committee:
Professor Larry R. Dalton
Department of Chemistry

This dissertation focuses on the intersection of two powerful technologies: organic electro-optic materials and silicon-based photonics. By combining the ever-increasing speed of the organics with the ubiquitous silicon, a new generation of photonic devices has been realized. The primary devices are ring resonator photonic components fabricated in silicon and integrated with electro-optic material to form electro-optic modulators for the purpose of converting data from the electronic to the optical domain. These devices represent a vast improvement over the current modulators used in fiber optic telecommunications networks worldwide. Two main types of devices are the focus: traditional ring resonators with single, monolithic waveguides and split-waveguide devices with the optical field concentrated between two electrically insulated rails separated by ~100 nm.

In order to capitalize on the benefits of silicon as a photonic medium significant challenges were overcome, the most significant of which was a large discrepancy between the dielectric breakdown point of the silicon resonators and the field needed to

electrostatically pole the electro-optic polymer integrated with the resonators. This was accomplished through the use of intricate 3D lithographic processing in the case of monolithic rings and by using the individual waveguide rails themselves as electrodes for split-waveguide devices. Additional problems overcome in pursuit of developing theses modulators include developing techniques for poling using doped silicon as an electrode instead of metal and the use of nanoimprint lithography for completely and repeatably filling the nano-scale features of these devices.

Complete and successfully functioning modulators of both types have been achieved with low drive voltages (~1 V), high speeds (MHz), and three orders of magnitude decrease in size when compared to current devices. An additional result was the creation of a nano-scale photodetector, capable of detecting optical signals six orders of magnitude smaller than previously reported results, by running the electro-optic modulator in reverse: inserting an optical signal into the resonator and generating an electrical signal. The end result is the development of two vital components for future photonic integrated circuits: a modulator and a detector. These are the first reported devices to perform these functions by combining organic electro-optic materials and silicon photonic resonators, two significant technologies which will likely shape the future of telecommunications for years to come.

Table of Contents

List of Figures

List of Tables

Acknowledgements

Thanks to the Scherer Group at Caltech and Boeing Phantomworks for their collaboration. This research was supported by the UW Department of Nanotechnology and DARPA.

Dedication

For Brooke, who has generously let me go to school for our entire life together.

Chapter 1 – Introduction and Summary

Section 1: The Convergence of Organic Electro-Optic Materials and Silicon Photonics

The purpose of this research is to combine the powers of two emerging fields of technology: organic electro-optic (EO) materials and silicon photonic devices. Until now silicon has primarily been known as a semiconductor material for electronic applications, yet it also has emerged as a photonic material for passive elements such as waveguides and ring resonators. Recently the Intel Corporation has significantly raised the interest of the photonics community by demonstrating high-speed electro-optic modulation of an optical signal using free-carrier injection.[1] By demonstrating that a traditionally passive optical material could be used to create a mass-produced optical modulator, the profile of the EO modulator was raised significantly.

Organic EO materials have also been a technology on the rise over the past few decades. A steady progression of increase in the key figure of merit, the EO coefficient r_{33}, has these materials now surpassing the inorganic gold-standard, lithium niobate, by an order of magnitude, with no end in sight for future increases. EO modulator devices have taken advantage of these increases by producing extremely fast and power efficient devices.[2]

Both of these promising technologies are not without difficulty, however. EO modulator devices based on the traditional all-polymer device structure, the Mach-

Zehnder (MZ),[3] have not shown any improvement in properties in many years. Even though EO materials are improving, the expected lock-step progression of device properties has not followed. This may be due to the extremely complex fabrication and poling methods needed to create an EO modulator.[4] Additionally, the MZ modulator is a relatively large device, on the order of a few centimeters, which has likely reached the limit of miniaturization in the current form. Additional size decrease must occur for the realization of photonic integrated circuits.

Silicon photonic modulators also face an uncertain future due to the constraints of silicon as an EO material. The work by Intel may have been the first reported silicon EO modulator but it may also define the extent of the speed at which these devices can operate. The ceiling for modulation speed may have already been reached. This is a stark contrast to the world of organic EO materials, which offer the endless opportunity to modify their molecular structures to produce ever-improving properties. There will surely be a limit on EO activity of organic EO materials but this seems like a distant event at this date.

By combining these two technologies, silicon photonics and EO materials, the benefits of both may be realized, and the deficiencies overcome.

Section 2: Organic Electro-Optic Materials

At the simplest level, these are materials that change refractive index (RI) through electrical stimulation. This is the product of the macroscopic electro-optic

coefficient, (usually) r_{33}, which arises from the non-centrosymmetric ordering of organic molecules. The chromophore molecules used primarily consist of an electron donor connected to an electron acceptor by a conjugated bridge.[5]

Because these molecules naturally pack centrosymmetrically, for the electro-optic effect to be of use on the device-scale the symmetry must be broken so that all molecules point in the same direction. This is primarily accomplished through electrostatic poling, although it has also been done through the "sequential synthesis" method.[6] Poling is usually accomplished by doping the EO chromophores into a polymer matrix with a glass transition temperature (T_g) around 100°C, heating this homogenous mixture above the T_g, applying a field of 50-150 V/micron for a short period of time, decreasing the temperature back to room temperature and finally removing the voltage. This process locks the orientation imparted by the poling by surrounding the molecules with a rigid polymer matrix.[7] An alternative poling technique, corona poling, uses plasma-onset conditions of an inert gas in a strong field to induce electrostatic alignment.[8] Corona poling is generally less repeatable and less effective in aligning the molecules, however the actually field applied to the device is smaller (~1 kV/cm).

For the purposes of this research, the most important aspects of EO materials are the EO activity and the poling process. We seek to induce the largest RI change with the smallest applied voltage; usually a direct correlation to r_{33}. In maximizing EO effect, the chromophore is of primary importance because it establishes the size of the

effect possible. In recent years, r_{33} has quickly moved from ~50 pm/V to over 300 pm/V. These are values generated by the simple reflection method, a non-device characterization method that is generally accepted as the standard for the field.[9] Device performance usually falls short of these ideal values due to both the complexity of fabrication and the difficulty of poling.

The complexity of poling in devices is one of the key issues facing the EO field today. To deliver 100 V/micron to micro/nano-scale structures without destroying them is a feat that requires precise control over all aspects of the fabricated structure: waveguides, substrate, cladding, and electrodes. This complexity makes device yield frustratingly small.

It is one of the goals of this research to solve the issue of poling by transitioning to nano-scale devices where the poling distance is reduced from ~10 microns to less than 100 nm, greatly reducing the overall voltage required. This will also bypass other obstacles to effective poling such as the need for thick cladding layers that separate the EO layer of a modulator from the electrodes in traditional devices.

Section 3: Ring Resonators

Given the promise of EO chromophores, new devices are needed to take advantage of the material properties. Ring resonators have been targeted as the next generation of EO devices, but this work has concentrated on all-organic resonator

devices, which tend to suffer from the same poling and fabrication issues encountered in MZ devices.[10] Passive ring resonator technology has been focused on silicon devices but they have never been "activated" to produce a tunable ring resonator capable of functioning as a modulator.

Ring resonators are photonic devices that are generally used as wavelength filters. When coupled to an optical waveguide, a resonator will selectively filter out certain wavelengths of light based on size of the ring and the refractive indices of both the ring waveguide material and the cladding surrounding the ring. The Q factor of a ring resonator defines how effective it is as a filter in terms of how narrow and deep the resonant peaks are. A high Q factor ring resonator will almost completely eliminate a very narrow band of wavelengths while allowing all others to pass. More resonator theory is developed in further chapters. It is of primary importance to this research that a very small change in the refractive index of the cladding surrounding the ring will significantly alter the wavelengths filtered by the resonator.

The ring resonators used in this research are fabricated in silicon-on-insulator (SOI). These substrates have a 100-200 nm single crystal silicon layer separated from a much thicker silicon wafer by a 1-2 micron layer of silicon dioxide. The buried oxide layer provides electronic insulation for SOI semiconductor devices, and provides an ideal lower cladding for optical devices fabricated on the upper silicon layer. This has become a standard device design in the field, with high Q factors and complex multi-

ring systems being realized.[11] Current research focuses on increasing Q factors and integrating rings into more complex photonic circuits.

Section 4: Summary of Major Results

By combining the properties of EO materials and SOI ring resonators the first reported tunable SOI resonator was created. Three types of devices were invented, fabricated, and tested.

The most simple was an initial proof-of-concept device using liquid crystal (LC) materials (Chapter 5). These materials are liquid and thus not stable at high temperatures, yet they have very large electro-optic properties, capable of a RI-shift on the order of 0.1, as opposed to EO chromophores which can currently only shift ~0.0001 units. By coating a SOI resonator with LC and modulating the cladding with surface electrodes the first organic EO/SOI resonator modulator was realized.

The first commercially viable hybrid modulator was fabricated using EO chromophores applied to an SOI resonator (Chapter 6). This was accomplished by overcoming the difficult issue of poling the EO material on silicon, which has a dielectric breakdown point far below the field needed for poling. The solution was a combination of complex, multi-layer photolithography and intelligent design of the SOI device below the EO layer. Slow AC results were achieved for a modulator operating in the 1500 nm telecom band.

The final device type fabricated used innovative device design to create a ring resonator where the waveguide was also the electrodes for poling and driving the device (Chapter 7). The ring resonator used a slotted waveguide geometry where the optical field was concentrated in a slot between two electrically isolated rails of highly doped silicon separated by ~100 nm. The EO material was filled into the slot, then poled and modulated by the walls of the waveguide. This device design provided a simple fabrication scheme and the smallest, most effective EO resonator modulator reported, surpassing the state of the art for all-polymer EO resonator modulators. The size of these devices is three orders of magnitude smaller than the current state-of-the-art commercial EO modulators.

In creating the above EO modulator devices a number of problems were addressed. Chapter 2 details the first reported study of poling EO materials using highly doped silicon, an essential component of the most promising devices, slotted ring modulators, which use doped silicon as poling and modulation electrodes. Chapters 3 and 4 address the use of EO materials with nanoimprint lithography (NIL), a lithography technique used to fill the nanostructured features of our devices. The degrading effect of the temperature used in the NIL process is detailed in Chapter 3 and this problem is addressed through the use of a smart-crosslinking polymer host in Chapter 4.

This dissertation is one that details the creation of an entirely new field. Until now the fields of EO materials and silicon photonics have been separated by many

technical challenges. By addressing and overcoming those challenges we have achieved impressive results for nascent devices and set the table for future improvements that will hopefully lead to the devices that will drive the telecommunications industry for years to come and create new opportunities for the realization of photonic integrated circuits.

Notes To Chapter 1

[1] A. Liu, R. Jones, L. Liao, D. Samara-Rubio, D. Rubin, O. Cohen, R. Nicolaescu, M. Paniccia, Nature, **2004**, *427*, 615.

[2] Yongqiang Shi, Cheng Zhang, Hua Zhang, James H. Bechtel, William H. Steier, Bruce Robinson, Larry R. Dalton. *Science*, *288*, **2000,** 119.

[3] L. Dalton, A. Harper, A. Ren, F. Wang, G. Todorova, J. Chen, C. Zhang, and M. Lee, "Polymeric electro-optic modulators: from chromophore design to integration with semiconductor very large scale integration electronics and silica fiber optics," *Ind. Eng. Chem. Res.*, **1999,** *38*, 8.

[4] Kuo, Y.-H.; Steier, W.H.; Dubovitsky, S.; Jalali, B. *Photon. Tech. Lett.*, 2003, *15*, 813.

[5] Dalton, L.R., "Nonlinear Optical Polymeric Materials", in *Advances in Polymer Science*, Vol. 158, pp. 1-86, Springer-Verlag, Heidelberg, 2001

[6] Keinan, S.; Zhu, P.; Ratner, M.A.; Marks, T.J. Self-Assembled Electro-Optic Superlattices, *Chem. Mater.*, **2004**, *16*, 1848-1854.

[7] Doctoral Dissertation of Marnie Haller, Materials Science and Engineering, University of Washington 2005.

[8] L.B.Loeb, Electrical Coronas, University of California, Berkeley, (1965).

[9] C.C. Teng, H.T. Man, "Simple reflection technique for measuring the electro-optic coefficient of poled polymers" *Appl. Phys. Lett.,* **1990**, *30,* 1734.

[10] Dalton, Steier, et al., *IEEE Quant. Elect.*, **2001**, 7, 826-835.

[11] Baehr-Jones T, Hochberg M, Walker C, Scherer A, *Applied Physics Letters.* **2004,** *85*, 3346.

Chapter 2 – Simple Reflection Measurement of Nonlinear Optical Activity Using Silicon as an Electrode

Section 1: Introduction

Recent progress has seen the electro-optic (EO) activity of specially designed polymer systems achieve new highs, easily surpassing lithium-niobate by a factor of at least two with respect to the critical figure of merit for the field, the electro-optic coefficient, r_{33}[1]. One method for characterizing the r_{33} of EO materials is the simple reflection method, which relies on an ITO coated glass slide as a conductive substrate that the polymer film is spin-cast upon[2]. Beyond simple testing of these EO materials, fabricated devices such as Mach-Zender type interferometers are typically fabricated using standard semiconductor processes on silicon wafers coated with gold to act as an electrode. While both of these substrate/electrode configurations have been very reliable for testing stand-alone devices and characterizing new materials, neither is ideal with respect to the current VLSI methods that dominate microelectronics fabrication. There is great interest in integrated photonic/electronic chips for the future, however, compatibility and ease of integration of EO polymer devices with semiconductor processing will be an important barrier to overcome. Furthermore, new generations of photonic devices integrating EO polymers with traditional architectures and new designs may require uniquely shaped electrodes or compatibility with CMOS technology. All of the above concerns are addressed through the use of doped silicon as an electrode for poling and modulating EO polymers. Previous work has been done

investigating the integration of EO-based modulators with VLSI electronics for the purpose of creating opto-chips containing both modulators encoding electronics[3]. These studies have focused on the effects of fabricating traditional metal-electrode EO modulators on VLSI circuits in vertical and horizontal configurations. The effect of high voltage poling on underlying electronics in the vertical integration scheme were also tested and it was found to be undamaging, assuming correct electrode shape and placement with respect to the sensitive electronics. A final area of VLSI electronic integration studied was the feasibility of laying a properly flat foundation for the building of the defect-sensitive EO modulator waveguides. Through the use of planarizing polymers, an acceptable flatness was achieved and all barriers to VLSI integration were overcome. This paper extends the investigation into VLSI integration of EO components by looking to silicon as an electrode for poling and modulation of these devices. There are decades of research built around the use of doped silicon as an electrode in semiconductor electronics and we seek to extend that knowledge further into the realm of EO polymer devices.

Section 2: Experimental

To determine the viability of silicon as an electrode in EO devices, a doped silicon wafer was substituted for the traditional ITO electrode in the simple reflection experiment. The parameters and characterization apparatus for our simple reflection

experiment are well documented[2]. Figure 2.1 illustrates the basic sample configuration and testing mechanism used in testing EO materials.

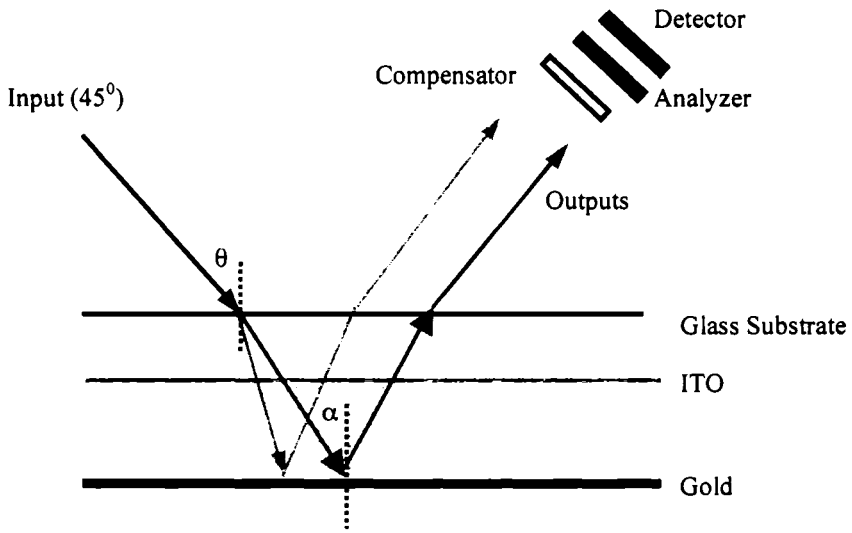

Figure 2.1: The simple reflection experimental detail

UV/VIS analysis determined that silicon was transparent at the telecom wavelengths of light (1.3 and 1.55 μm), as shown in Figure 2.2. Since silicon meets the transparent and conducting requirements for the bottom electrode in the simple reflection experiment, the technique provides a convenient method for evaluating the potential of silicon as a poling and modulation electrode for future generations of EO devices.

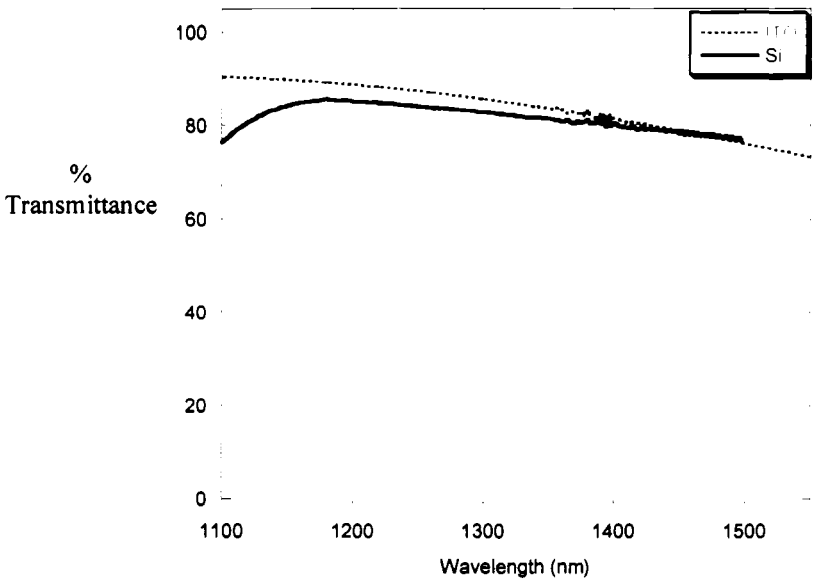

Figure 2.2: Near-IR transmission of ITO/glass and doped silicon

Section 3: Sample Preparation

Sample preparation begins with a clean substrate of either ITO/glass or double side polished doped silicon chips cleaved from wafers of varying doping concentrations and oxide thicknesses. Two types of silicon wafers were used, a highly doped (HD) and a lightly doped (LD). The HD substrate was a double side polished 4-inch <100> wafer doped with arsenic, with a resistivity of 0.002 Ω–cm. The LD substrate was a double side polished 4-inch <100> wafer with phosphorous doping, with a resistivity of 0.8 Ω–cm. All silicon substrates were cleaned with a buffered oxide etch and some were oxidized in a wet oxygen environment. 100 nm of oxide was grown on the oxidized

wafers and then etched back with buffered oxide etch to various thicknesses. Oxide depth was measured using a Nanospec 210.

The guest-host polymer system was made by combining a mix consisting of 15 wt % nonlinear optical chromophore 1, shown in Figure 2.3, in 75000 Dalton molecular weight poly(methyl methacrylate) (PMMA). The mix was dissolved in cyclopentanone at a solid loading level of 15 wt % and filtered through a 0.2 μm PTFE filter. The NLO chromophore 1, 2-[3-cyano-4-(2-{5-[2-(4-diethylaminophenyl)vinyl]thiophen-2-yl}-vinyl)-5,5-dimethyl-5H-furan-2-ylidene] malononitrile is a simple derivative of the FTC family[4] and its synthesis will be published at a later date.

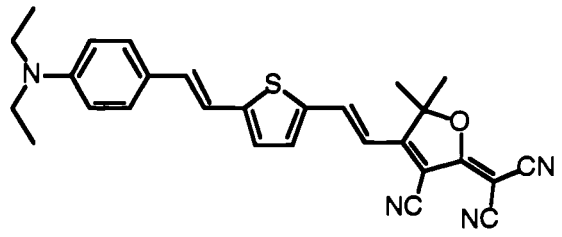

Figure 2.3: Structure of Chromophore 1

The thin film preparation involved spin coating, soft baking at 65 °C for approximately 10 minutes, then hard baking under vacuum for more than 12 hours at 65 °C. The final EO polymer film thickness ranged from 1 to 3 microns and was measured by a profilometer (Dektak 3030) to determine poling field strength requirements. Once the EO material was deposited, the device was completed by sputtering on a thin gold

top electrode and making contact to the silicon and gold electrodes with wires bonded by silver paste. The films were poled at 72 °C for 5 minutes under nitrogen and a fresh sample was used for each measurement. All of the electro-optic coefficients were measured using a laser diode of 1.3 micron. Figure 2.4 depicts the traditional ITO/glass sample stack compared to the doped silicon sample configuration.

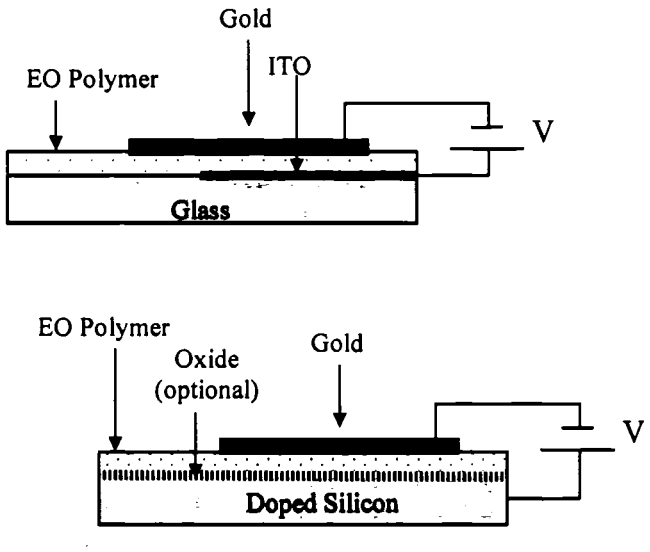

Figure 2.4: Sample configurations for the traditional ITO/glass (above) and the doped silicon (below) substrates.

Section 4: Results and Discussion

The successful poling and modulation of multiple EO materials was achieved. Figure 2.5 illustrates data from the Chromophore 1 system compared through variation of poling field strength and substrate type. Taking the ITO value of 17 pm/V as the standard to which all silicon values were compared, it can be seen that there is a wide range of possible results when using silicon as an electrode. The maximum value achieved for all systems was the highly doped bare silicon poled at 2.0 MV/cm, yielding a value of 28 pm/V. One benefit of silicon is that higher poling fields can be achieved when compared to ITO, likely due to the far superior flatness of the surface on the single crystal wafers in contrast with the extremely rough ITO surface – an attribute that usually causes shorts above 1.0 MV/cm in guest-host systems. These higher fields then translate into a more efficient orienting of the chromophores during the poling process.

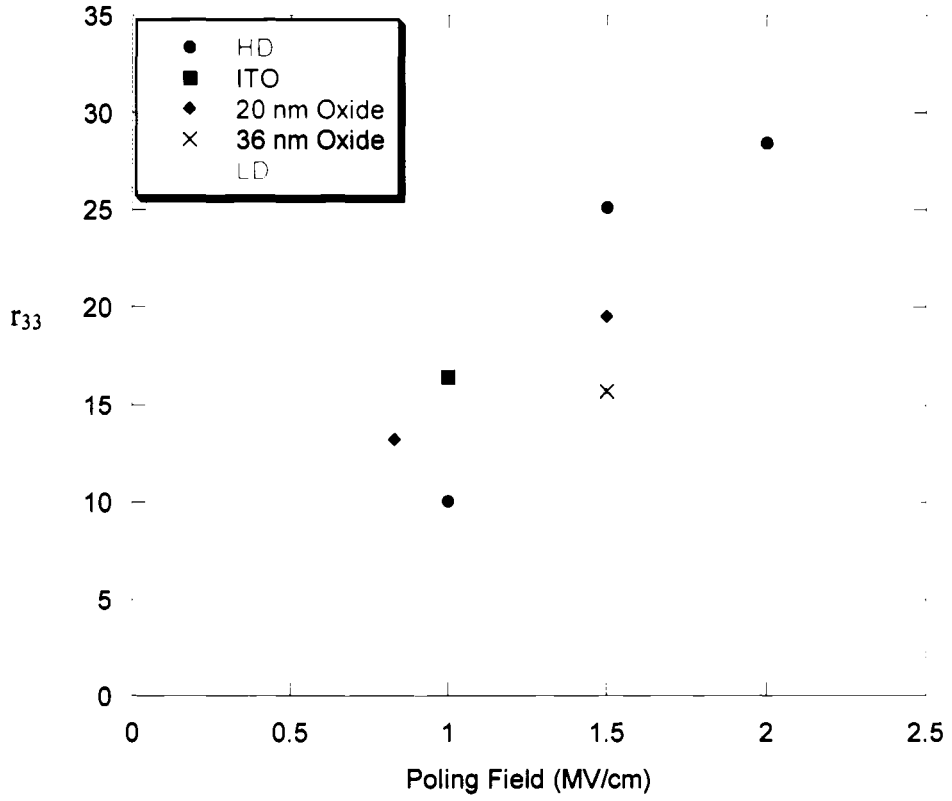

Figure 2.5: Comparison of electro-optic coefficient versus poling field for differing substrates. HD – highly doped silicon; ITO – indium tin oxide coated glass; X nm Oxide (X = 20 or 36) – HD substrates with thermally grown, wet oxide; LD – lightly doped silicon.

The highly doped bare silicon substrate was shown to be the most effective analog to ITO. This is a natural result since the high doping makes the inherently semiconducting substrate more metallic, and the lack of an oxide layer maximizes the amount of field dropped across the EO material[5]. While the HD has the potential to achieve greater EO activity than ITO, when comparing the two at the same field strength the silicon is slightly less effective as an electrode. This is caused by the

slightly lower conductivity and small contributions of native oxide layers to the contact resistance, when connecting the device to poling or testing equipment, and as a small barrier layer at the EO material/substrate interface. It can be seen that in terms of applied electric field the HD sample appears to have reached its poling saturation. There was little improvement in the EO coefficient, rising only from 25 to 28 pm/V, when the field was increased from 1.5 to 2.0 MV/cm. This may be due to the attributes of the substrate, or possibly an inherent limit of the chromophore being tested. Regardless, results show that by achieving higher fields with the silicon substrate, a greater amount of electro-optic activity was achieved.

The effect of adding an oxide layer to the bare silicon is that of a barrier between the electrode and polymer, thus lowering the overall performance of the EO material. The series of samples in Figure 2.5 that were poled at 1.5 MV/cm demonstrate this oxide effect. The highest electro-optic effect was seen with the bare HD silicon, and as the oxide layer was grown thicker, the effect decreased. It is notable, however, that even with a dampened effect, because of the higher poling fields afforded by silicon, the performance of the oxide samples can still equal or outperform the ITO samples at the higher field strength.

One difference that was noted during the poling process was that the silicon took longer to begin poling, in fact the sample does not really begin to pole until almost three fourths of the voltage has been applied – when gauging the amount of poling by the current leaking between electrodes. This differs from ITO samples, which usually

begin to have an increase in leakage current near the 50% mark. This helps to explain the lower EO coefficient for silicon when compared to ITO at 1.0 MV/cm, since less "poling" occurred.

A common device fabrication problem with EO polymers is that the current during poling is too high and causes damage to the electrodes, active layer or cladding layers. Typically a bottom metallic electrode is deposited on to the undoped silicon substrate to pole the polymer. Using doped silicon instead could eliminate the need for the bottom electrode as well as dramatically lower the current during poling. Figure 2.6 demonstrates the maximum current during poling for each of our samples. The standard ITO sample has a maximum current of approximately 350 nAmps poling at 1.0 MV/cm. While the samples poled at 1.5 MV/cm have a current range of 10-20 nAmps with approximately the same EO coefficient.

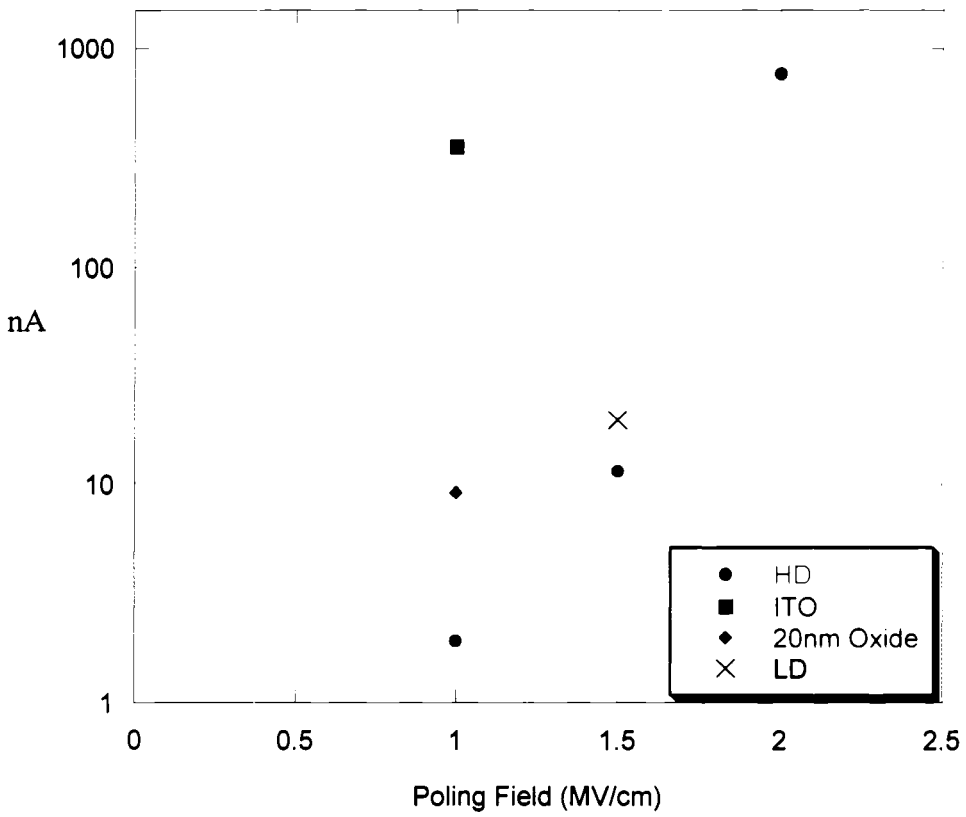

Figure 2.6: Poling current versus poling field applied to various substrates

While the performance of the simple reflection experiment done with silicon electrodes worked well in the context of the experiments presented, there were a few difficulties should be noted. The surface of silicon/silicon dioxide was not always as compatible with the standard EO polymer hosts traditionally used for simple reflection or device fabrication – PMMA and amorphous polycarbonate (APC). The most common effects of this lack of compatibility were films with pinholes or other defects that could lead to shorts during poling. This problem can be engineered around through

the use of surface treatments on the silicon or higher molecular weight polymer hosts. Another issue that may arise when considering the use of silicon as an electrode is its ability to modulate at high frequencies. During the testing process an AC current of 1 kHZ was applied to the silicon samples, which resulted in a response similar to that of ITO; yet since the silicon is not entirely metallic in its conduction there may be issues when trying to modulate at an extremely high frequency for encoding applications.

Section 5: Conclusion

In conclusion, highly doped silicon substrates can be used as an effective transparent electrode for testing electro-optic polymers at an infrared wavelength by the simple reflection method. The silicon substrate has the advantage of higher applied electric fields during poling, a lower poling current and improved poling efficiency. The use of silicon has the additional advantage of possessing a tremendous history of knowledge built around its processing and manipulation. Because of this, it has the potential to be a highly customizable electrode in new photonic band gap devices incorporating EO polymers. Further, since this work has shown the viability of poling through thermally grown silicon dioxide layers, the possibility exists for fabricating waveguide devices which use silicon as an electrode and the oxide as a cladding layer.

Notes to Chapter 2

1. Dalton, L.R., "Nonlinear Optical Polymeric Materials", in *Advances in Polymer Science*, Vol. 158, pp. 1-86, Springer-Verlag, Heidelberg, 2001

2. C.C. Teng, H.T. Man, "Simple reflection technique for measuring the electro-optic coefficient of poled polymers" *Appl. Phys. Lett., 30,* pp. 1734-1736, 1990

3. L. Dalton, A. Harper, A. Ren, F. Wang, G. Todorova, J. Chen, C. Zhang, and M. Lee, "Polymeric electro-optic modulators: from chromophore design to integration with semiconductor very large scale integration electronics and silica fiber optics," *Ind. Eng. Chem. Res.*, *38*, pp. 8-32, 1999

4. B. Robinson, L. Dalton, A. Harper, A. Ren, F. Wang, C. Zhang, G. Todorova, M. Lee, R. Aniszfeld, S. Garner, A. Chen, W. Steier, S. Houbrecht, A. Persoons, I. Ledoux, J. Zyss, A. Jen, "The molecular and supramolecular engineering of polymeric electro-optic materials", *Chemical Physics, 245,* pp. 35-50, 1999

5. J. Grote, J. Zetts, R. Nelson, F. Hopkins, L. Dalton, C. Zhang, W. Steier, "Effect of conductivity and dielectric constant on the modulation voltage for optoelectronic devices based on nonlinear optical polymers," *Optical Engineering, 40(11),* pp. 2464-2473, 2001

Chapter 3 Nanoimprint Lithography of Organic Functional Materials

Section 1: Introduction

Given the impressive progress of organic functional molecules in both electronic and photonic applications, there is a great interest in these materials as they have now begun to equal or improve upon the performance of their inorganic counterparts. Of particular interest are organic electro-optic (EO) materials, which have now achieved electro-optic activity (as defined by the electro-optic coefficient, r_{33}) as much as 9 times greater than the inorganic standard, lithium niobate.[1] The importance of these new materials in future telecommunications applications has already been detailed elsewhere[2], but it should be noted that continued improvement in EO materials will increase the speed and bandwidth of the vital electrical-to-optical data conversion process leading to not only improved current devices but also entirely new device applications. [3]

While EO material progress has been rapid and produced many breakthroughs over the past five years, the devices that make use of EO materials, specifically Mach-Zehnder EO modulators, are still made using traditional lithography. The solvents used in photolithography are known to damage various layers of the multiple-polymer stack comprising a device, and because of this, great lengths are taken to make EO devices compatible with photolithography.[4] This incompatibility between materials and methods has generated interest in the use of non-traditional lithography, with specific attention paid to soft lithography.[5] Here we detail the use of another new lithography

technique, nanoimprint lithography (NIL), in conjunction with EO materials. In particular, the solventless nature of the NIL process provides an elegant solution to patterning films that show sensitivity to the solvents used in photolithography.

Nanoimprinting has recently developed into a viable method for patterning highly detailed nanoscale features in polymers[6] and small molecule organic films.[7] The fundamental process, illustrated in Figure 3.1, requires a press with heated platens, capable of applying a specific temperature and pressure profile to a sample. While any press capable of these will suffice, there are now clean-room compatible presses available specifically for use with NIL, meaning that this method has the opportunity to be integrated into large-scale production.[8]

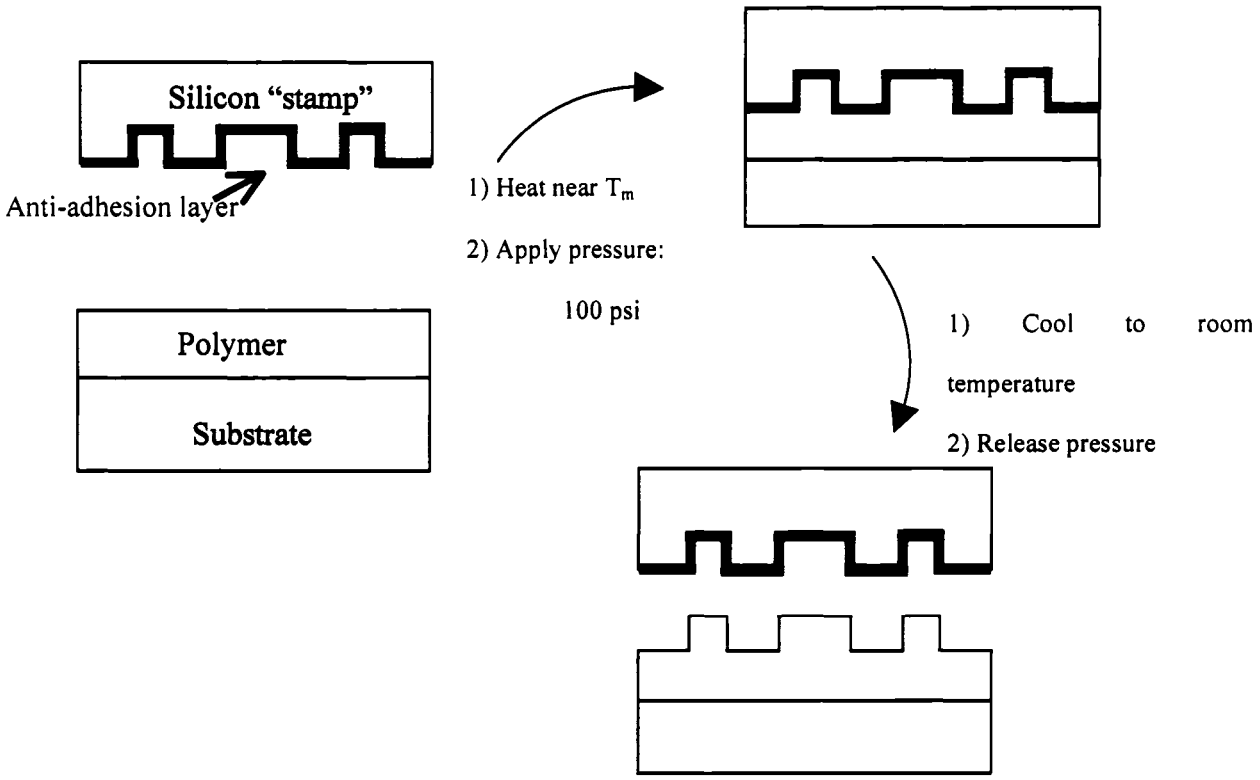

Figure 3.1: Schematic of the nanoimprint lithography process.

In addition to the press, the other pieces of the process are a "stamp" and a substrate coated with the material to be stamped. The stamp is usually formed in silicon, or an equally robust material, and patterned using some type of lithography (photo, e-beam, soft, NIL) followed by an etch step. Considerations for the formation of the stamp include the fact that the pattern should be the negative of the desired pattern, with the etched feature depth equal to the desired height for the stamped feature. The substrate upon which the stamped material is deposited can be any robust material, including silicon, glass, or metal. The NIL experiment proceeds by sandwiching the material to be stamped between the substrate it is coated on and the etched stamp. The platens of the press are closed around the sample to the desired pressure and heated above the glass transition temperature (T_g) of the film (in the case of polymers). The pressure is kept constant while the temperature is reduced to room temperature and the platens separated. The stamp and film are separated, yielding a reusable stamp and a high fidelity image of the stamp imprinted in the film. Depending on the application of NIL, the imprinted polymer has been used as an etch-mask (essentially mimicking the role of photoresist in photolithography),[6] or to directly pattern features in the film. Much recent work has focused on the use of NIL to imprint an etch mask since this allows a non-imprint-compatible material to be patterned via reactive ion etch or liquid etch. While this makes good use of the solvent-less nature of NIL, it does add an additional step not necessary when working with EO materials

(which can be patterned directly). For that reason, we have concentrated our efforts on direct imprinting NIL.

Section 2: Experimental

Our implementation of NIL for EO materials follows the standard procedure described above. The specific details are as follows: a Tetrahedron MTP-13 press was used for all experiments. Stamps were fabricated in silicon by e-beam (nanoscale features) or photolithography (micron-scale features), followed by reactive ion etching. Further treatment of the stamp involved the application of an anti-adhesion self-assembled monolayer (SAM) using a fluorinated alkane-trichlorsilane.[9] The EO materials were loaded into a polymer matrix and spin cast upon 1 in^2 ITO coated glass slides and dried in a vacuum oven overnight. The electro optic materials used consisted of one new molecule PAS 172[10], and two that are well-characterized, CLD-1[11] and Disperse Red-1 chromophores.[12] All are illustrated in Figure 3.2.

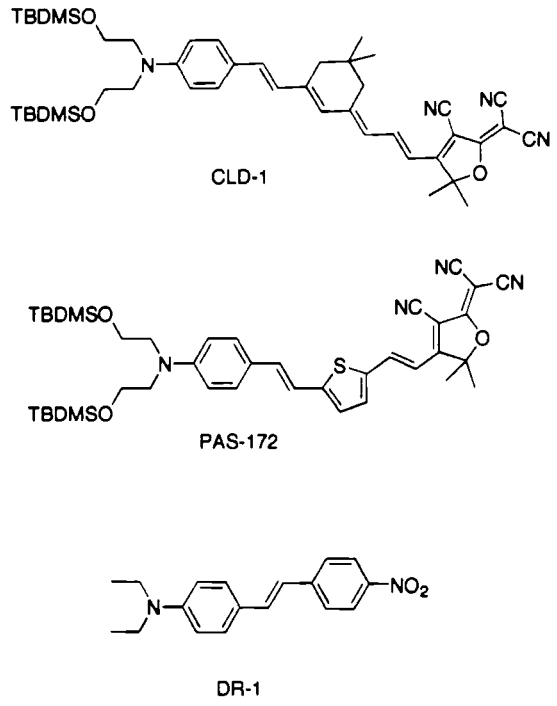

Figure 3.2: The electro-optic chromophores used.

With the press platens open, the film/substrate was first placed on the lower platen with the film face-up. The stamp was then placed feature-side-down on top of the film/substrate. The platens were closed to a pressure of 100 psi and heated to T_g+100°C. This softens the matrix of the polymer and allows it to flow into the features of the stamp. The maximum temperature was held for 10 minutes and the platens were cooled to room temperature with pressure still applied. Upon cooling, the platens were separated, releasing the stamp from the substrate, as well. Due to the lack of adhesion between stamp and film, no residue is left in the features of the stamp, rendering it reusable. As an indication of the longevity of the stamps used in this work, some have been used for 18 months and still perform like new. Analysis of the stamping fidelity was done by scanning electron (SEM), optical, and atomic force (AFM) microscopy.

General. All chemicals were obtained from Aldrich unless otherwise noted. UV-VIS measurements were taken with a Shimadzu UV-1601 (Kyoto, Japan). Scanning electron microscopy (SEM) was done using a JEOL-6300F (Peabody, MA) operating at 5 kV. Polymer samples imaged by SEM were coated with ~25 nm of gold for imaging.

Basic Imprinting. In NIL, a pattern is transferred from an etched silicon "stamp" into a polymer film by applying temperature and pressure. A typical imprinting experiment involves placing an etched silicon stamp in contact with a polymer film coated on a solid substrate. This stack is placed on the lower platen of a heated press. The platens are closed to the desired pressure and the temperature ramped above the polymer glass transition. The heat is removed while pressure is still applied. When the platens are cooled to room temperature the pressure is released and the imprinted film separated from the stamp.

Stamp Fabrication. This is done using a traditional technique such as photolithography (micron-scale features) or ebeam lithography (nano-scale features to define the desired pattern in photoresist). The pattern defined by lithography must be the inverse of the desired features stamped in the polymer. Once the pattern is defined, traditional reactive ion etching transfers the resist pattern to the silicon substrate. Once the resist is removed, the stamps are treated with a fluorinated alkane self-assembled monolayer (SAM), which facilitates the separation of stamp and imprinted film once the NIL process is done. The SAM is deposited using a procedure modified from Ref. 9.

First the silicon was cleaned using concentrated hydrofluoric acid for 10 minutes, then rinsed briefly in DI water. The surface is oxidized using a 30% hydrogen peroxide rinse for 10 minutes and then rinsed in DI water briefly. The stamp is then rinsed in 2-propanol for 5 minutes followed by a rinse in iso-octane for 5 minutes during which the stamp in the rinsing solution is transferred to a glove box with an argon environment. In the glove box, the stamp is transferred to the SAM containing solution, comprised of 1 mM trichloro(1*H*,1*H*,2*H*,2*H*-perfluorooctyl)silane in iso-octane, for 10 minutes. The silicon is then transferred to iso-octane for 10 minutes, followed by 5 minutes in 2-propanol and a final rinse in water.

Stamping. The NIL process is done in a MTP-13 hot press (Tetrahedron Associates, San Diego, CA) with fully programmable pressure and temperature controlled platens. The polymer to be imprinted is spin cast on the desired substrate (silicon, glass, ITO/glass) and placed in the press. The SAM-coated silicon stamp is placed on top of the polymer (areas do not have to match). The press is closed to 100 psi and heated to near the polymer melting temperature for 10 minutes. The platens are then cooled to room temperature and the pressure released. The stamp and film separate as the platens of the press open.

Testing the compatibility of NIL with this model EO chromophore is done by doping (15% wt.) the molecule into two different polymer hosts: poly methyl methacrylate (PMMA, 75k Polysciences) and an amorphous polycarbonate (APC, Aldrich). The mixture is dissolved in cyclopentanone (20% wt. total solids) and mixed

for 24 hours on a tumbler. The resulting solution is filtered through 0.2 micron PTFE filters (Whatman) and spin-cast onto 2.54 cm^2 ITO coated glass slides (Aldrich) to a thickness of 2 microns. At this point, some samples of each polymer host-type are taken through the NIL process while others are not imprinted. The PMMA-based polymer is stamped at 220°C (~T_g+100°C) and the APC-based polymer is stamped at 280°C (~T_g+100°C). Both stamped and unstamped samples of each polymer-type are then coated with 100 nm of gold using a bench-top sputter coater (Denton Vacuum) and a shadow-mask defining an open (i.e. gold coats) 1 cm square in the center of the sample area.

Section 3: Nanoimprinting Results on Electro-Optic Films

The quality of stamping into EO films was very high. Figure 3.3 shows typical images of a test pattern both in silicon and an imprinted EO film (CLD1). 100 nm feature size is readily achievable.

Figure 3.3: SEM images of the silicon stamp (left) and an imprinted CLD1/PMMA film (right).

Looking first at the most standard EO materials available, CLD1 has been long recognized as one of the most active and widely studied EO chromophores, with a wide variety of devices produced using it as an active layer, including the lowest reported halfwave voltage (V_π) in a Mach-Zehnder modulator.[11] DR1 was one of the early successful EO chromophores and is one of the few that are commercially available. The standard matrices used for EO materials are polymethylmethacrylate (PMMA) and amorphous poly carbonate (APC), both of which have relatively low loss in the near IR region and exhibit high glass transition temperatures. Our initial test used these two chromophores mixed individually with each of the polymer hosts as the directly imprinted NIL material. PMMA was imprinted at 220°C and APC was imprinted at 280°C.

The EO coefficient of each EO system was tested using simple reflection[13] on both a stamped and unstamped film. Additionally, each sample was also tested by UV-vis spectroscopy. By comparing the difference (between stamped and non-) in these two tests, the effect of NIL on the films was determined.

To the eye, there is an obvious difference between the stamped and non-stamped films in terms of color. While there is only a lightening of the color in the stamped PMMA samples, all color is gone from the imprinted APC samples. The chromophores decompose at the high temperature, even though it is not more than a few minutes. To quantize this, the UV-vis data in Figure 3.4 shows the dramatic difference caused by the NIL process.

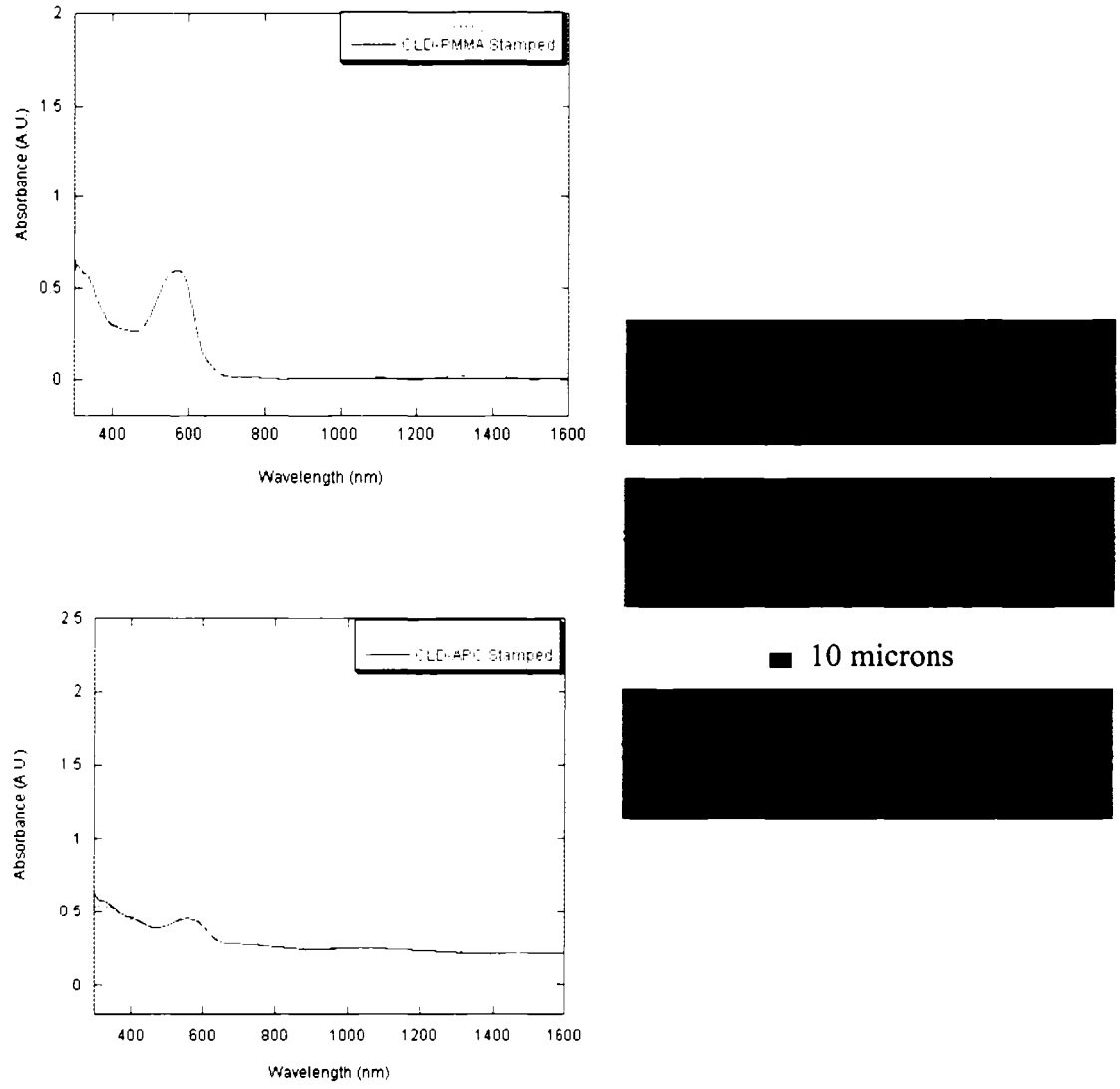

Figure 3.4: UV-vis spectra for CLD in both PMMA and APC and optical micrographs (200X) of a non-stamped (top), stamped PMMA/CLD (middle) and stamped CLD/APC (bottom) film.

The data for DR1 are similar in illustrating a serious degradation in the chromophore character as illustrated in Figure 3.5. This was further characterized by simple reflection, which yielded no EO effect for any of the four combinations of EO

chromophore and polymer used. Neither chromophore withstood the harsh temperatures of NIL, even with the lower T_g PMMA.

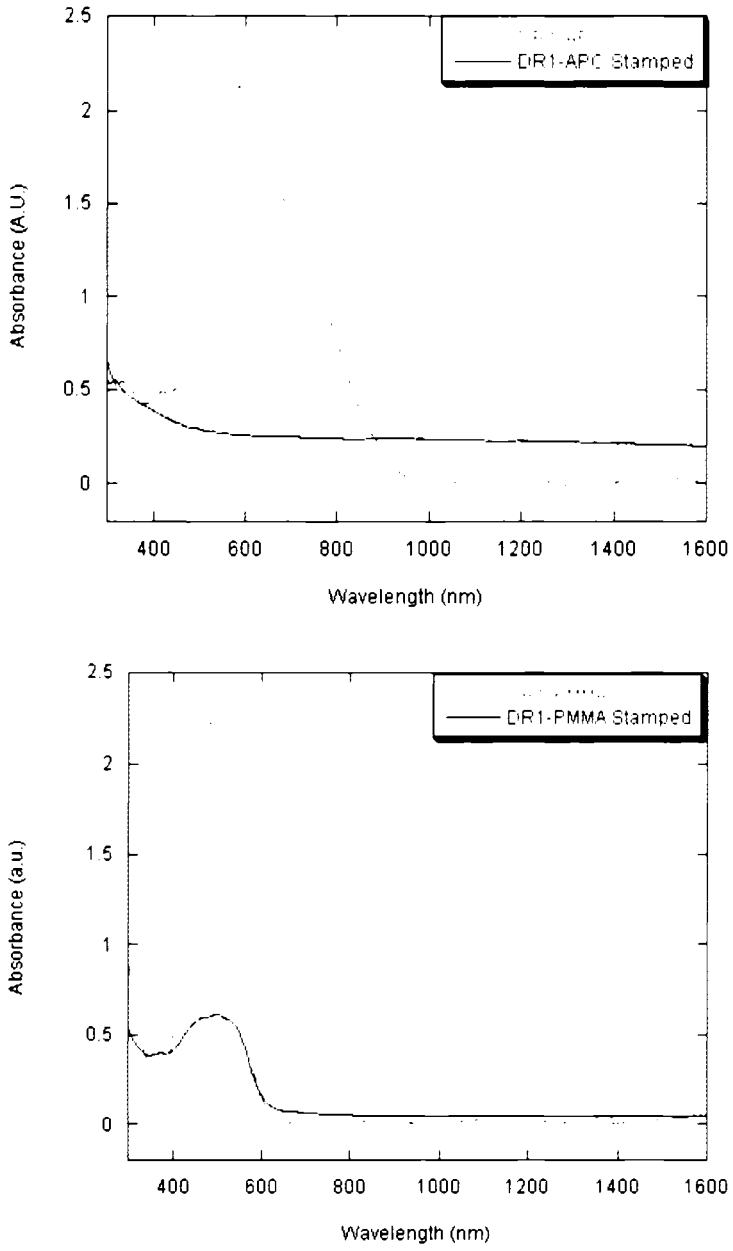

Figure 3.5: UV-vis spectra for CLD in both PMMA and APC

After the failure of the classic EO chromophore systems, we synthesized a temperature-resistant chromophore that was designed with temperature stability as a primary attribute. Nonlinear optical chromophores exhibiting large substituent induced charge density asymmetry have classically followed a push-pull design paradigm. An electron donor moiety was attached to a conjugated bridge terminated by an electron-withdrawing group. The stability of these systems is limited by the relative stability of the components. A tradeoff between optical nonlinearity and material stability has been observed when aromatic rings such as thiophene, are used as conjugated bridge components.[14] The chromophore PAS172 was designed as a simple test model patterned after the well-known FTC-type EO chromophore. This model demonstrates the gain in stability associated with the use of aromatic bridge components as well as the incorporation of a robust electron acceptor such as TCF.[15]

After imprinting PAS172, it was once again visually apparent that the chromophore did not survive the high temperature APC imprinting process, but the PMMA version looked unaffected. UV-Vis confirmed this, as shown in Figure 3.6, and simple reflection testing showed that the electro optic functionality of the chromophore was eliminated in the APC samples but preserved in the PMMA matrix imprinting.

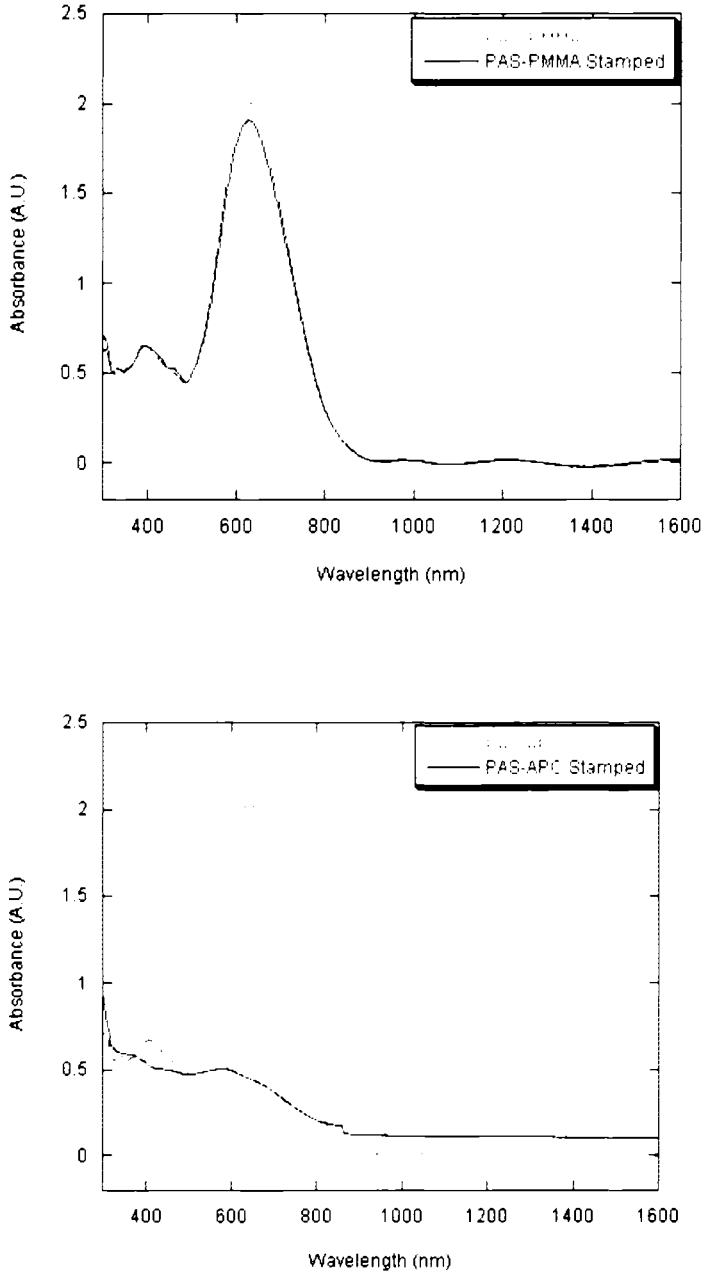

Figure 3.6: UV-vis spectra for PAS172 in both PMMA and APC.

By designing PAS172 as a high temperature-resistant molecule, it can be seen that NIL can be compatible with common polymeric EO materials. A notable area for

improvement in the union of EO and NIL is the polymer matrices. PMMA and APC have many desirable traits that make them ideal hosts for EO materials. Having a high glass transition temperature means that they are very rigid at room temperature but their matrix can be loosened with heating. In EO processing, this is essential because the guest EO molecules in the polymer must be electrostatically poled within the matrix to induce non-centrosymetric orientation. This is achieved by heating the polymer near the glass transition and applying an electric field. The field is left on while the polymer is cooled to room temperature, thus locking in the order as the matrix hardens.

When thinking about NIL and EO matrices, we encounter a problem because as a matrix becomes more rigid (higher T_g – APC in our case) it also requires a higher temperature to imprint. APC is considered to be a premier EO host material, but NIL on APC destroys even the temperature-stability designed molecule in this study. Further temperature stable molecules could be designed but designing in temperature stability may cause a negative trade-off to occur between the stability and the EO effect, which is of primary importance. This trade off is seen when going from CLD1 to the very similar but temperature stable PAS172. CLD1 was tested with r_{33} = 25-30 pm/V, while PAS yielded only 3-11 pm/V.

For this reason, alternative matrices must be explored to reap the benefits of NIL. Of primary interest would be crosslinkable materials that would be able to be stamped at a low NIL temperature but then crosslink (UV or thermal) during the stamping process.

Section 4: Conclusion

If NIL is to be a tool for processing EO materials the significant difficulty of temperature degradation of the materials must be addressed. There is a severe degradation in the properties of traditional EO materials as a result of the NIL process, yet more robust materials can be realized through rational design and the strengthening of the bridge of the molecules. While there are material issues that must be addressed with respect to how well an organic functional material survives the NIL process, the technique has great promise as a solvent-less alternative to photolithography and a route to parallel (as opposed to serial methods like ebeam) nano-scale lithography. Not only can NIL be useful to EO material processing but it may also show promise in working with other functional materials such as organic light-embitters and organic semiconductors.

Notes To Chapter 3

(1) Liu, S.; Haller, M. A.; Ma, H.,; Dalton, L. R.; Jang, S.-H.; Jen, A. *Adv. Mater.* **2003**, *15*, 603.

(2) L. R. Dalton, in *Advances in Polymer Science*, Vol. 158, Springer-Verlag, Berlin **2002**.

(3) Kuo, Y.-H.; Steier, W.H.; Dubovitsky, S.; Jalali, B. *Photon. Tech. Lett.*, **2003**, *15*, 813.

(4) Zhang, C; Dalton, L. R.; Oh, M.-C.; Zhang, H.; Steier, W. H. *Chem. Mater.* **2001**, *13*, 3043.

(5) Paloczi, G. T.; Huang, Y.; Yariv, A.; Luo, J.; Jen, A. *Appl. Phys. Lett.* **2004**, *85*, 1662.

(6) Chou, S. Y.; Krauss, P.; Renstrom, P. J. *Science* **1996**, *272*, 85.

(7) Cedeno, C.C.; Seekamp, J.; Kam, A.P.; Hoffmann, T.; Zankovych, S.; Sotomayor Torres, C.M.; Menozzi, C.; Cavallini, M.; Murgia, M.; Ruani, G.; Biscarini, F.; Behl, M.; Zentel, R.; Ahopelto, J. *Miroelectronic Eng.* **2002**, *61*, 25.

(8) The EV520HE wafer bond system made by EV Group, Austria is one example.

(9) Srinivasan, U.; Houston, M. R.; Howe, R. T.; Maboudian, R.J. *Microelectromech. Syst.* 1998, *7*, 252.

(10) See supporting material.

(11) Shi, Y.; Zhang, C.; Zhang, H.; Bechtel, J. H.; Dalton, L. R.; Robinson, B. H.; Steier, W. H. *Science*, **2000**, *288*, 119.

(12) Dalton, L.; Harper, A.; Ren, A.; Wang, F.; Todorova, G.; Chaen, J.; Zhang, C.; Lee, M. *Ind. Eng. Chem. Res.* **1999**, *38*, 8.

(13) Teng, C.C.; Man, H. T. *Appl. Phys. Lett.* **1990**, *56*, 1734.

(14) (a). Breitung, E. M.; Shu, C. –F.; McMahon, R. J. *J. Am. Chem. Soc.* **2000**, 122, 1154-1160.

(b) Varanasi, P. R.; Jen, A. K-Y.; Chandrasekhar, J.; Namboothiri, I. N. N.; Rathna, A. *J. Am. Chem. Soc.* **1996**, 118, 12443-12448.

(15) (a) Albert, I. D. L.; Marks, T. J.; Ratner, M. A. *J. Am. Chem. Soc.* **1997**, 119, 6575-6582.

(b) He, M. Q.; Leslie, T. M.; Sinicropi, J. A. *Chem. Mater.* **2002**, 14, 4662-4668.

Chapter 4 : Mild Temperature Nanoimprint Lithography Using Smart-Crosslinking Polymers For Organic Functional Material Applications

Section 1: Introduction

The excitement generated by organic functional materials is unavoidable and well founded, with organic light emitting diodes (OLED), transistors, photovoltaics, and electro-optic (EO) modulators comprising a few of the more prominent devices based on these molecules targeted by researchers in recent years. In many of these areas organics have begun to rival or surpass their inorganic analogs while demonstrating additional benefits such as mechanical flexibility and inexpensive fabrication. For example, EO modulators based on functional polymers and dendrimers have now surpassed the inorganic state-of-the-art, lithium niobate, by a factor of four in the key figure of merit, electro-optic coefficient (r_{33}).[1] Similarly, organic semiconductors are competitive with amorphous silicon in electron mobility[2] and OLEDs can now shine as brightly as traditional light sources.[3] A similarly young field, nanoimprint lithography (NIL, also known as embossing lithography), has made much progress as an alternative to conventional photolithography that can provide the same parallel processing capabilities without the use of photoresists and the solvents associated with their processing.[4] In the present work we address the compatibility of NIL and organic functional materials, with an emphasis on electro-optic chromophores, a class of organic functional materials that is known to be sensitive to environmental conditions[1] (such as those in NIL), yet would benefit greatly from the attributes of this new lithographic technique.

The basic NIL experiment involves a patterned "stamp" (usually etched silicon or a similarly robust material) being pressed into a heated polymer film, and then separated after cooling, leaving the polymer film imprinted with the inverse pattern of the stamp. Sub-100 nm features can reproducibly be stamped[4] and the entire process is cleanroom compatible. The solvent-less aspect of NIL makes it a very attractive technique for working with organic functional materials, due to their historical sensitivity to solvents. As with traditional photolithography, there are two types of lithographic modes when using NIL, positive and negative, as shown in Figure 4.1. We are primarily interested in negative NIL stamps due to our work fabricating optical rib waveguides patterned in a functional material.

Figure 4.1: Stamp nomenclature.

Problems arise when the necessary heating stage of NIL is performed, since the temperatures for patterning a standard thermoplastic, such as polymethyl methacrylate (PMMA, T_g 85-100°C), are near 200°C (T_g +100°C) since they must be able to flow into the stamp features. At these temperatures, many functional organic materials will decompose, sublime, or otherwise be rendered inactive, especially in an oxygen atmosphere. High temperatures are even more necessary if a negative stamp is used.

Because this stamp type requires much more polymer area to be compressed than the "positive" version, a highly malleable matrix is needed. This is traditionally achieved through higher heating. Room and low temperature NIL have been shown, but these are almost always "positive" stampings into films that are used as an etch mask resist, and not for direct imprinting.[5]

There are a number of solutions to the difficulty incorporating functional materials with imprint lithography. One simple approach is the use of a "softer" polymer, a material with a lower glass transition temperature that would then be able to imprint at a lower, hopefully less destructive, temperature. This is a poor solution for most applications, however, due to the decrease in overall film stability that comes with using a softer material. This will manifest itself not only in the quality of the imprinted surface, but also in the overall stability of any type of device incorporating the imprinted layer. In EO polymer devices, such as modulators, this leads to a relaxing of molecular ordering imposed by field-induced poling, thus reducing the performance and effective lifetime of the device.[6]

A second, more elegant, solution is Step and Flash Imprint Lithography (SFIL).[7] Through the use of a transparent stamp, a UV-curable precursor is imprinted, with no heating, due to the low viscosity of the uncured monomer. After the stamp is applied, the film is cured and the stamp is removed. This method is generally used in the same way as photolithography in that once the film is patterned it is subsequently used as an

etch mask for patterning a material below the UV-curable imprinted film. Unless incorporated as a component of a UV-curable monomer,[8] patterning a functional organic material would then require the SFIL monomer to be cast upon it, a step that introduces the same type of material compatibility issues raised with photoresists used in photolithography. Additionally, photopolymerization can be very dangerous to functional molecules due to the strength of radicals or ions generated.

This issue of material compatibility can prove difficult during processing. For example, the common EO host material amorphous polycarbonate (APC) is dissolved by almost all current positive-tone photoresists. Because of this sensitivity, heroic efforts and many different photoresists must be explored to enable photolithography for patterning device waveguides.[6] It can be expected that similar material compatibility may arise with SFIL.

A final solution to low temperature imprinting that is truly solvent-less and provides direct patterning of organic material is presented here. The enabling aspect of our solution is a thermally crosslinkable polymer system that can act as a host to small-molecule organic functional materials or be incorporated as a co-polymer with a functional element. In either case, the Diels-Alder [4+2] cyclo-addition reaction, as used in "self-healing" polymers,[9] provides a thermally controlled crosslinking element at a relatively low temperature (~80°C). The Diels-Alder (DA) groups are attached to a polystyrene chain that can be copolymerized with other polymers. The polystyrene,

Diels-Alder (PSDA) matrix used in this work also benefits from a furan-capped malemide group that inhibits the DA crosslinking until the furan group is released by heating to ~100°C.[10] The result of the polymer composition is a material that is very soft when initially cast as a thin film (T_g~80°C), but when heated enough to release the protecting furan group, the Diels-Alder crosslinkers are "activated." Once activated, a temperature dwell at ~80°C will facilitate the DA crosslinking, and when cooled to room temperature the film is fully cured with a T_g~130°C and resistance to common solvents.

Recent work by our group has focused on testing these PSDA-type polymers as electro-optic materials by copolymerization with an EO-chromophore element.[10] Great benefit was realized in this combination since a very stable matrix is needed for EO devices yet the functional molecules are very sensitive to high temperatures. The EO-functional PSDA molecules have now produced high electo-optic activity (r_{33} = 97 pm/V)[10] and very impressive stability (80% effective after 500 hours at 85°C).[11] These encouraging results demonstrated the promise of PSDA as a host/co-polymer for functional materials.

By incorporating PSDA material into an imprinting process, great benefits can be realized. Essentially acting as two materials, first soft then hard, PSDA can be imprinted in the initial "soft" state at a low temperature and then cooled to the "hard", crosslinked, state. The final result is a robust, highly customizable, polymer system that

can be imprinted with nanoscale fidelity at a temperature suitable for organic functional materials.

Section 2: Experimental

The PSDA incorporated imprinting process is shown in Figure 4.2.

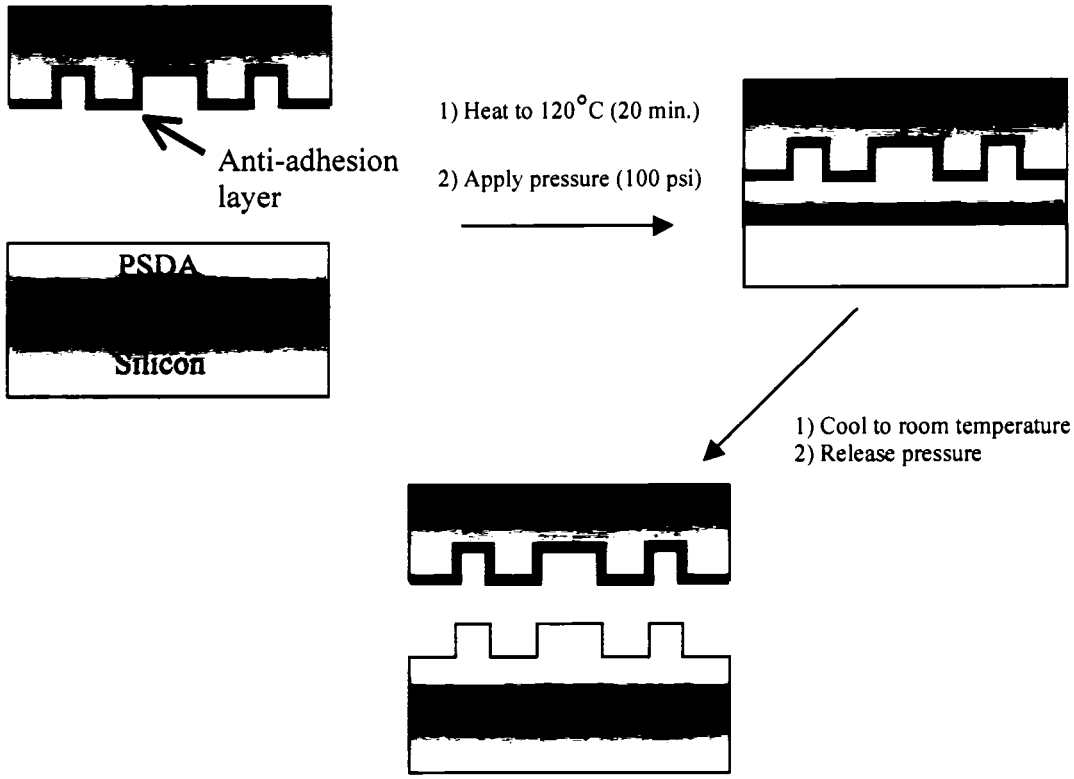

Figure 4.2: Imprinting a polymer film.

In this work, silicon stamps based on a photonic crystal design were fabricated using ebeam lithography. These photonic crystal designs are not intended as actual functional

devices but are used for their nanoscale features and diverse surface patterns. Stamps were coated with the fluorinated anti-adhesion layer 1H,1H,2H,2H-perfluorodecyltrichlorosilane (FDTS) using a previously published procedure.[12]

The Diels-Alder polymer, PSDA, is shown in Figure 4.3.

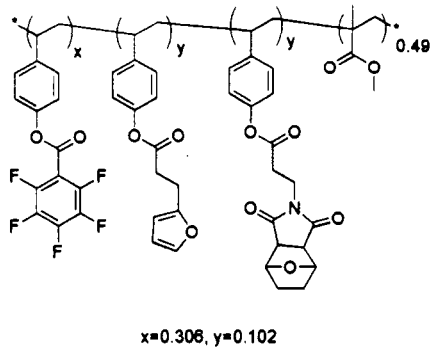

Figure 4.3: Synthesis of thermally crosslinking PSDA.

Thermal analysis by differential scanning calorimitry (DSC), shown in Figure 4.4, demonstrates the difference between the initial, furan protected, non-crosslinked polymer and the deprotected, hardened material. A shift in glass transition temperature of +50°C is shown.

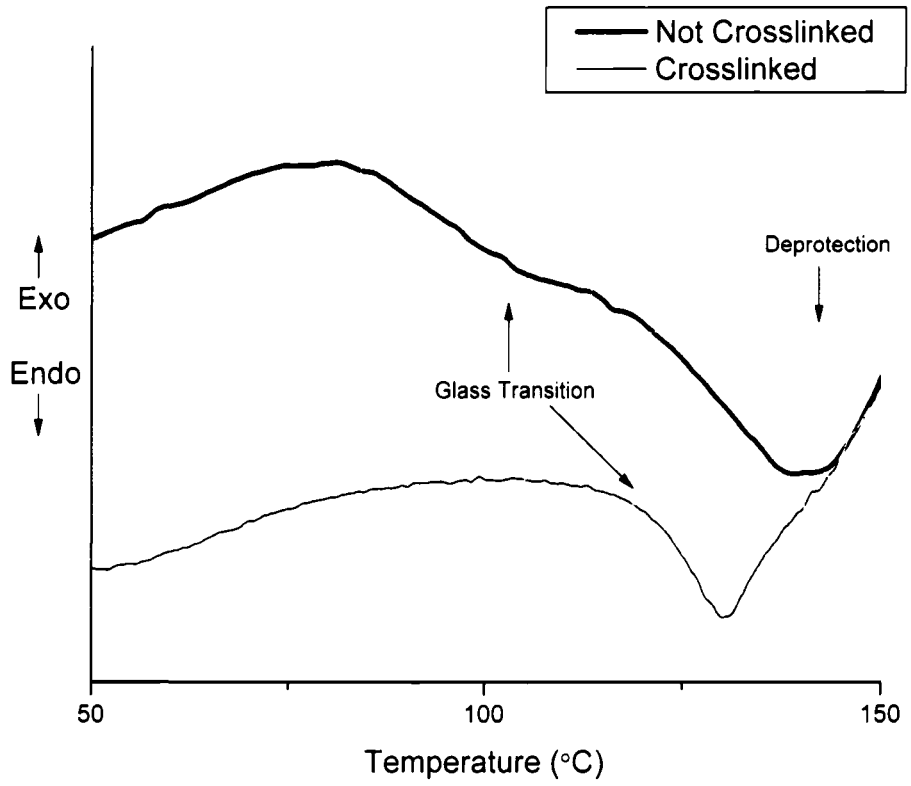

Figure 4.4: DSC of PSDA before and after crosslinking, note the dissociation of protecting furans seen in the non-crosslinked scan.

PSDA was spin-coated onto cleaned Si<100> chips (1 cm^2) giving films from 1 to 2 microns thick. The films were then solidified (not crosslinked) in a vacuum oven for four hours at 70°C.

Imprinting was done using a Tetrahedron MTP-13 hot press. First the polymer-coated chip was placed in the open press and the platens were heated to a maximum of 120°C for 20 minutes. This "deprotects" the polymer, evaporating the protecting furan group and allowing crosslinking to occur when cooled. The etched silicon stamp was

then placed on top of the polymer and the press was closed to 100 psi. The press was then cooled to 90°C for up to one hour as crosslinking proceeded. Finally, the press was cooled to room temperature and the pressure released. The stamp and polymer separated as the press opened, leaving the polymer imprinted and the stamp indefinitely reusable. Based on the nature of the organic molecule (guest/host or copolymer) the temperatures and times will change slightly, as will the stability of the overall finished film (i.e. a guest/host system will have a slightly lower T_g than the pure PSDA film).

Section 3: Imprinting Results

Using the passive polymer, PSDA, imprinting was performed with a maximum temperature of 120°C using an ebeam written photonic crystal. The results are shown in Figure 4.5, including a comparison to PMMA imprinted with the identical stamp at 200°C. Profilometer analysis confirmed the close match between stamp and imprinted film features in both height and area.

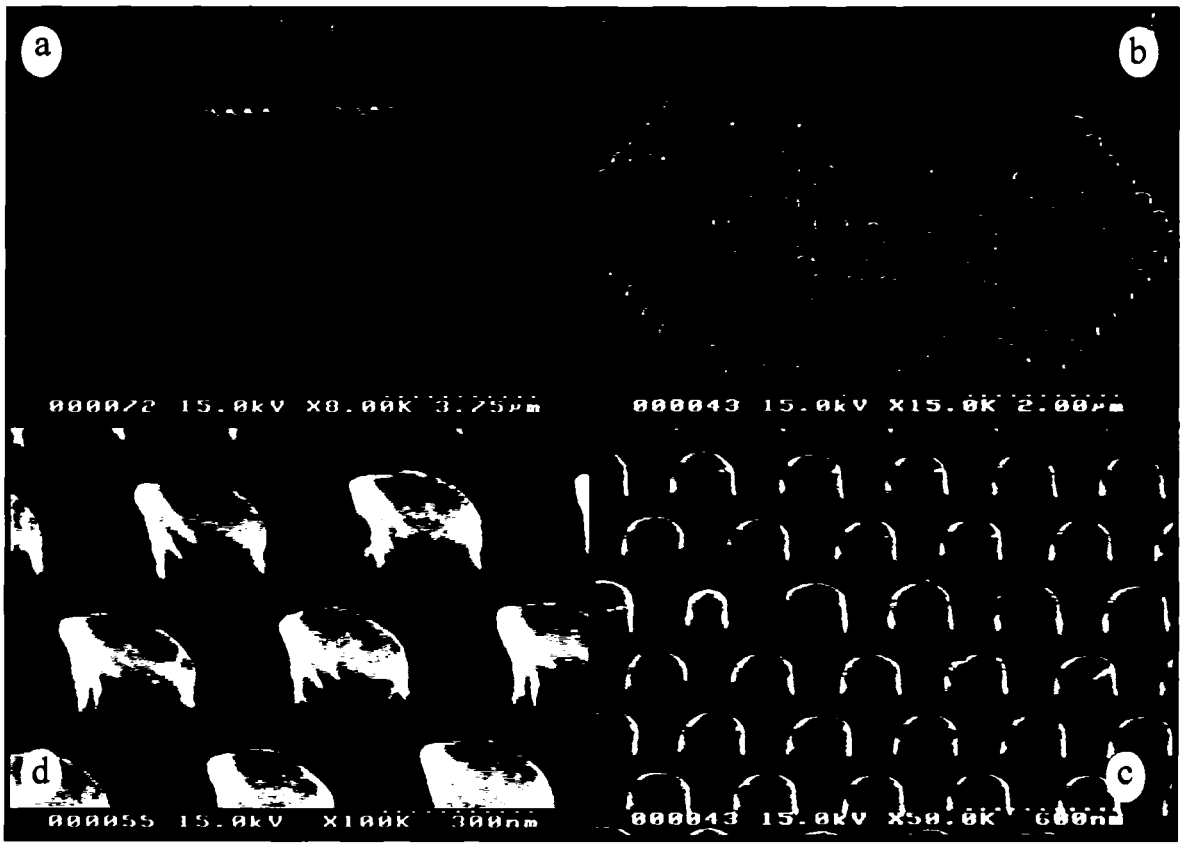

Figure 4.5: SEM images of 120°C stamped PSDA films: a) Photonic crystal silicon stamp (post imprinting) b) Imprinted PSDA film c) Detail of the stamped PSDA d) Imprinted PMMA film stamped at 200°C. Circled feature is the 100 nm wide, 200 nm tall "central defect" of the photonic crystal.

From Figure 4.5 it can be seen that the photonic crystal design is reproduced with very high fidelity. Paying specific attention to the "central defect" of the photonic crystal design, a 100 nm wide, 200 nm tall post, the nanoscale range of this method can be seen.

While the fidelity of pattern transfer is impressive, the most exciting aspect is the low temperature that this direct imprinting is achieved at. Through the use of the crosslinkable PSDA, the temperature needed to imprint was reduced almost 100°C when compared to imprinting of PMMA. An identically stamped PMMA film is shown in Figure 4 for comparison to the PSDA results. While the stamping fidelity in PMMA is still good, close inspection reveals distortions in the shape of the posts. This defect is likely due to the mechanical separation of stamp and imprinted film. Even though PMMA is considered a fairly rigid matrix, it is soft compared to the crosslinked PSDA, which is stamped with no distortion and at a much lower temperature.

In order to insure the compatibility of NIL, PSDA, and functional materials, a model study was performed by imprinting an EO polymer film. The organic functional material used was a guest/host EO polymer consisting of the small molecule electro-optic chromophore AJL8[13], shown in Figure 4.6, doped 20% by weight into PSDA.

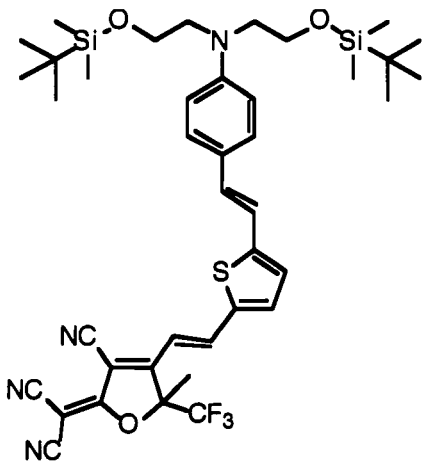

Figure 4.6: Structure of AJL8 electro-optic chromophore.

This solution was spin cast onto ITO/glass substrates which were then divided into two groups: one to be imprinted and the other not. The imprinted samples were taken through the NIL process described above while the other samples were cured using the same temperature profile but in an oven instead of a press. Due to the nature of the characterization experiment for EO materials, a flat polymer surface is needed, and so a featureless silicon stamp was used. After imprinting, gold electrodes were evaporated onto all samples for poling and electro-optic testing using the simple reflection method.[14] The functionality of EO chromophores depends on a non-centrosymmetric ordering of the molecules within the polymer host.[6] This is achieved though electrostatic poling, where the polymer host is heated near its glass transition temperature, thus loosening the matrix, and then applying an electric field of 100 V/micron. There was no discernable difference in the electrostatic poling behavior

(monitored by current) of the stamped samples versus the non-stamped samples. Similarly, the electro optic coefficient (r_{33}) also showed no difference between the two sample types. The average EO coefficient of both sample types was 90 pm/V. The long-term stability of the low temperature cross-linkable sample is quite good in comparison to a guest host system. This stability was demonstrated by periodically monitoring (by simple reflection) the electo-optic activity of AJL8 doped into PMMA and PSDA as the samples were baked in an 85°C vacuum oven. The results of this experiment are shown in Figure 4.7 and demonstrate the overwhelming stability of PSDA as a host when compared to PMMA. In fact, the stability of these PSDA devices rivals previously published reports of APC stability, considered the current state of the art for thermal stability within the field.[15]

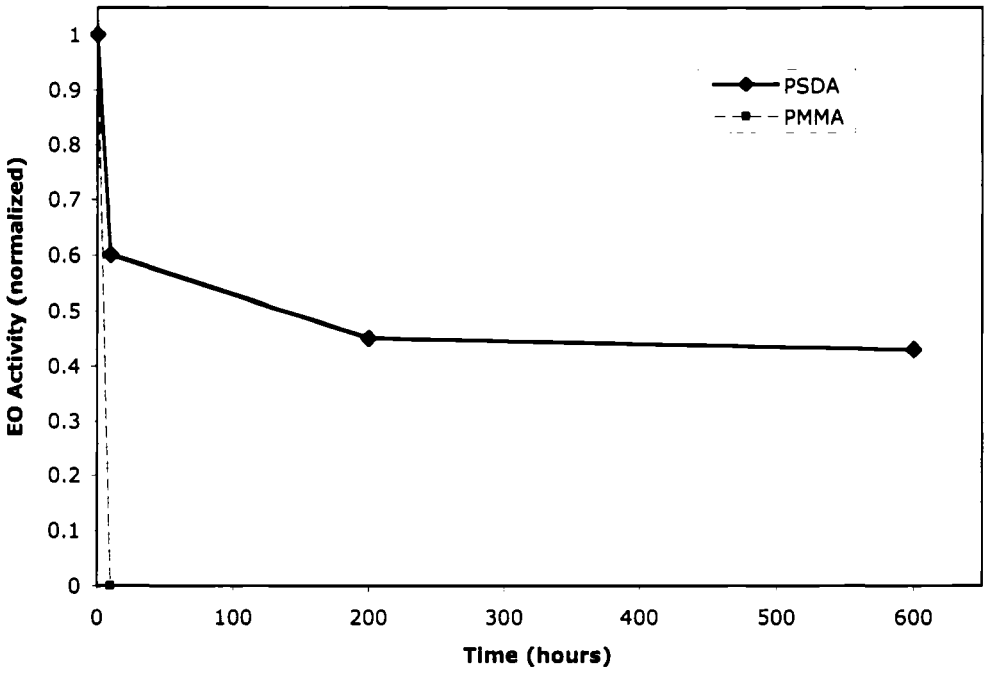

Figure 4.7: Thermal stability of AJL8 chromophore at 85°C using PSDA and PMMA host materials.

Section 4: Conclusion

Patterning organic active polymeric materials using the solvent-less nanoimprint lithography (NIL) technique is an area of great interest, yet the harsh heating conditions required by the process are generally such that the functionality of the film is endangered. A system was developed enabling the use of imprint lithography at mild temperatures so as to avoid this problematic aspect yet still produce high fidelity

nanoscale features. This was accomplished through the use of a controlled crosslinking process that creates a malleable, easily imprinted, film at a relatively low temperature and then crosslinks and hardens as it cools. The final result is an extremely stable imprinted film that can easily be the host of a number of organic functional materials and preserve their unique characteristics.

Notes To Chapter 4

[1] S. Liu, M. A. Haller, H. Ma, L. R. Dalton, S.-H. Jang, A. K.-Y. Jen, *Adv. Mater.* **2003**, *15*, 603.

[2] V. C. Sundar, J. Zaumseil, V. Podzorov, E. Menard, R. L. Wllett, T. Someya, M. E. Gershenson, J. A. Rogers, *Science*, **2004**, *303*, 1644.

[3] X. J. Wang, J. M. Zhao, Y. C. Zhou, Z. Z. Wang, S. T. Zhang, Y. Q. Zhan, Z. Xu, H. J. Ding, G. Y. Zhong, H. Z. Shi, Z. H. Xiong, Y. Liu, Z. J. Wang, E. G. Obbard, X. M. Ding, *J. Appl. Phys.* **2004**, *95*, 3828.

[4] S. Y. Chou, P. R. Krauss, P. J. Renstrom, *J. Vac. Sci. Technol. B* **1996**, *14*, 4129.

[5] D.-Y. Khang, H. Yoon, H. H. Lee, *Adv. Mater.* **2001**, *13*, 749.

[6] L. R. Dalton, in *Advances in Polymer Science*, Vol. 158, Springer-Verlag, Berlin **2002**

[7] M. Colburn, S. Johnson, M. Stewart, S. Damle, T. Bailey, B. Choi, M. Wedlake, T. Michaelson, S. V. Sreenivasan, J. Ekerdt, C. G. Wilson, *Proc. SPIE*, Vol. 3676, **1999**, 379.

[8] M. Behl, J. Seekamp, SS. Zankovych, C. M. S. Torres, R. Zentel, J. Ahopelto, *Adv. Mater.* **2002**, *14*, 588.

[9] X. Chen, M. A. Dam, K. Ono, A. Mal, H. Shen, S. R. Nutt, K. Sheran, F. Wudl, *Science* **2002**, *295*, 1698.

[10] J. Luo, M. Haller, H. Li, T.-D. Kim, A. K.-Y. Jen, *Adv. Mater.* **2003**, *15*, 1635.

[11] M. Haller, J. Luo, H. Li, T.-D. Kim, Y. Liao, B. H. Robinson, L. R. Dalton, A. K.-Y. Jen, *Maromolecules* **2004**, *37*, 688.

[12] U. Srinivasan, M. R. Houston, R. T. Howe, R. Maboudian, *J. Microelectromech. Syst.* **1998**, *7*, 252.

[13] J. Luo, S. Liu, M. A. Haller, J.-W. Kang, T.-D. Kim, S.-H. Jang, B. Chen, N. Tucker, H. Li, H.-Z. Tang, L. R. Dalton, Y. Liao, B. H. Robinson, A. K.-Y. Jen, *Proc. SPIE* Vol. 5351 **2004** 36.

[14] C.C. Teng, H. T. Man, *Appl. Phys. Lett.* **1990**, *56*, 1734.

[15] C. Zhang, L. R. Dalton, M.-C. Oh, H. Zhang, W. H. Steier, *Chem. Mater.* **2001**, *13*, 3043.

Chapter 5 – Electro-optic tuning of a silicon ring resonator using liquid crystal cladding

Section 1: Introduction

Micro-ring resonators, fabricated with conventional semiconductor processing methods in silicon, offer significant advantages over the existing telecommunication filter technology and may be the foundation of future dense-wavelength-division-multiplexing (DWDM) filters[1-5]. The high RI contrast available in SOI ring resonators enables low loss and high-Q filters fabricated with radii down to a few microns[6-7]. Such resonators can be designed as notch filters for adding or dropping individual channels in the telecommunication bands and can be densely integrated in photonic networks. For reconfigurable DWDM systems, and to compensate for temperature changes, it is desirable to tune the precise channel frequency dropped by such resonator add/drop multiplexers.

Two primary methods exist to control the optical path length of a ring resonator and thus tune its resonant frequency. To statically tune a ring resonator one can either adjust the physical dimensions (in particular its circumference) or the refractive indices of the constituent materials of the resonator. Dynamically tunable resonators can most practically be obtained by dynamically controlling the refractive indices of the constituent materials. Such dynamic tuning is commonly achieved by thermally changing the RI, i.e. by introducing a heater close to the resonator[8], and provides another level of functionality over that of statically tuned resonators. However, power

dissipation may provide a serious problem in such tunable ring resonator designs, especially when many resonators have to be integrated in a DWDM multiplexing system. Here we demonstrate the dynamic tuning of a ring resonator by changing the RI of its cladding via the orientation of a nematic liquid crystal (NLC).

Section 2: Experimental

The resonator system under study, as shown in Figure 5.1, was fabricated from a SOI wafer with silicon thickness of 205 nm, ring radius of 5 μm, and ring and waveguide widths of 500 nm.

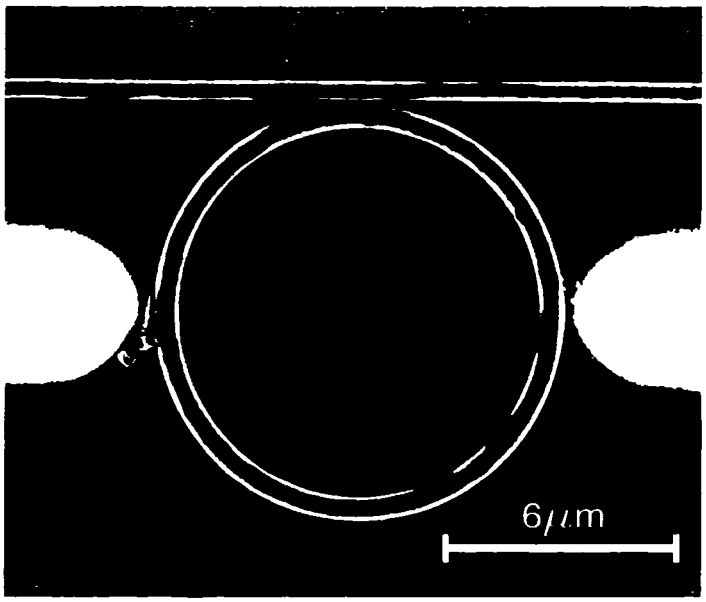

Figure 5.1: SEM image of the ring resonator with modulation electrodes (and NLC remnants).

The resonator was coupled to one waveguide, which served as both the input and output port and was separated from the resonator by a 100 nm gap. Modulation electrodes were then photolithographically defined and deposited using standard lift-off processing. The left and right electrodes were approximately 4.0 microns wide and were spaced about 400 nm and 300 nm from the resonator respectively. The modulation electrodes were designed to preferentially orient the directors of the NLC molecules parallel (azimuthally oriented) to the resonator. To minimize their electrostatic energy, the NLC molecules rotate and orient their directors along the direction of the applied electric field[9]. Figure 5.2 shows the simulated electric field generated by the electrodes designed for the azimuthally biased orientation of the NLC. The NLC E63 (n_e = 1.744, n_o = 1.517 at 589 nm) from Merck was used for the resonator cladding and was applied to the resonator by spinning at 4000 RPM for 40 seconds. Light from a tunable semiconductor laser was grating coupled, both into and out of the respective ports. The grating couplers selectively coupled and transmitted the waveguide's single TE mode (electric field in the plane of the resonator). The resonator's resonances were measured by recording the power from the output port while sweeping the wavelength of the laser. Scans were taken with different electric potentials applied across the electrodes.

The resonances of the rings correspond to the wavelengths of light coupling into the resonator which undergo a phase shift of an integer multiple of 2π upon one

roundtrip in the resonator. The resonance wavelengths can therefore be determined by modifying the Fabry-Perot etalon resonance equation to obtain[10]:

$$\lambda_m = 2\pi R n_{eff}/m \quad (1)$$

Where,

m = 1,2,3...

λ_m = wavelength of the mth resonator mode

R = radius of resonator (measured from the center to midpoint of ring)

n_{eff} = effective RI of waveguide mode

From Eq. (1), we can infer that the essence of tuning the resonator lay in changing n_{eff}. Fortunately, the TE waveguide mode contains evanescent tails that penetrate into the NLC cladding and consequently n_{eff} is partly dependent upon the cladding RI, n_{clad}.

For the TE guided mode, the contribution to n_{clad} of a NLC molecule is given by[11]:

$$1/n_{clad}^2 = \cos^2(\theta)/n_e^2 + \sin^2(\theta)/n_o^2 \quad (2)$$

Where, θ = the angle between the NLC director and the radial axis.

Section 3: Results and Discussion

With the electrode configuration shown in Figure 5.2, the application of an electric field will preferentially orient the NLC azimuthally.

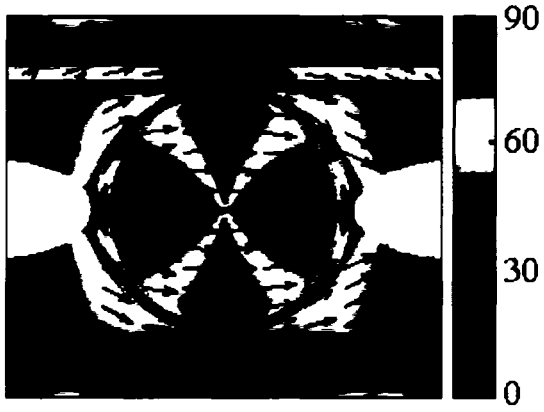

Figure 5.2: Electric field generated by electrodes. Arrows indicate direction of field and color-scale indicates angular difference between presumed director alignment (parallel to electric field direction) and radial axis.

Eq. (2) shows that n_{clad} is expected to decrease towards n_o, in turn decreasing n_{eff}. A decreasing n_{eff} causes the resonances to shift to shorter wavelengths, Eq. (1). We recorded wavelength scans while applying potentials of 0-20V across the electrodes and monitored the resonator drop frequency with a tunable laser. The resulting data for three resonances are shown in Figure 5.3. Note that the resonance shift is in the opposite direction as expected if the resonator were being heated (by absorption of the laser or leakage currents across the electrodes)[12].

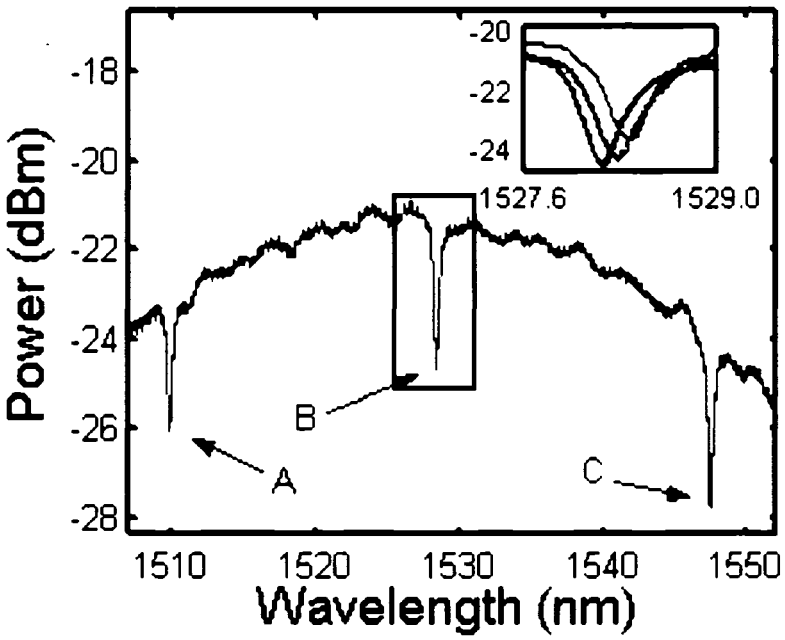

Figure 5.3: Wavelength scan showing three resonances A, B, and C at 0 V. (inset) Close-up of resonance B at 0, 10, and 20 V.

We obtained a maximum resonance shift of approximately 0.22 nm (27.5 GHz at 1.55 μm) by applying 20V. To correlate our experimental results with the degree of NLC alignment, we start with a modified form of Eq. (1) and obtain:

$$\Delta\lambda_m = (\partial n_{eff}/\partial n_{clad})\, \lambda_m\, \Delta n_{clad} / n_{eff} \quad (3)$$

Where,

$\Delta\lambda_m$ = the shift in resonance wavelength

$\partial n_{eff}/\partial n_{clad}$ = the derivative of n_{eff} with respect to n_{clad}

Δn_{clad} = the change in the cladding RI due to NLC alignment

We assumed that with zero applied electric field the NLC was randomly oriented[13]. For E63, this corresponds to an n_{clad} of 1.619. We subsequently used this n_{clad} to simulate n_{eff} and $\partial n_{eff}/\partial n_{clad}$ for the three resonant wavelengths under study. Then, by using Eq. (3) (and for small n_{clad} changes) we solved for $\partial \lambda_m/\partial n_{clad}$ and obtained the resonance wavelength sensitivity to n_{clad}. Using this in conjunction with the wavelength shift data, we obtained a Δn_{clad} of only -0.0012 for all three resonances. Based on our electrostatic modeling for the azimuthally biased electrode configuration, in the NLC saturation field regime we would expect a Δn_{clad} of -0.0342. Though the applied field was expected to exceed E63's saturation field of 0.52V/μm, the resonances instead continued to shift through the maximum applied field. This indicated the applied electric field was insufficient to achieve complete NLC alignment and it partly explains the disparity between the calculated and measured Δn_{clad} values. Another possible explanation for the disparity between Δn_{clad} values is that the fabricated electrodes were not identical to the electrodes used in the electrostatics modeling. As can be seen in Figure 5.2, the tuning electrodes used in this study align the NLC azimuthally, radially, or in a linear combination of the two, depending on their position around the ring. Therefore, the actual resonance tuning results from the relative imbalance between azimuthal and radial NLC alignment, which in turn is extremely sensitive to the electrode geometry. The electric field generated by the fabricated electrodes may then differ substantially

from the simulated field and thus explain the significant difference between measured and simulated Δn_{clad} values.

As expected, the resonance shifts were independent of field polarity and were completely reversible. After removing the electric field, we observed the resonances slowly return to their original wavelengths. The long (approximately 5 min) resettling time further suggests negligible surface induced NLC alignment by the ring. Instead of snapping quickly into a surface-induced alignment, the NLC slowly flows and undergoes Brownian motion until it returns to a completely randomized state[14].

Section 4: Conclusion

In conclusion we have demonstrated an electrically tunable ring resonator using NLC as the cladding. The resonance wavelengths could be reversibly controlled up to a 0.22 nm range by applying an electric field across the resonator to align the NLC cladding. In the future we intend to investigate increasing the tuning range of the resonator and shortening the resettling time by using alternate electrode designs, higher electric fields, and a NLC alignment layer on the surface of the ring.

Notes To Chapter 5

[1] M. K. Chin, C. Youtsey, W. Zhao, T. Pierson, Z. Ren, S. L. Wu, L. Wang, Y. G. Zhao, and S. T. Ho, IEEE Photon. Technol. Lett. **11**, 1620 (1999).

[2] B.E. Little, S. T. Chu, H. A. Haus, J. Foresi, and J.–P. Laine, J. Lightwave Technol. **15**, 998 (1997).

[3] S. Suzuki, Y. Hatakeyama, Y. Kokubun, and S. T. Chu, J. Lightwave Technol. **20**, 745 (2002).

[4] K. Oda, N. Takato, and H. Toba, J. Lightwave Technol. **9**, 728 (1991).

[5] S. T. Chu, B. E. Little, W. Pan, T. Kaneko, S. Sato, and Y. Kokubun, IEEE Photon. Technol. Lett. **11**, 691 (1999).

[6] D. Rafizadeh, J. P. Hagness, A. Taflove, K. A. Stair, and S. T. Ho, Opt. Lett. **22**, 1244 (1997).

[7] D. Rafizadeh, J. P. Zhang, R. C. Tiberio, and S. T. Ho, J. Lightwave Technol. **16**, 1308 (1998).

[8] P. Heimala, P. Katila, J. Aarnio, and A Heinamaki, J. Lightwave Technol. **14**, 2260 (1996).

[9] P. J. Collings, *Liquid Crystals: Nature's Delicate Phase of Matter*, 2nd ed. (Princeton University Press, Princeton, 2002), Chap. 3, pp. 33-34.

[10] B. E. A. Saleh, and M. C. Teich, *Fundamentals of Photonics*, 1st ed. (Wiley, New York, 1991), Chap. 9, pp. 314.

[11] *Handbook of Liquid Crystals*, 1st ed. (Wiley-VCH, New York, 1998), Vol. 1, pp. 215-217.

[12] We observed the resonance wavelengths shift in the opposite direction to longer wavelengths when increasing the temperature of the resonator with zero applied electric field.

[13] An electrode configuration, which balanced the azimuthal and radial orientation of the NLC around the ring, was used to probe for possible surface-induced NLC alignment by the resonator edges. We observed no resonance shift upon application of an electric

field with this electrode configuration, which suggests little to no surface-induced NLC alignment.

[14] *Handbook of Liquid Crystals*, 1st ed. (Wiley-VCH, New York, 1998), Vol. 1, pp. 215-217.

Chapter 6 – Hybrid Organic-Silicon Ring Resonator Electro-optic Modulator (Monolithic Ring)

Section 1: Introduction

In the semiconductor electronics industry, miniaturization is a constant fact of progression. Gordon Moore established the trend with his "law" and it continues to hold today, as transistors on computer chips continue to shrink in size at a steady rate. In the relatively young field of photonics, there is no law to guide development, as the field is still emerging; yet shrinking devices size, while maintaining defining characteristics is almost always smiled upon in any industry. This miniaturization of photonic components has been the driving force behind the Defense Advanced Research Projects Agency's (DARPA) Chip-Scale Wavelength Division Multiplexing (CSWDM) program. Along with a group at The Boeing Company's Phantom Works research division and Dr. Axel Scherer's Electrical Engineering group at the California Institute of Technology, the Dalton group has played a vital role in CSWDM.

The goal of this research is ambitions: to shrink the process of wavelength division multiplexing from the current board-scale (~1 ft^3 volume) to the millimeter chip-scale. This shrinkage would reduce cost, complexity, power consumption, weight, and size. Aside from the potential commercial benefits of a superior technology, this technology will also enable more processing power, and higher instrumentation density in space constrained environments; this will be particularly advantageous in applications such as satellites, hence the involvement of Boeing.

While the entire WDM process is not the focus of this research, the fundamental function it performs is: the encoding of electronic data onto an optical signal. Integrating electro-optic material with micron-sized photonic resonators and dithering the resonant wavelength will accomplish this modulation function here. The materials used for modulation are electro-optic polymers (EO) and liquid crystals (LC). The resonators used are micro-rings.

Electro-optic modulation has been achieved in the past by integrating EO materials into Mach-Zehender modulators[1] and recently using EO ring-resonators.[2] The resonator structures used here are very different from any prior art due to the use of silicon-on-insulator (SOI) substrates that provide waveguide structures in the high refractive index (RI) single-crystal silicon surface layer. These SOI resonators do not use an EO material as the active waveguiding layer but relinquish them to the role of cladding layer. This seemingly counterintuitive decision is made primarily because the high index-contrast afforded by using silicon as a waveguide for resonators can generate extremely high quality factors (Q) for very small (~5 micron) structures. If a large enough Q is obtained, the evanescent field interaction with an EO cladding can be large enough to shift the resonant wavelength the small amount needed for modulation applications.

Ring resonators act as notch filters when coupled to optical waveguides. A ring is defined in close proximity, ~100 nm, and is evanescently coupled to a rib waveguide, as shown in Figure 6.1.

Figure 6.1: A ring resonator is defined on an SOI chip next to an optical rib-waveguides

Based on the radius of the ring and the refractive indices of the core and cladding, a specific wavelength of light will be filtered from the coupled waveguide. The efficiency and bandwidth of the filter is defined by the Q of the resonator. A high Q resonator is defined as a very efficient narrow bandwidth filter. The ring resonators used in this work are high Q (Q>1000). A typical ring resonator spectrum is shown in Figure 6.2.

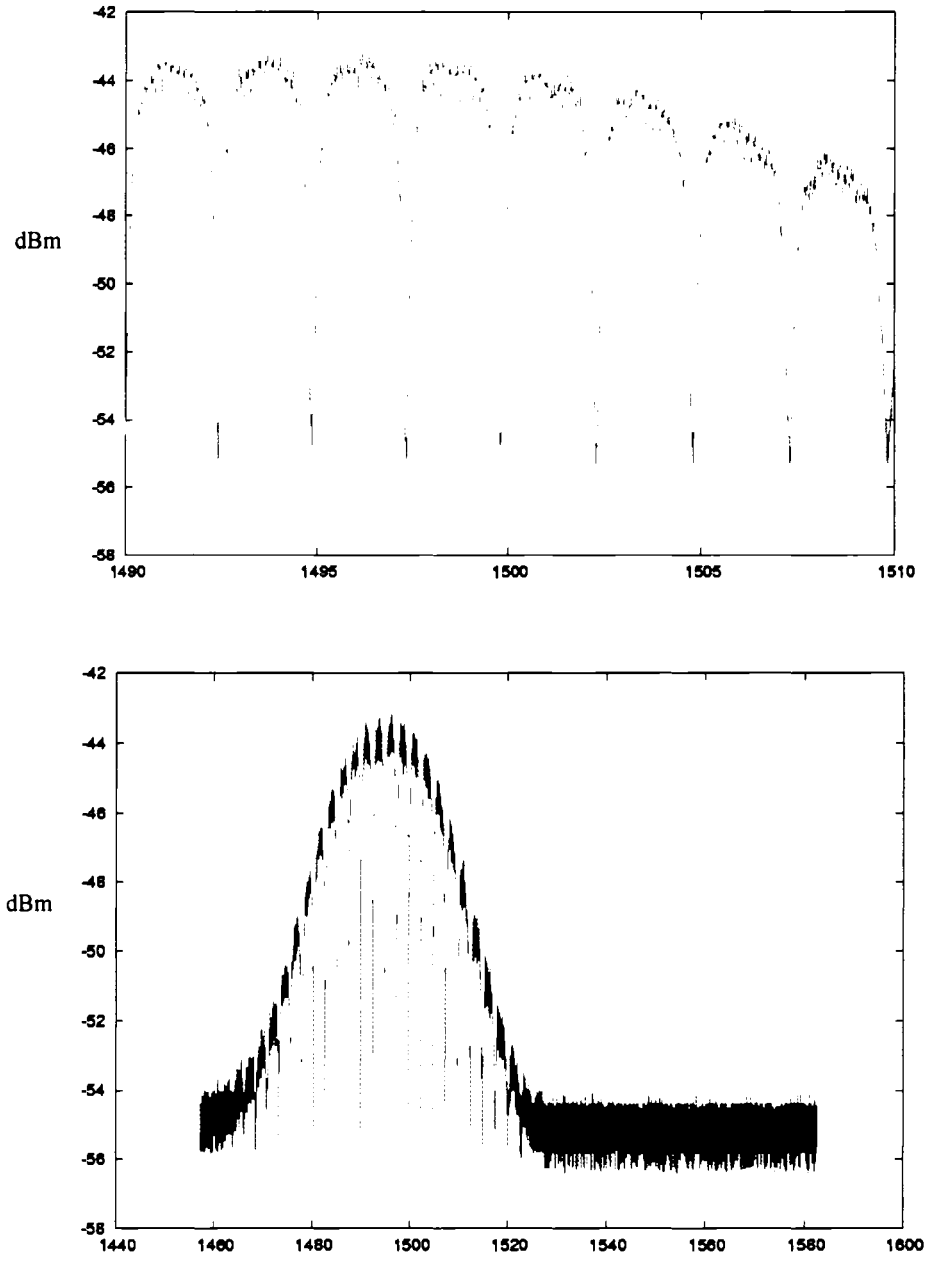

Figure 6.2: Transmission spectra of a passive SOI resonator optimized for the 1.5 micron telecom band.

Based on the (high) quality of the resonators used in this work, it is known that a detectable resonance shift can be seen if the refractive index of the cladding is shifted on the order of 0.0001 units. For our goal of modulation, this means that the task is to apply an EO material to these resonators and modulate that material at a sufficient speed and magnitude. Both liquid crystals and electro-optic polymers are suitable in this situation and both EO materials were pursued in conjunction with both resonator types.

While these polymers come in a variety of compositions, the current work focuses on small-molecule electro-optic chromophores doped into a polymeric host material. Operating by the Pockel's Effect, an applied electric field will cause a shift in the bulk refractive index of the polymer. The Dalton/Jen groups have created some of the most efficient EO polymers to date, and these are used in this work. The magnitude of RI shift can be calculated using the Pockel's Equation:

$$\Delta n = \frac{r_{33} n^3}{2} \mathrm{E}$$

Table 6.1 shows the estimated RI shift for a selection of EO polymers and a typical LC. From this table, it can be seen that EO polymers can easily achieve the needed 0.0001 RI shift needed to tune a high-Q resonator. While this minimum can be reached, devices would ideally have a much larger shift available. To reach higher levels of tuning, larger voltages (70 V) will be needed for the current generation of EO materials. What these materials lack in magnitude of RI shift they make up for in speed; they are

capable of GHz modulation due to the intra-molecular electron shift that leads to the Pockel's Effect.

Table 6.1: Calculated properties of select EO materials. EO polymers: CLD1, G1 – Current generation, G2 – next generation; LC – Nematic liquid crystal. Calculations assume a 7 micron electrode gap across a resonator.

EO Material	r_{33} (pm/V)	Δn	E Field (V/m)	Applied Voltage	Shift (nm)
CLD1	60	0.00122	1E7	70	1.2
G1	110	0.00225	1E7	70	2.1
G2	300	0.00061	1E6	7	0.58
LC	NA	0.2	1E5	1	193

Difficulty arises when integrating EO polymers into devices because they require large electric fields (50-150 V/micron) to orient the chromophores within the polymer host. This is especially critical when working with silicon-based devices – such as the resonators used in this work – because this poling voltage exceeds the breakdown voltage of silicon (30 V/micron).

The data in Table 6.1 illustrates that the liquid crystal entry offers orders of magnitude more RI shift with less field required. This large EO effect is the result of a complete molecular rotation experienced by the LC molecules with a shift in alignment

force. This force can be an electronic, magnetic, or surface contact induced ordering. LC molecules are interesting because they are liquid; yet have varying degrees of order based on the LC type. In this work we use nematic LCs, which are defined by one degree of orientational order. While work with LCs benefits from their large RI change, their detraction lies with the speed at which the RI can shift, usually on the order of milliseconds at the fastest. This switching speed is orders of magnitude slower than EO polymers, which can shift RI on the nanosecond scale.

The maximum tuning shown by the LC tuning experiments in Chapter 5 is 0.2 nm of shift with an applied 20 V. This is much smaller than the expected shift of tens of nanometers but can be attributed to the rudimentary nature of the experiment. While an external electronic field is used to orient the LC molecules between the electrodes, there is no counter force to reorient the LC to an orthogonal – maximum RI difference – configuration. This fact also contributes to the slow switching speeds seen in these first devices, on the order of minutes to return to the original, disordered, state of the LC bulk.

Similar experiments have been performed, successfully, using photonic crystal resonators/lasers.[33] The results suffer from similar shortcomings. The maximum tuning demonstrated was 1 nm with an applied voltage of 20 V. This can be attributed to the larger contribution of the LC material to the effective refractive index of the photonic crystal (where the LC material is actually integrated into the PC cavity) when compared to the resonator (where the LC is merely a cladding and so only evanescently influential on the effective refractive index). It is evident that the issues facing both resonator

types when considering LC tuning are the same: switching speed and magnitude of RI shift. Because of the severe limitation of LC switching speed, EO polymers are the only feasible option for a GHz+ electro-optic modulator system.

The integration of fast switching, robust EO polymers into resonator structures is the primary goal of the CSWDM program, yet it is also the most difficult in terms of realizing complete, functional devices. This difficulty stems from many issues: filling nano-scale features with a viscous polymer; electrode configuration, design, and fabrication; and poling EO polymers on silicon substrates.

An initial concern for polymers and micro-resonators lies in how well a viscous polymer will fill the nanometer-scale features of a photonic crystal or ring resonator. It is known that even with micron-scale waveguide features, such as inverted-rib waveguide Mach-Zehender modulators, spin-coating or dip-coating EO polymers results in incomplete wetting of fine features.[4] For this reason, it may be necessary to "force" the polymer into the resonator features. Chapters 3 and 4 detailed this imprinting technique, which was initially used in processing resonators. There was minimal improvement, however, in the performance of resonators with a polymer layer imprinted when compared to a similar spin cast film.

Embossing is accomplished fairly simply, and requires only a specially outfitted press that can apply a level, constant pressure to a sample, while simultaneously heating or cooling in a controlled manner. The press used in this work is a Tetrahedron Press housed at Boeing Phantom Works. The experiment is very straightforward and consists of placing an SOI resonator in the press with an EO polymer coated silicon chip on top

of it. The two pieces are pressed together while heating the polymer above the glass-transition temperature (Tg). The softened polymer is forced into the features of the resonator. A resonator device fabrication procedure is shown in Figure 6.3.

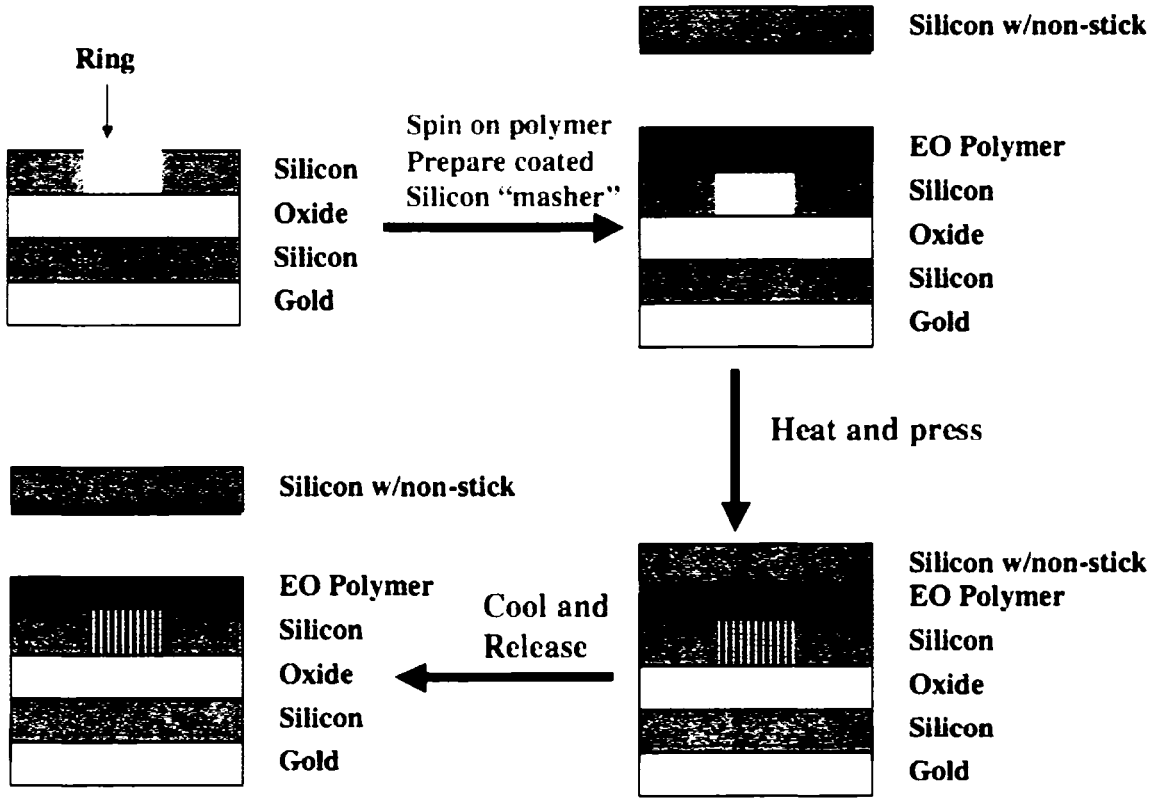

Figure 6.3: Embossing fabrication of ring resonator device

The polymer filling of nano-features has been resolved at this point, as has the question of how to properly electrode EO polymers. Traditional EO polymer devices do not rely on a directly electroded EO layer, but usually have electrodes on UV-curable cladding layers that are much more robust than a non-crosslinked guest-host EO polymer. The essence of these experiments was the discovery of lift-off photoresists as

the best method for patterning electrodes on EO polymers due to the use of more benign chemicals and fewer processing steps.

Section 2: Dielectric Breakdown

One of the largest obstacles to integrating EO materials with SOI photonic devices is the dielectric breakdown point of silicon, which is very low (30 V/micron) when compared to the standard poling voltage for an EO material (100 V/micron). The ability to electrode EO polymers was critical to pursuing dielectric breakdown experiments. Directly electroding the SOI substrate and attempting to pole will result in dielectric breakdown as shown in Figure 6.4. Table 6.2 compares the dielectric breakdown of the materials used in this experiment.

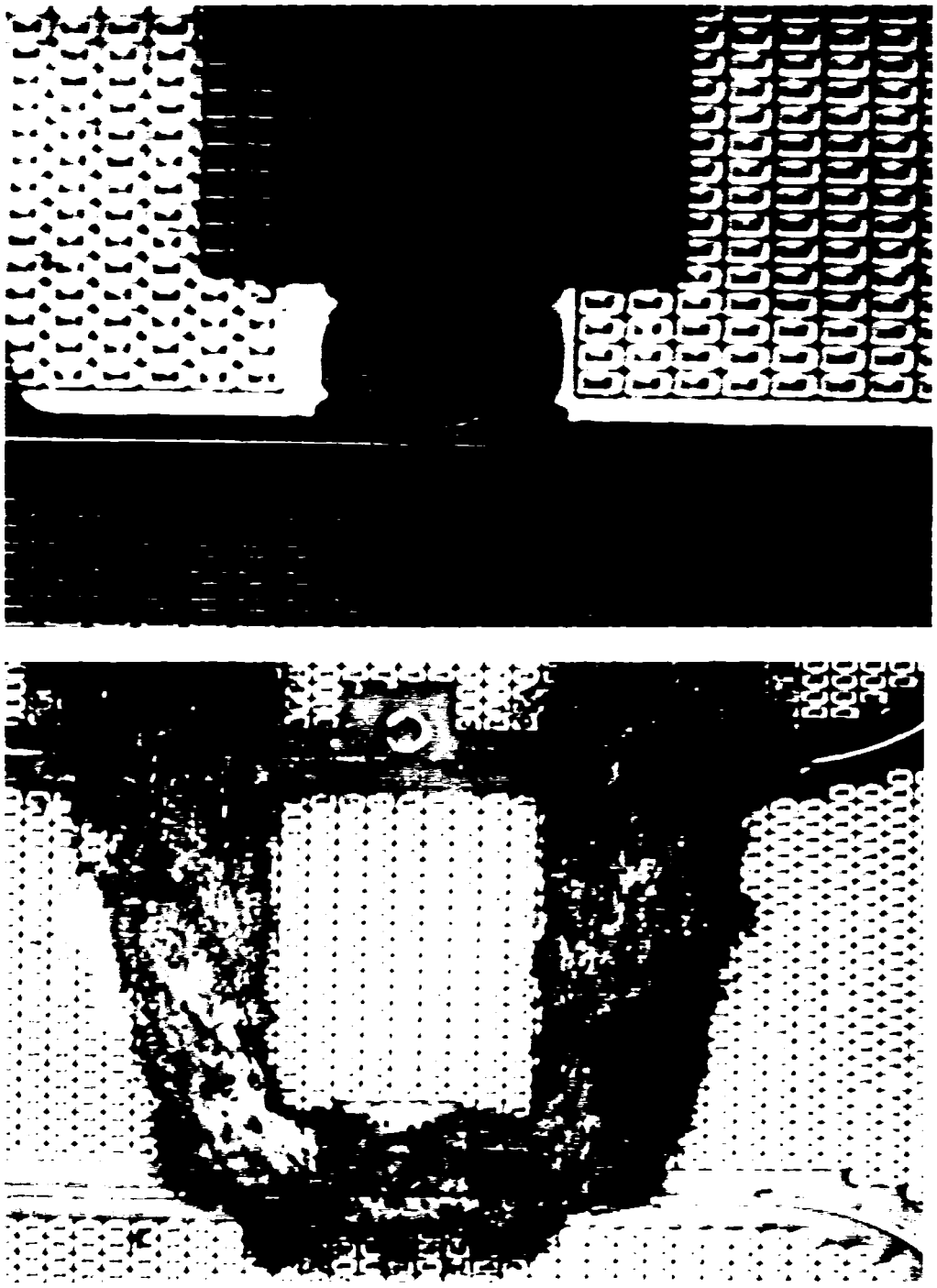

Figure 6.4: A ring resonator (top) destroyed by dielectric breakdown (bottom) while attempting EO poling at 50 V/micron across a 10 micron gap.

Table 6.2: Relevant electronic properties of some materials used in this experiment.

Materials	Dielectric Constant	Poling Fields	Dielectric Breakdown Strength	Electrode Field Penetration Depth
		(V/um)	(V/um)	(um)
Silicon	11.9	N/A	~ 30	N/A
Silicon Dioxide	3.9	N/A	1000	N/A
Poled EO Polymer	3.5	100 to 300	>300	N/A
Self-Assembled EO Polymer	3.5	N/A	>300	N/A
Doped Silicon	See Si	See Si	See Si	N/A
Metal	N/A	N/A	N/A	7 um

From the information above, it is apparent that in order to pole EO polymers on SOI, dielectric breakdown must be engineered around. By electroding on top of the EO material, a potential route is realized since the polymer will act as an insulating buffer between electrode and substrate.

To test this, we have fabricated blank samples (no resonators) with (in-plane) electroded EO polymer layers as shown in Figure 6.5.

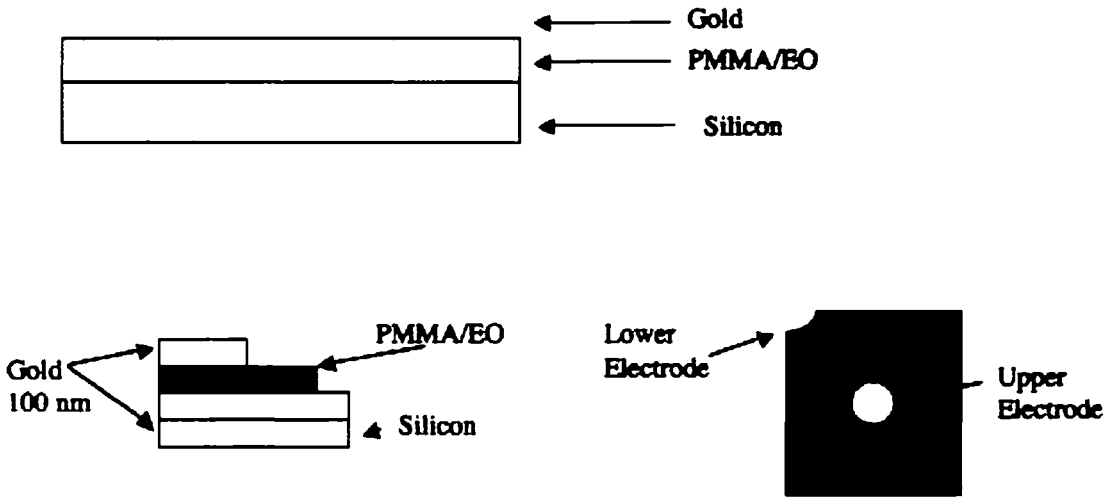

Figure 6.5: Horizontal (top) and vertical (bottom) schemes for poling and breakdown experiments.

Micrographs of horizontal dielectric breakdown samples are shown in Figure 6.6.

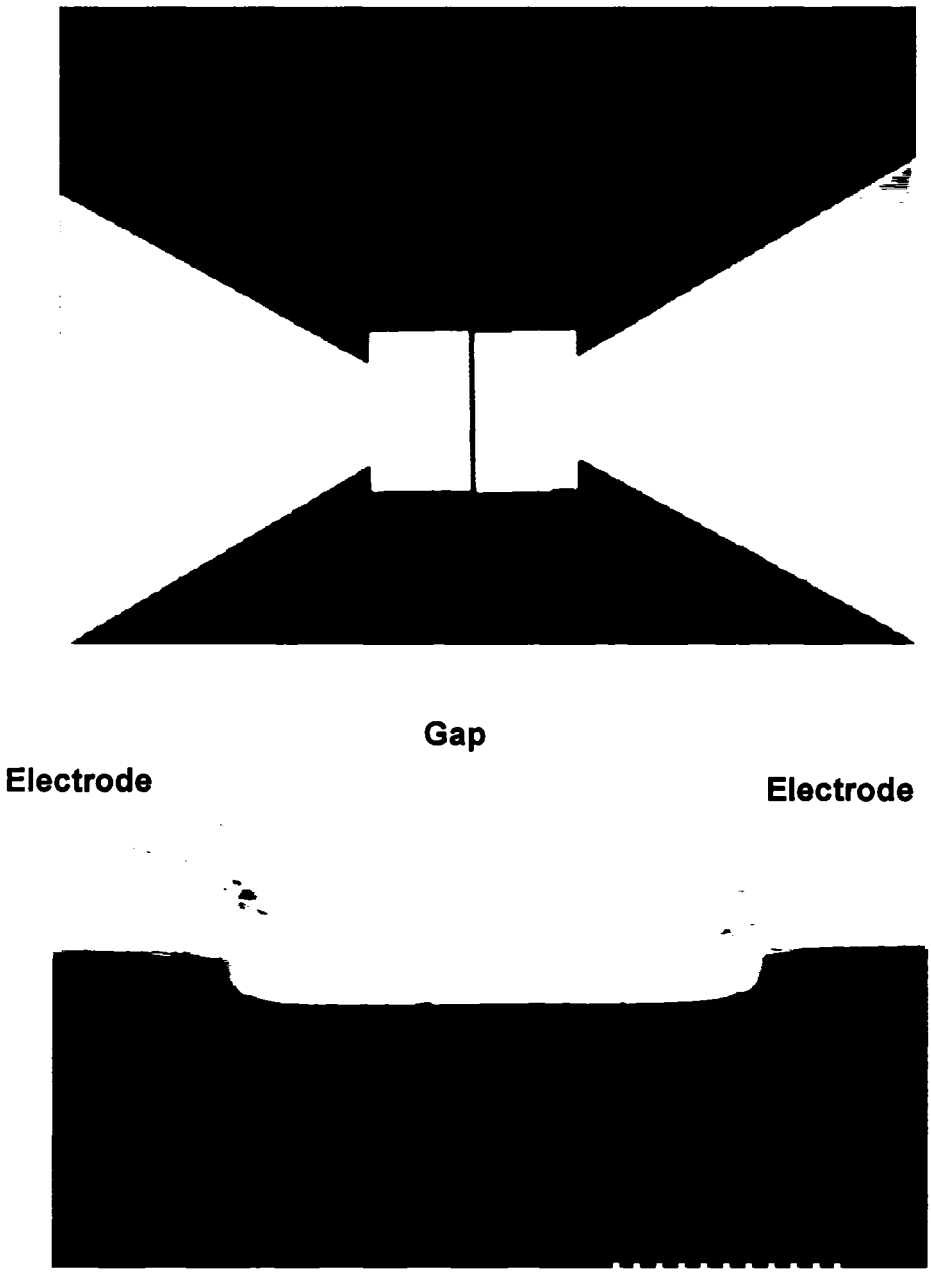

Figure 6.6: Optical micrograph (top) and SEM (bottom) of a 50 micron gold gap lithographically defined on top of a polymer film.

Based on the testing in the both horizontal and vertical configurations we have been able to raise the achievable fields to ~30 V/micron (before dielectric breakdown), still short of the minimum of 50 V/micron needed to begin poling and EO polymer and well short of the 100-150 V/micron traditionally used. This figure if fairly consistent over all EO/polymer or EO/dendrimer blends.

From these values a very large issue emerges for the creation of hybrid EO/SOI devices due to the large disconnect between the amount of field needed to effectively pole EO materials and the field that silicon is able to withstand before dielectric breakdown.

Section 3: Fluid Tuning

Before any EO tuning could be attempted, a calibration of the effect of resonator cladding on the resonance was studied. By using a series of index matching fluids (Cargille, Cedar Grove, NJ) the performance of a resonator was measured and the position of a selected peak was monitored and charted based on the refractive index change from a blank PMMA standard cladding value. The resulting calibration is shown in Figure 6.7.

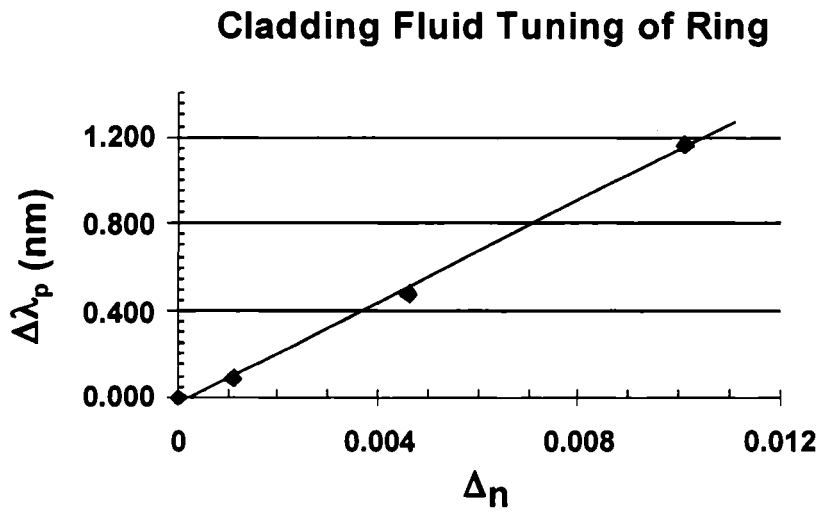

Figure 6.7: Shift in resonance as a result of cladding refractive index change.

The resonance of this device varied 1.15 nm (in the 1500 nm telecom band) per percentage of index change (i.e. a 0.01 RI change will shift a resonant peak 1.15 nm). This is illustrated in Figure 6.8.

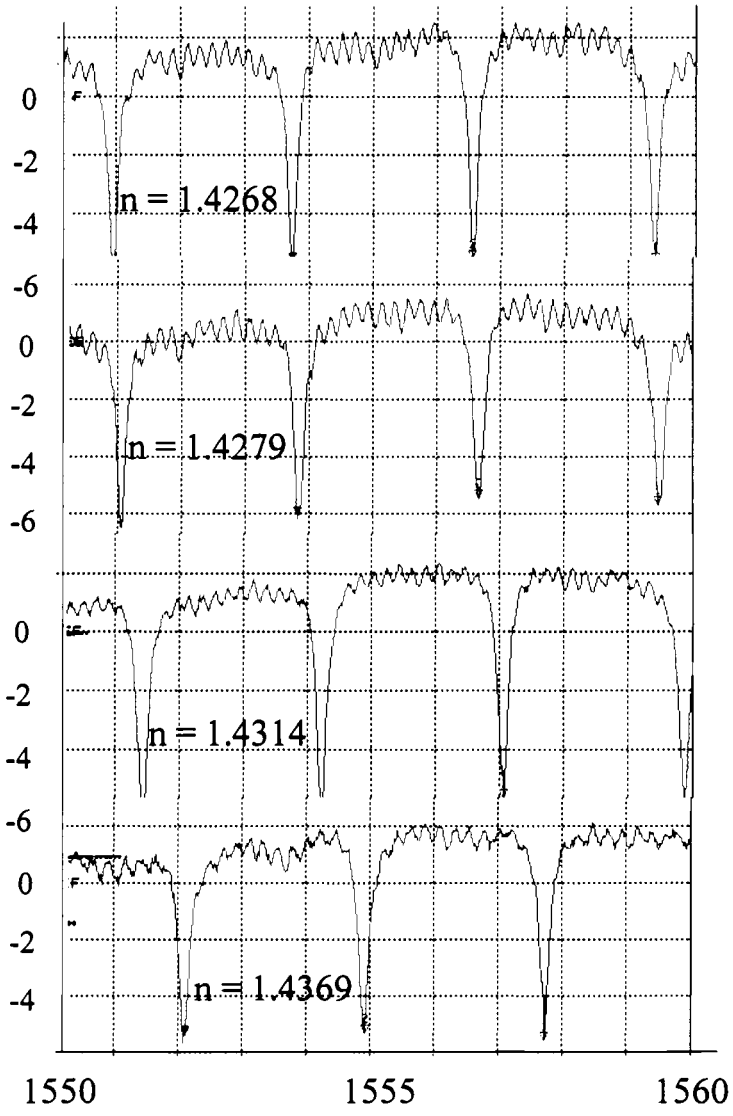

Figure 6.8: Shifting resonance as a result of cladding index change.

From the generated calibration curve, a working EO-resonator can be analyzed based on the amount a resonant shift by tracing the shift back to a refractive index change. From the refractive index change the EO activity, r_{33}, of the material can be determined using the Pockel's equation where Δn is derived from the liquid tuning

calibration, n is the refractive index of the EO material and E is the applied electric field:

$$\Delta n = \frac{r_{33} n^3}{2} E$$

This method provides a simple route to analyzing tuned EO resonator devices in order to determine EO activity.

Section 4: Temperature Tuning

Given the temperature dependence of a material's refractive index it is also possible to modulate a resonator using heating/cooling. While the speed of this heating would not be fast enough for high-speed data networks, other applications, such as sensors, could be realized. Additionally, because EO-resonator devices may be used in telecom, aerospace, and satellite applications, all of which are variable temperature environments, the effect of temperature on resonator devices must be understood in order to correct and control those effects for device stability.

To test for temperature effects a heating stage was integrated into the device-testing set-up, which allowed for controlled heating of the device under test. An initial resonant scan was taken at room temperature and a second scan was taken after a small increase in device temperature. The incremental change in temperature was only 5°C because a larger temperature change may have resulted in peak aliasing, leading to

uncertainty as to how far the monitored peak actually traveled. In other words, when monitoring a window of frequencies, such as in Figure 6.7, a large temperature increase might lead to the monitored peaks from the initial peaks moving so far that new peaks move into the monitored window, causing confusion as to the direction and extent of peak travel.

The temperature dependence has only been briefly addressed here due to the highly evolutionary stage of device development underway. Once a more mature and consistent device system is settled on, temperature characterization should be undertaken more earnestly.

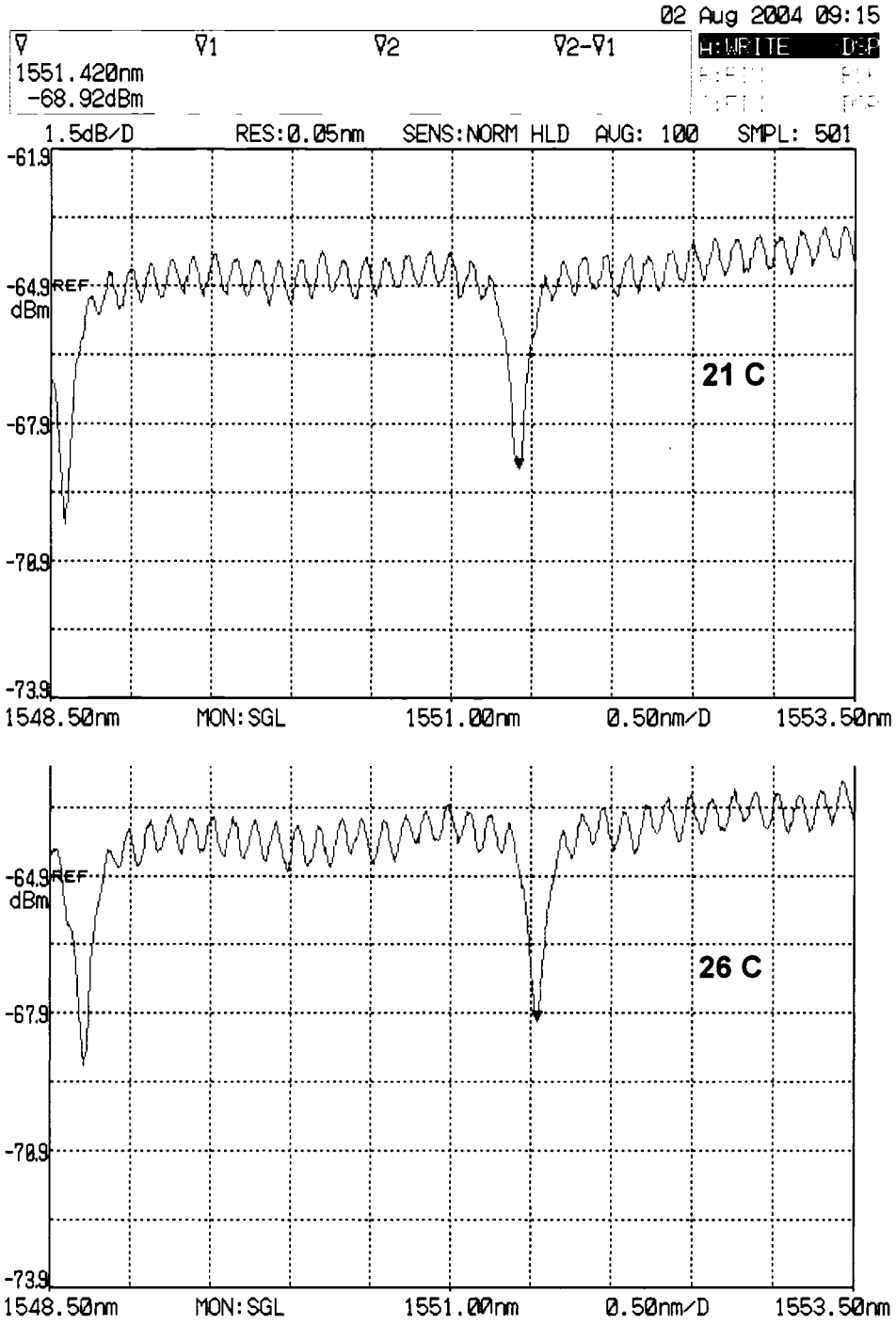

Figure 6.9: Changing resonance position as a result of temperature.

Section 5: Contact Poling

Contact poling is the traditional route to creating EO devices. Traditionally this is done by heating the EO material above T_g, applying a field to orient the chromophores, cooling, and removing the field field. While the sequence sound simple enough, the large field needed to orient the molecules, 50-150 V/micron, creates difficulty when integrating EO materials with silicon resonators.

Because of this large field requirement, many potential device fabrication schemes were envisioned for applying the appropriate field to create a working device. Figures 6.11, 6.12, and 6.13 all are early fabrication schemes for potential devices. The original thinking was to isolate the electrodes above a dielectric layer and so poling would be done with the high field only reaching the silicon of the modulated device. The hope was that because there was EO polymer surrounding the device the field would primarily concentrate in the polymer, where it was needed for poling, and the silicon of the device would survive. Additionally, preliminary tests with photonic crystal resonators (abandoned early on due to fabrication difficulties) showed that EO polymer would not fill the holes of the crystal without NIL embossing the polymer into the features. Thus, each of the following figures shows an attempt to not only circumvent dielectric breakdown but also to include NIL in the processing. Devices of the type shown in Figure 6.11 (vertical poling) were never created due to the extreme difficulty of fabricating a device by tunneling through the backside of a 500 micron

thick SOI wafer. Devices of the type shown in Figures 6.10 and 6.12 were both fabricated but dielectric breakdown prevented any device poling or operation.

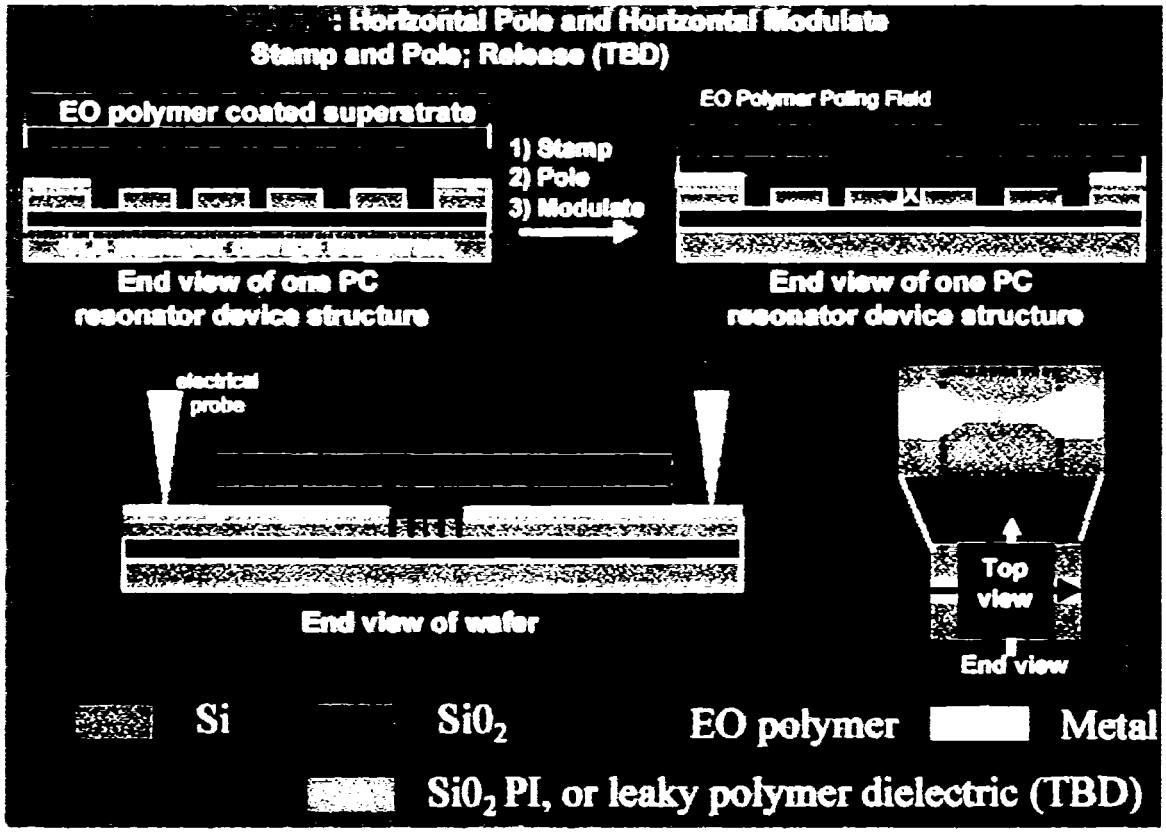

Figure 6.10: Fabrication schematic of a horizontally contact poled resonator modulator.

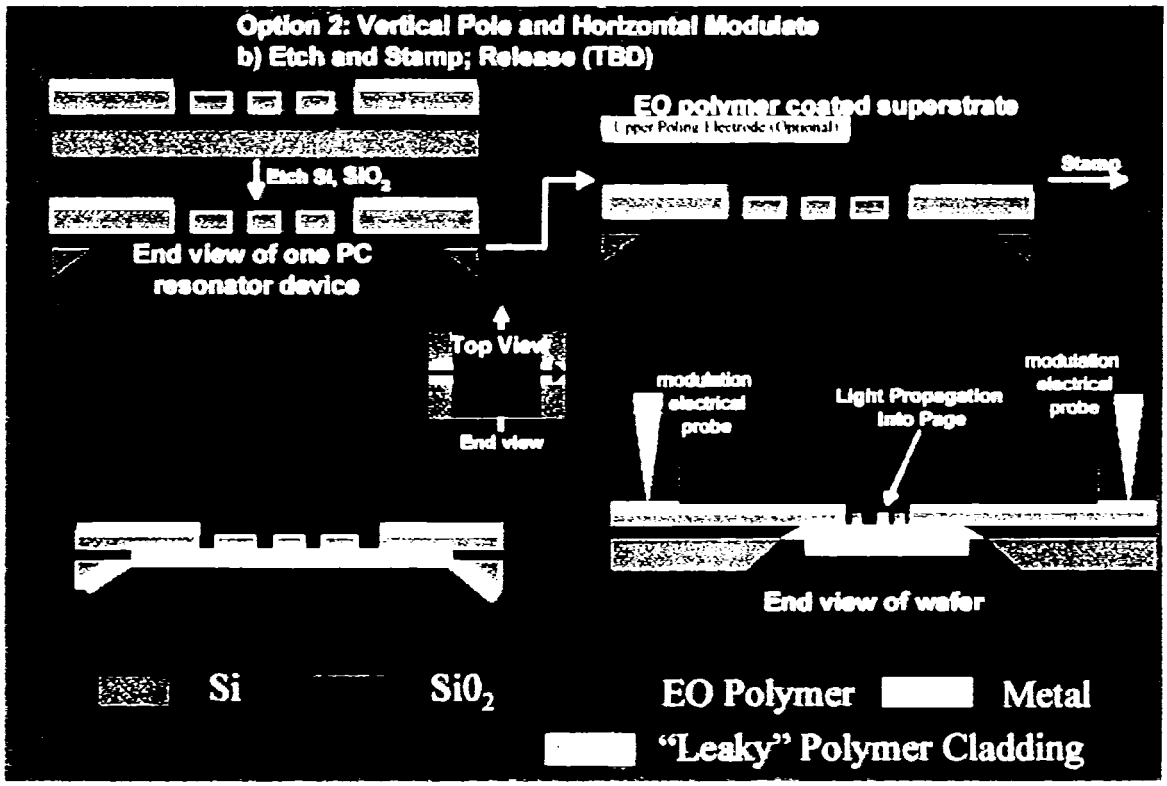

Figure 6.11: Fabrication scheme of a vertically poled resonator modulator.

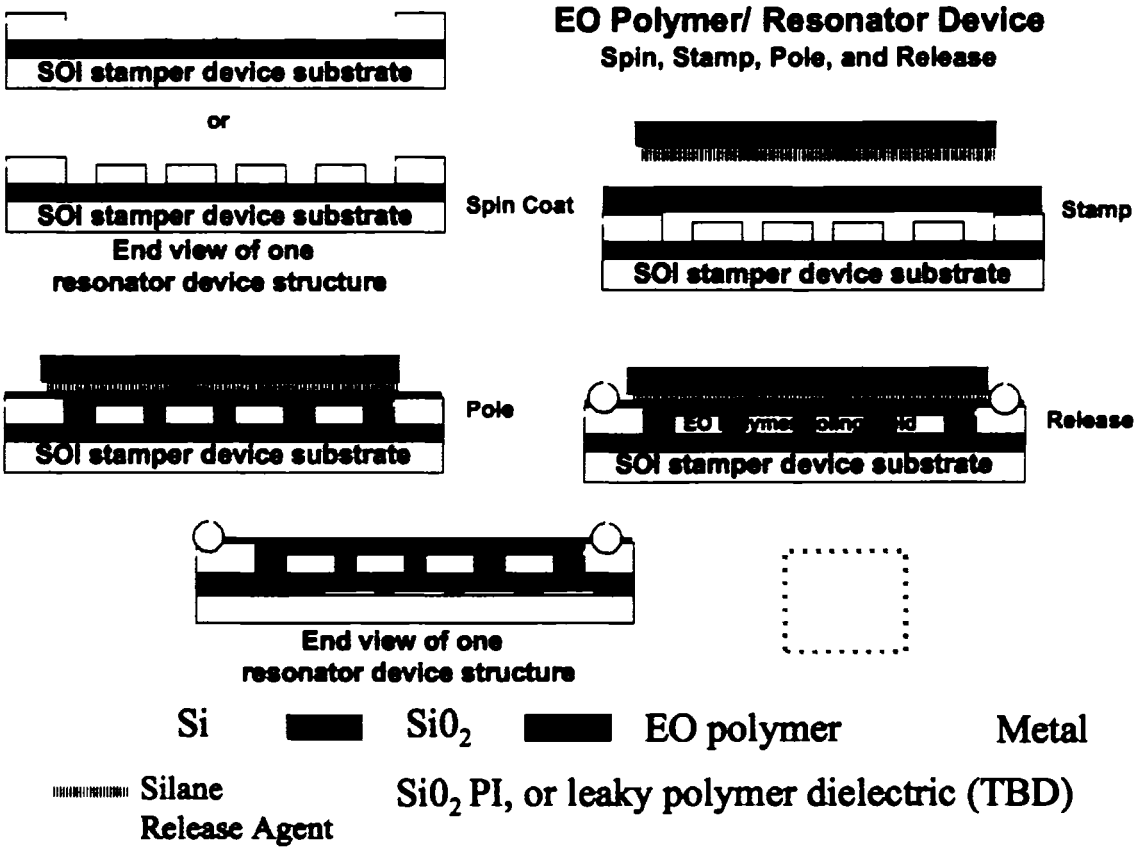

Figure 6.12: Fabrication scheme of a horizontally poled resonator modulator with NIL used to force the polymer into the nanoscale features.

By excluding all silicon from the surface of the SOI chip except for the resonator/waveguide features, there was less of an opportunity for dielectric breakdown. The practical result is that the poling/drive electrodes rested on the silicon dioxide layer of the SOI wafer and so higher fields could be applied. Because of the large field needed, it was determined that even if a full field were to be applied, the distance between the electrodes in devices such as those in the above figures (50 microns) would require many thousand volts to pole and hundreds to operate. To overcome this, a central electrode scheme was devised to drastically shrink this distance. Figure 6.13 illustrates an attempt at this configuration. The resulting device, however, suffered too much optical loss in the bridge section where the electrode crosses the waveguide, even though an oxide layer protected the waveguide in an attempt to avoid this. Additionally, poling through the entire SOI/EO stack was attempted in a device shown in Figure 6.14 yet this attempt was doomed to failure by the thickness of the sample.

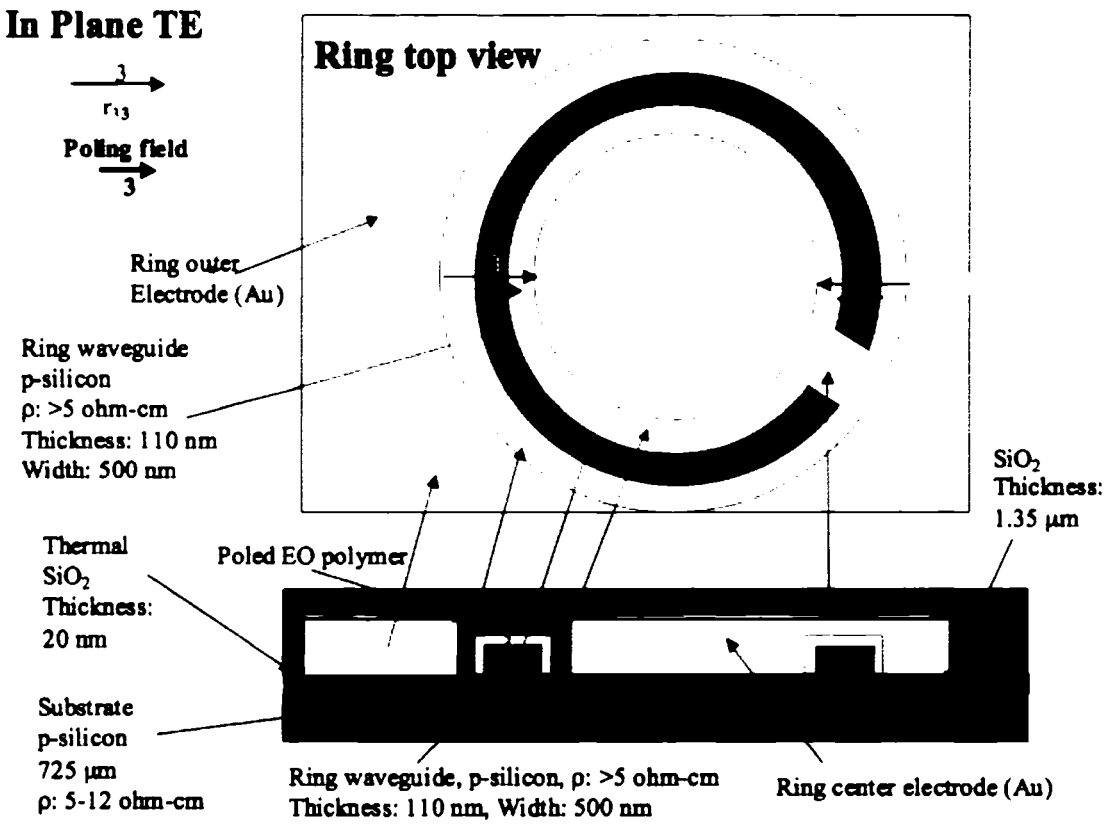

Figure 6.13: Horizontally poled and modulated resonator.

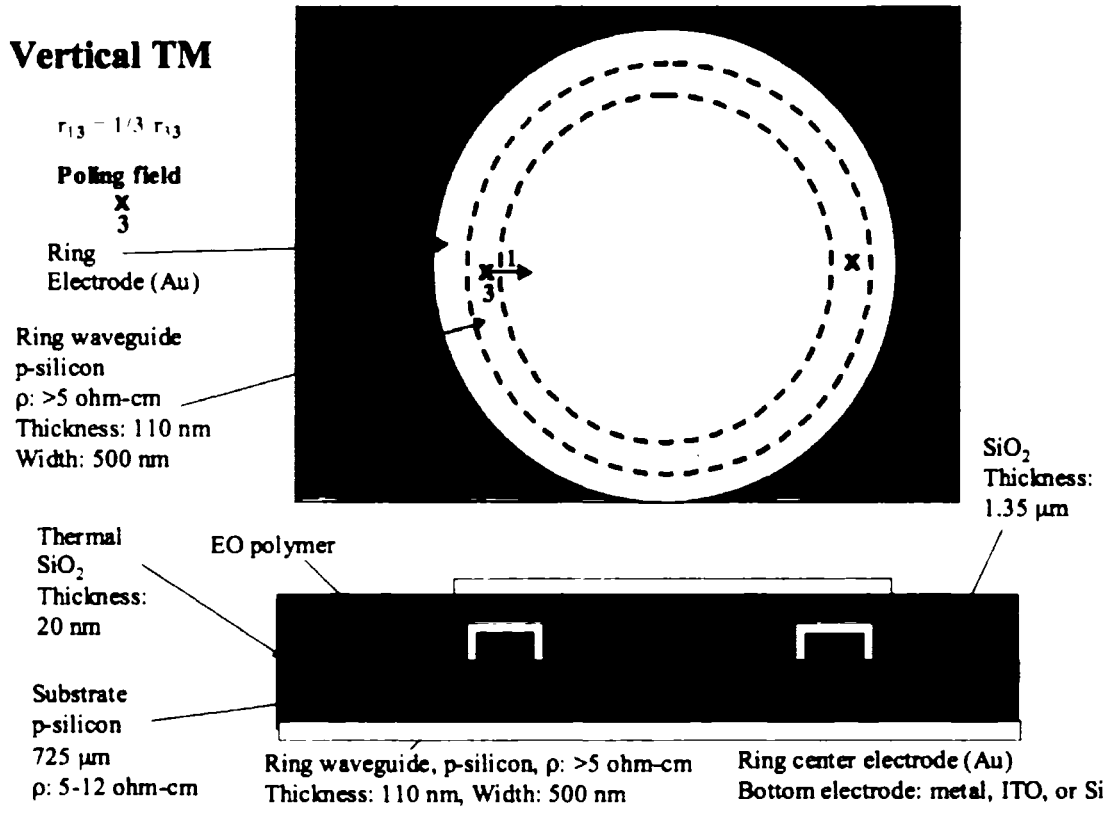

Figure 6.14: Vertically poled and modulated resonator.

In the end, the years of failed contact poled devices taught the route to success. The device must have the electrodes resting on the SOI oxide layer, with the only surface silicon being the optical components, and there must be an electrode in the center of the ring but the electrode cannot come close to the waveguide or optical loss will be prohibitive. The result of these lessons is shown in Figure 6.15 and 6.16. These are devices that connect the electrode in the center of the resonator to an upper electrode defined on top of the EO material by way of a metal via. Unfortunately, this is a very

photolithography intensive process, requiring three levels of lithography not including defining the ring and waveguide in the SOI.

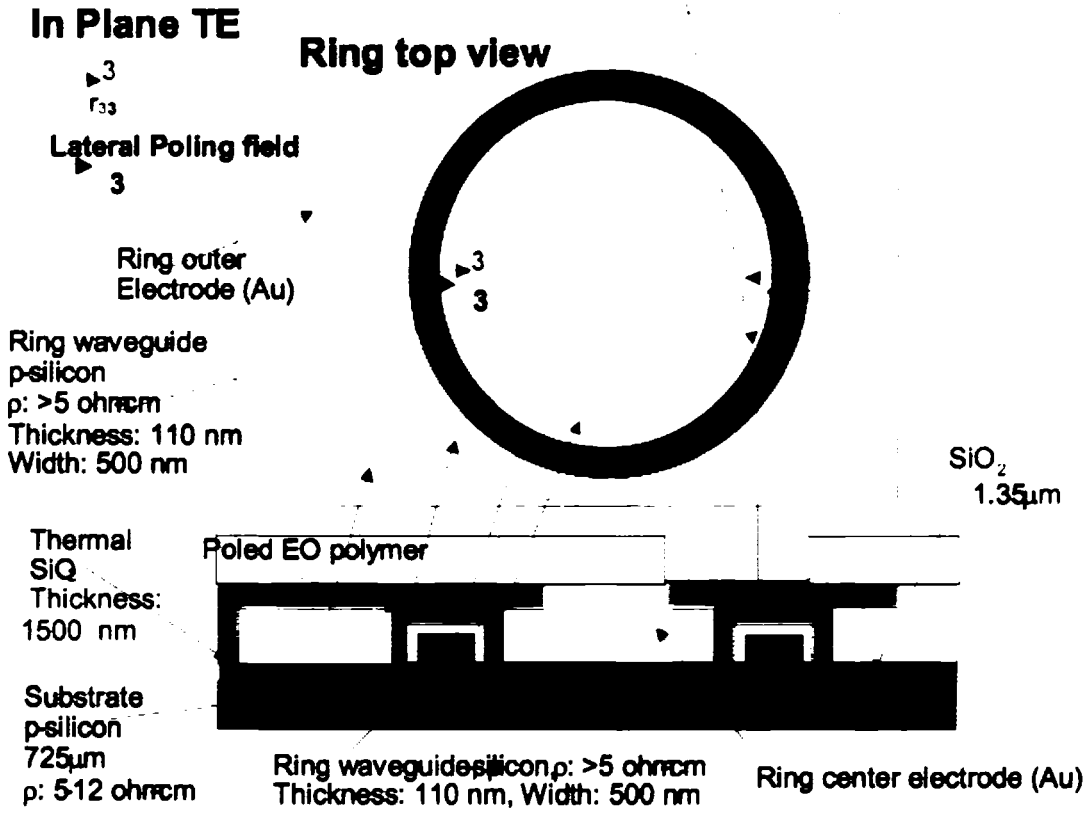

Figure 6.15: Vertically poled and modulated resonator with via.

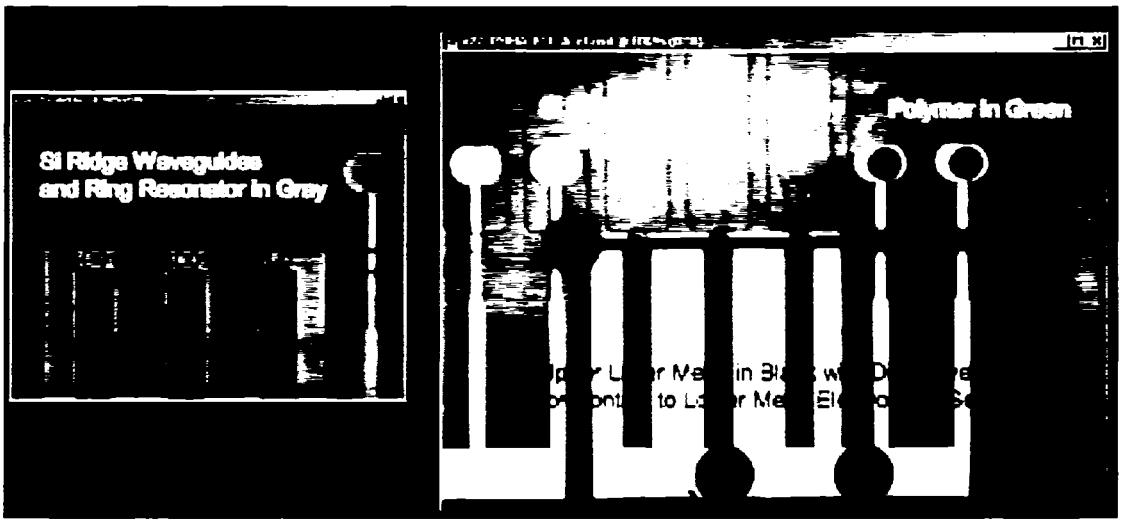

Figure 6.16: Optical micrographs of 50 micron, horizontally poled and modulated resonators with vias.

Very early stage devices of this type have now been realized. Modulation is shown in Figure 6.17 of a device with a 3 micron gap between the inner ring electrode and the outer electrode. Vpp is the peak to peak voltage applied, FWHM is the full-width half-max of the resonant peak. The r_{33} of this device is only ~10 pm/V compared to the ~100 pm/V expected for the YL124/APC material based on simple reflection measurements.

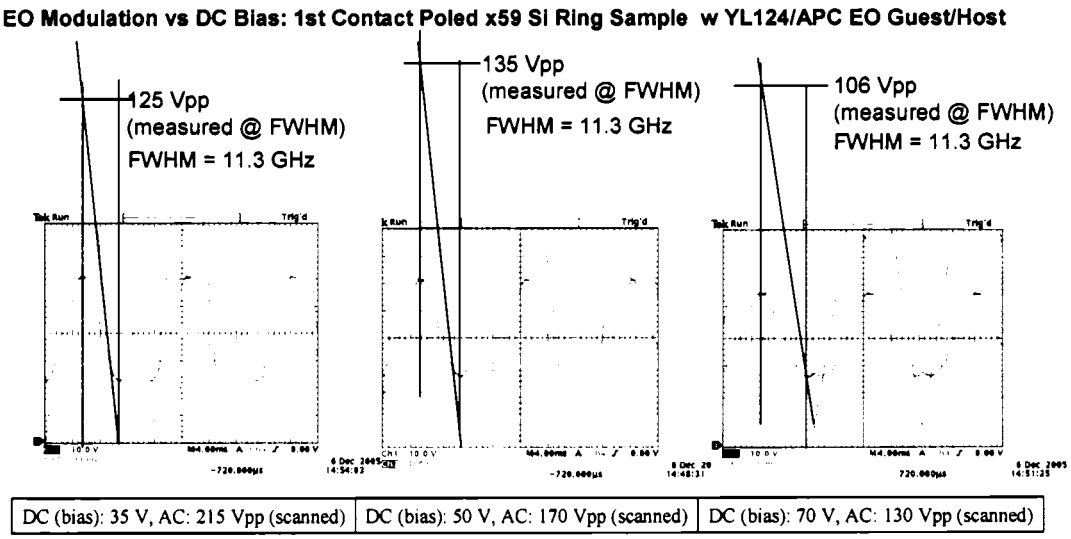

Figure 6.17: Modulation of a first generation contact poled device with a 3 micron electrode gap.

Development of this device type continues but it can safely now be said that the issue of contact poling, when integrating EO materials into silicon photonics, has been solved.

Section 6: Corona Poling

While contact poling is the traditional poling method for fabricating EO devices, corona poling is a known alternative that allows for poling with lower fields, yet in a limited configuration. As a quick route to working EO/SOI resonator devices, corona poling is an ideal method. The limitation is that there can only be poling in a vertical

direction, which differs from contact poling which is directionally limited only by electrode configuration.

Corona poling, involves ionizing an inert gas above a sample, which imparts an electrostatic effect on the sample surface.[5] This is done in a vertical configuration with an SOI chip electroded with gold on the backside and with an EO polymer film on the top. A tungsten filament electrode is place 4 cm above the sample surface and the environment is filled with nitrogen. A voltage of ~3 kV is applied between the filament and the backside electrode while heating the sample above the polymer T_g. As the gas is ionized a potential develops on the surface of the sample inducing alignment of the EO chromophores. By cooling to room temperature with the voltage still applied, the order imparted to the film is locked in.

While the most logical scheme for device operation is to pole and modulate in the same direction, thus utilizing the r_{33} component of the chromophore, the r_{13} component can also be access by modulating at 90° to the poling direction. The r_{13} component is generally 1/3 the size of r_{33} but given the difficulty of contact poling EO/SOI devices, any EO activity is acceptable. Figure 6.18 illustrates both the corona poling process and the two device configurations. Figure 6.19 shows an actual device in the horizontal configuration (vertical poling, horizontal modulation).

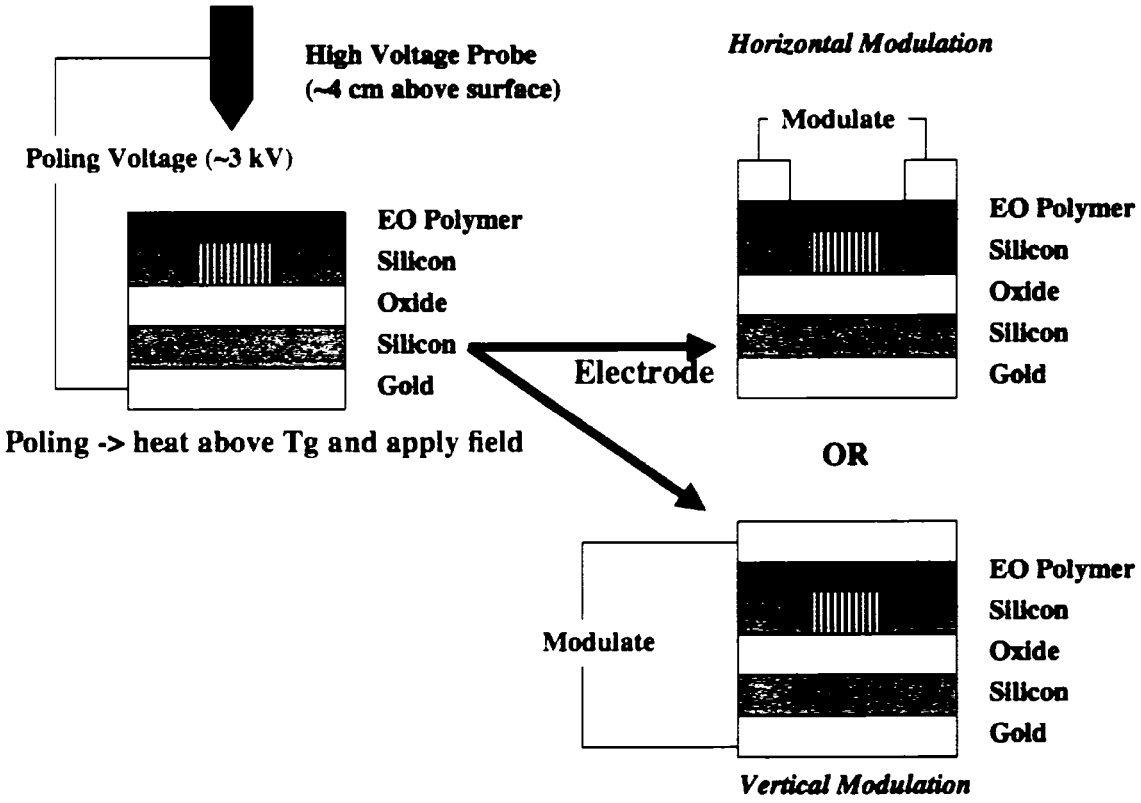

Figure 6.18: Corona poling of resonator devices.

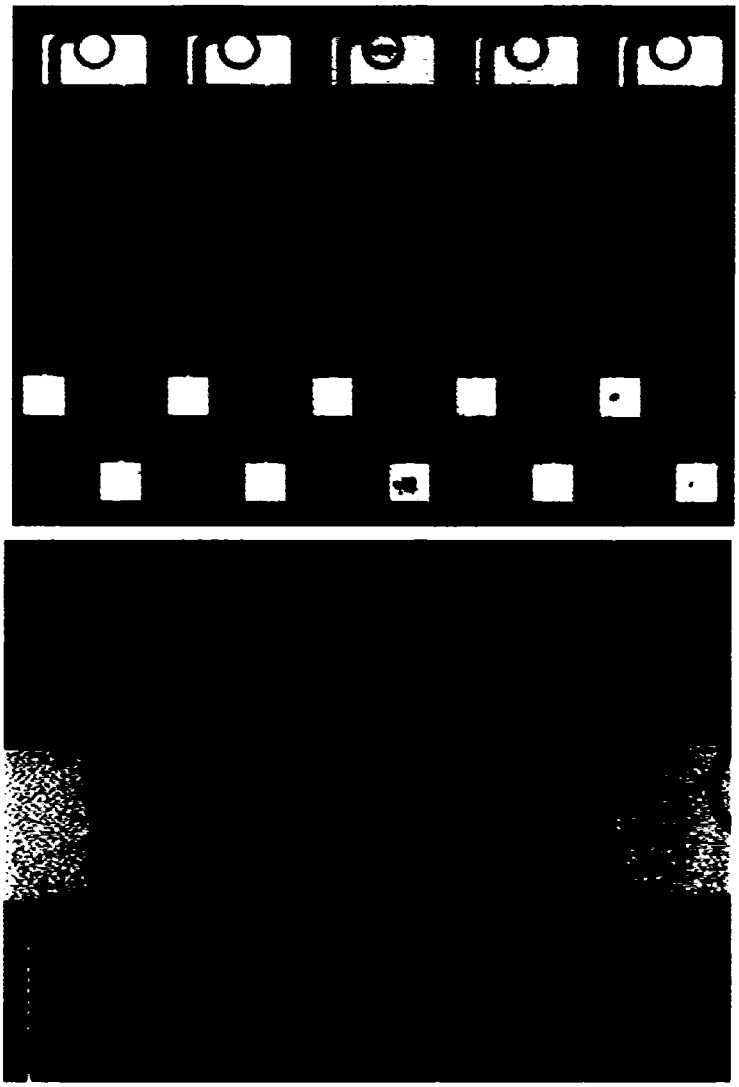

Figure 6.19: Optical micrographs of gold electroded 100 micron SOI ring resonators.

Immediate success was realized with the corona poling fabrication scheme; the resonance of an early device is shown in Figure 6.20. While the voltage to modulate remains high, this is an expected result given the inefficiency of corona poling.

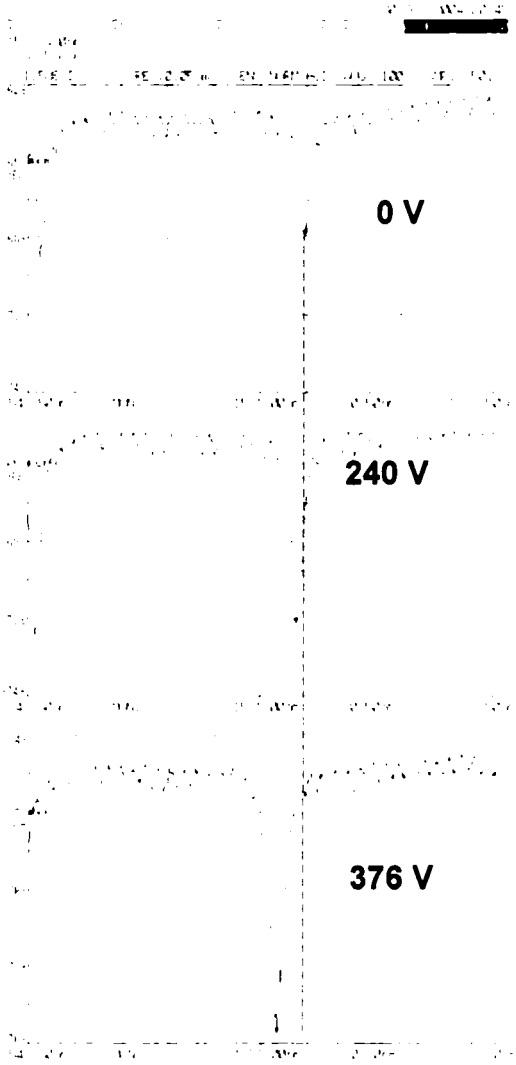

Figure 6.20: Electrical tuning of a corona poled EZ-FTC/PMMA ring resonator modulator.

An interesting illustration of the r_{33}/r_{13} relationship was demonstrated using the vertically corona poled devices. By poling in the vertical direction and then modulating in both the vertical and then horizontal, the resulting resonant shift in the horizontal, r_{13}, direction is 1/3 as large as that in the vertical, r_{33} direction. This comparison is shown in Figure 6.21.

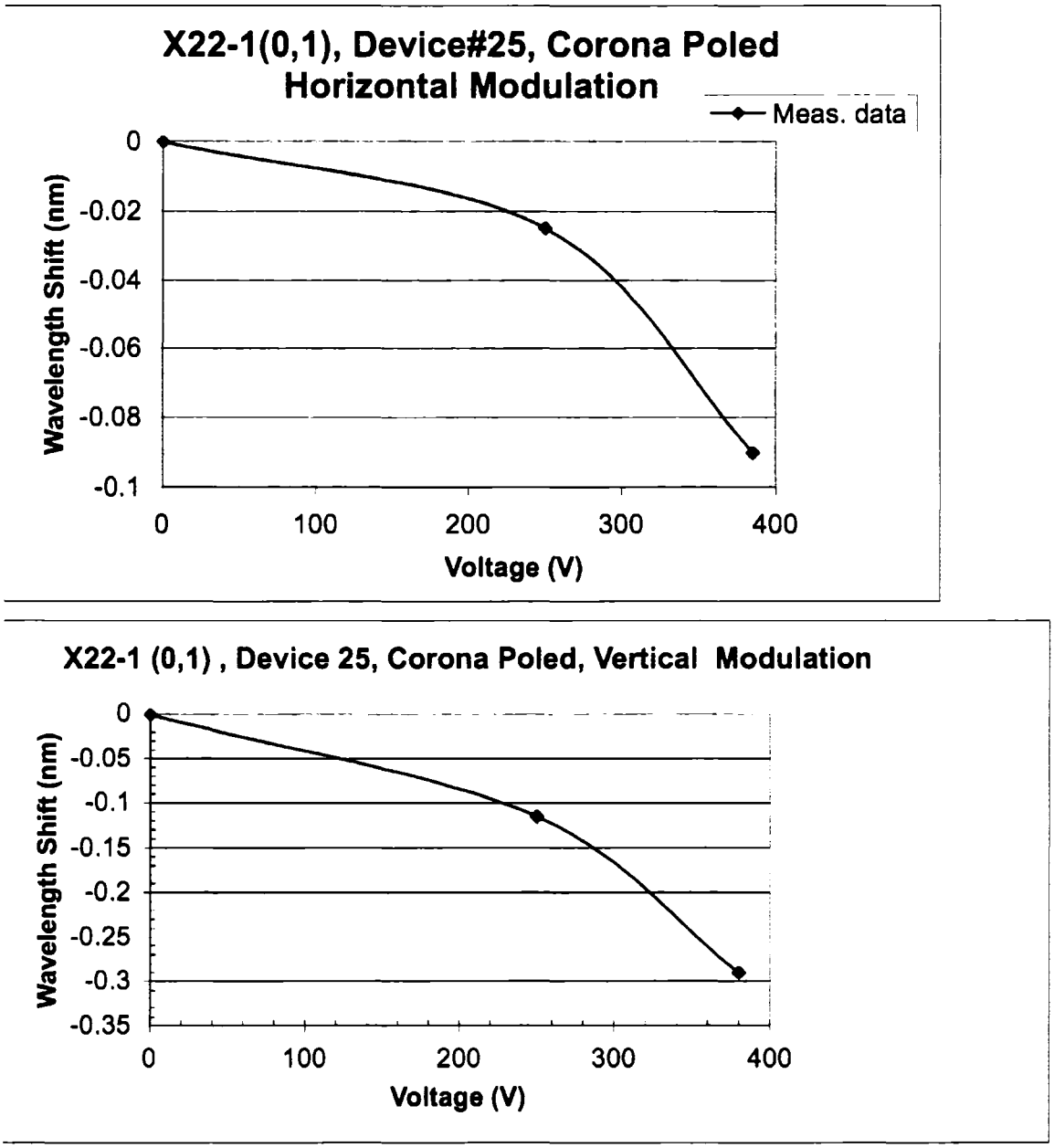

Figure 6.21: Comparison of horizontal (top) and vertical (bottom) modulation of a vertically corona poled device.

In a demonstration of a real world application of a corona poled device an EO modulator was demonstrated by driving the device with an AC voltage while monitoring the optical output. Figure 6.22 is a screen shot showing both the electrical and optical domains. In the experiment a single wavelength was input into the device and that wavelength monitored at the output. By applying a voltage the changing refractive index of the EO material also changes the wavelength of the resonant peak position. At the 0 V point there is no resonant peak in the optical output. As the voltage increases to 100 V a resonant peak moves on to the monitored wavelength. This is repeated at ~100 Hz, a slow modulator when compared to the GHz regime of commercial devices, but this is the embryonic stage of device development.

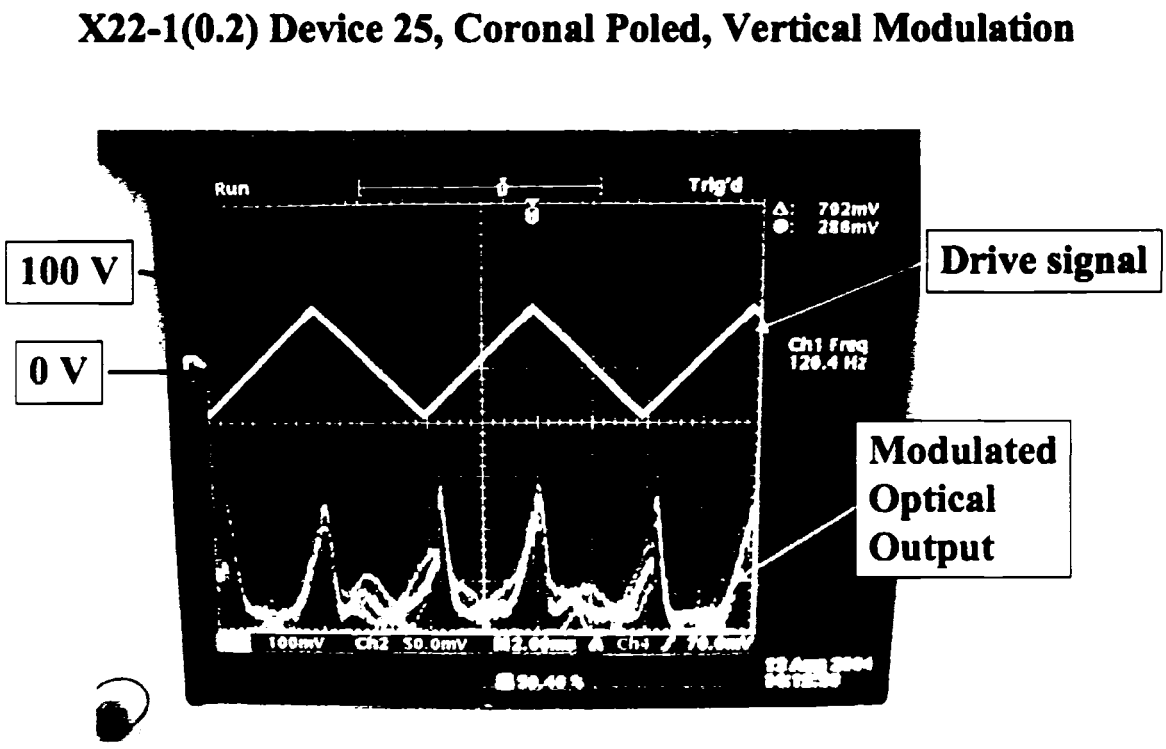

Figure 6.22: AC modulation of a ring resonator showing both drive voltage and optical output.

Section 7: Experimental Methods

The devices described here were fabricated in electronic grade silicon-on-insulator (SOI) with a top layer thickness of 110 nm and an oxide thickness of 1.3 microns. EO polymers were then spin-deposited onto the waveguide structures and subsequently poled.

Lithography was performed using a Leica EBPG 5000+ electron beam system at 100kv. Prior to lithography, the samples were manually cleaved, cleaned in acetone and isopropanol, baked for 20 minutes at 180C, coated with 2 percent HSQ resist from Dow Corning Corporation, spun for two minutes at 1000 rpm, and baked for an additional 20 minutes. The samples were exposed at 5 nm step size, at 3500 $\mu C/cm^2$. The samples were developed in AZ 300 TMAH developer for 3 minutes, and etched on an Oxford Instruments PLC Plasmalab 100 with chlorine at 80 sccm, forward power at 50 W, ICP power at 800 W, 12 mTorr pressure, and 33 seconds of etch time. The samples were then implanted with phosphorous at normal incidence, 30keV energy, and $1x10^{14}$ $ions/cm^2$ density. The sample was annealed under a vacuum at 950C in a Jipilec Jetstar rapid thermal annealer, and the samples were dipped in buffered hydrofluoric in order to remove the remnants of electron beam resist from the surface.

After initial optical testing, the samples were coated with YLD 124 electrooptic polymer, and in one case with dendrimer-based electrooptic material [14]. The samples

were stored under a vacuum at all times when they were not being tested, in order to reduce the chances of any degradation.

Section 8: Conclusion

Our goal was to integrate EO materials into ring resonator structures with the hope of creating the first generation of electrically tunable micro-resonators for electro-optic data conversion. To this end we have successfully demonstrated the first ever reported functioning, functional EO ring-resonator modulators. While these devices are not yet optimized, we have now passed the proof-of-concept phase and are continuing on towards well-characterized devices. Both contact and corona poled devices have been fabricated and AC/DC modulation of both device types demonstrated. A maximum modulator speed of 100 Hz was achieved for a first generation device operating at 100 V. Additionally an EO activity, r_{33}, of 30 pm/V was achieved for a material that produces ~50 pm/V under ideal conditions. The slow device operation, high drive voltage, and lower than expected EO activity should all be very addressable issues for future generations of devices that have optimized poling and take advantage of advanced-generation EO materials with r_{33} values of 300+ pm/V. This work represents the first ever hybrid EO/Silicon photonic devices reported, a groundbreaking development in both the field of organic EO materials and semiconductor photonic

devices. In the future the highly refined semiconductor industry will hopefully be able to seamlessly add EO functionality to VLSI devices for commercial applications.

Notes To Chapter 6

[1] Dalton, Steier, et al., *IEEE Quant. Elect.*, **2001**, 7, 826-835.

[2] Dalton, Steier, et. al., *J. of Light. Tech.*, **2002**, 20, 1968-1975.

[3] B. Maune, M. Loncar, J. Witzens, M. Hochberg, T. Baehr-Jones, D. Psaltis, A. Scherer, and Y. Qiu, Appl. Phys. Lett., **2004**, *85*, 360.

[4] Dr. Bill Steier, Ying-Hao Kuo, University of Southern California, Department of Electrical Engineering, personal communication.

[5] L.B.Loeb, Electrical Coronas, University of California, Berkeley, (1965).

Chapter 7 – Hybrid Organic-Silicon Ring Resonator Electro-optic Modulator (Slotted Ring)

Section 1: Introduction

Waveguide-based integrated optics in silicon [1] provides an ideal platform for concentrating and guiding light at the nanoscale. The high index contrast between silicon and common cladding materials enables extremely compact waveguides with very high mode field concentrations, and allows the use of established CMOS fabrication techniques to define photonic integrated circuits [2-4]. It has recently become possible, by using slotted waveguides [5], to further concentrate a large fraction of the guided mode into a gap within the center of a silicon waveguide. This geometry greatly magnifies the electric field associated with the optical mode, resulting in electric fields in excess of 10^6 V/m for continuous-wave, sub-millitwatt optical signals. Moreover, since the slotted geometry consists of two silicon strips which can be electrically isolated, a convenient mechanism for electro-optic interaction is provided. Such waveguides can be fabricated with low loss of -10dB/cm [6].

Here we exploit both the high intensity of the optical field and the close proximity of the electrodes for several purposes. First, and perhaps most significantly, we demonstrate standard Pockels' effect based modulation [11], which is enhanced by means of the very small scale of our device. The close proximity of the electrodes, and ready overlap with the optical mode, causes an external voltage to produce a far larger

effective electric modulation field, and therefore refractive index shift, than would be obtained through conventional waveguide designs [12]. We demonstrate this through the tuning of the resonance frequencies of a slot waveguide ring resonator.

Additionally, we demonstrate detection of optical signals via direct conversion to electrical energy by means of nonlinear optical rectification [7]. Our device consists of a ring resonator with an electro-optic polymer based χ^2 material deposited as a cladding [8, 9]. Inside the slot, the high optical field intensity creates a standing DC field, which creates a virtual voltage source between the two silicon electrodes, resulting in a measurable current flow, in the absence of any external electrical bias. Though optical rectification has been observed in electro-optic polymers elsewhere [10], typically instantaneous optical powers on the order of 1 kW are needed for observable conversion efficiencies, often achieved with pulsed lasers. We demonstrate measurable conversion with less than 1 mW of non-pulsed input, obtained from a standard, low power tunable laser near 1500 nm.

Section 2: Electro-optic Modulation

Utilizing the experience gained in monolithic ring devices from the previous chapter and taking advantage of technological breakthroughs in the development of passive SOI resonator devices have realized a new generation of EO modulator devices. In many ways this project represents the culmination of this dissertation. The proof that

silicon can be used as an electrode for both poling and driving EO devices (Chapter 2) was important in giving us the confidence to invest a massive amount of time and energy in designing slotted ring resonators that were electrically active. Similarly, the research of monolithic ring resonator devices (Chapter 6) gave us the confidence and experience needed to design and test these next generation devices.

Figure 7.1 details the complete geometry of the resonators used in this work, including a cross section of the slotted waveguide. In Figure 7.1(A), the optical mode was solved using a finite-difference based Hermetian Eigensolver [15], and has an effective index of approximately 1.85 at 1500nm. Most of the electric field is parallel to the plane of the chip, and it is possible to contact both sides of the slot in a slotted ring resonator, as shown in Figure 7.1(B). Electrically isolated contacts between the silicon rails defining the slotted waveguide introduce only about 0.1 dB of optical loss. Figure 7.1(C) details the layout of a complete slotted ring resonator, with two contact pads connected to the outer half of the ring, and two pads electrically connected to the inner half of the ring. A shunt resistor provides a means of confirming electrical contact, and typical pad-to-pad and pad-to-ring resistances range from 1MΩ to 5 MΩ. Figure 7.1(D) displays a typical electrically contacted slotted ring described in this study.

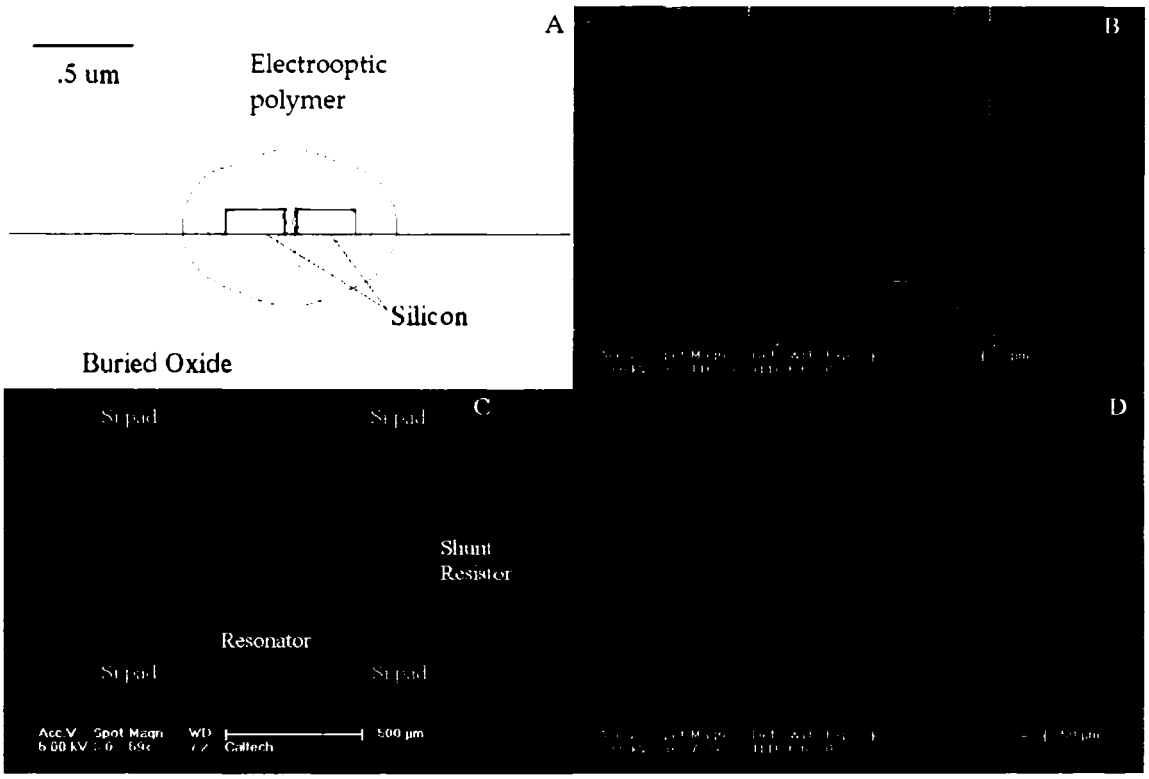

Figure 7.1: . Panel A shows a cross section of the geometry with optical mode superimposed on a waveguide. Panel B shows a SEM image of the resonator electrical contacts. Panel C shows the logical layout of device, superimposed on a SEM image. Panel D is an image of the ring and the electrical contact structures.

These devices offer a tremendous advantage over any other EO modulator technology. Given the extremely small poling gap (~100 nm) a device poled at 100 V/μm will only require 10 V to pole and under 1 V to modulate. The most power-efficient EO polymer modulator reported to date operated at 0.8 V but this was a very processing-intensive push-pull Mach-Zehender modulator. There is additional promise

in the ease of manufacture. While the nanostructured SOI resonators require advanced ebeam or (current generation) photolithography capable of defining features in the 100 nm range, once these structures are fabricated a device is completed by simply coating the EO polymer on top of the structure. This is extremely simple when compared to traditional EO device fabrication[1] or even the devices detailed in Chapter 6.

A typical split ring resonator scan is shown in Figure 7.2. The performance of these devices are almost indistinguishable from monolithic rings and the Q factor can be either intentionally spoiled or pushed into the 100,000's with accurate fabrication.

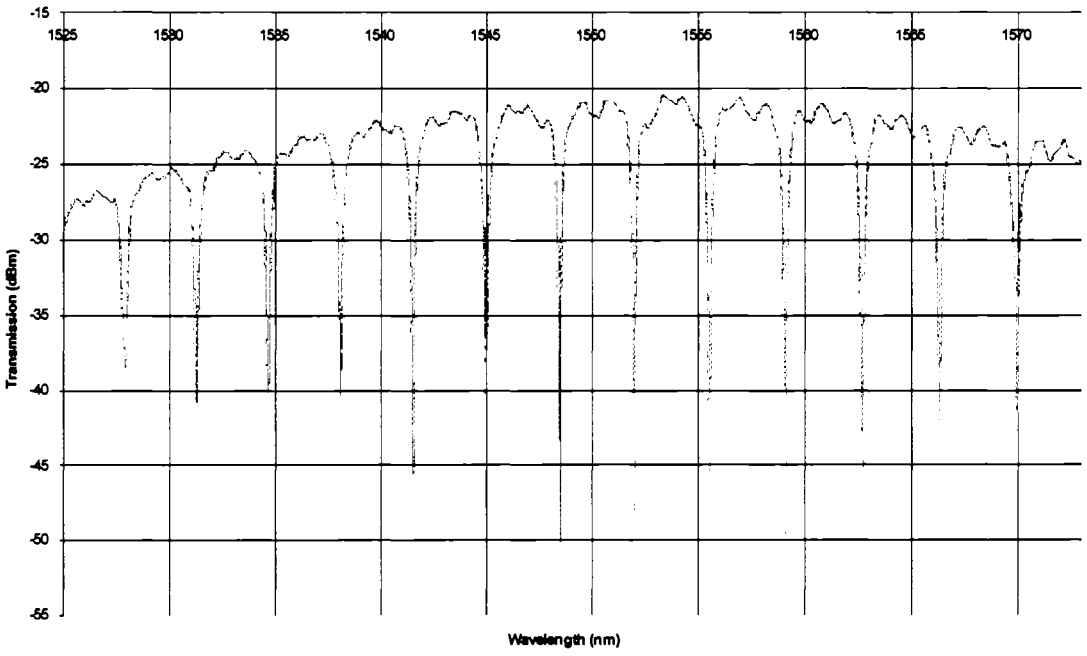

Figure 7.2: Passive resonance of a split ring resnator.

At DC, the Pockels effect was measured by applying varying voltages to the device and observing the device transmission as a function of wavelength. For devices with working modulation, the resonance peaks were shifted, often to a noticeable degree.

At AC, a square wave input voltage was put across the device. The input wavelength was tuned until the output signal had the maximum extinction. It was determined what power levels were implied by the output voltage, and then the observed power levels were fit to a wavelength sweep of the resonance peak. This readily allowed the tuning range to be calculated. We successfully measured AC tuning up to the low MHz regime; the limitation at this speed was noise in our electrical driving signal path, not, as far as we can tell, any roll-off in the modulation process itself. In Figure 7.3, a result at approximately 6 MHz for the use of these structures as electro-optic modulators is shown.

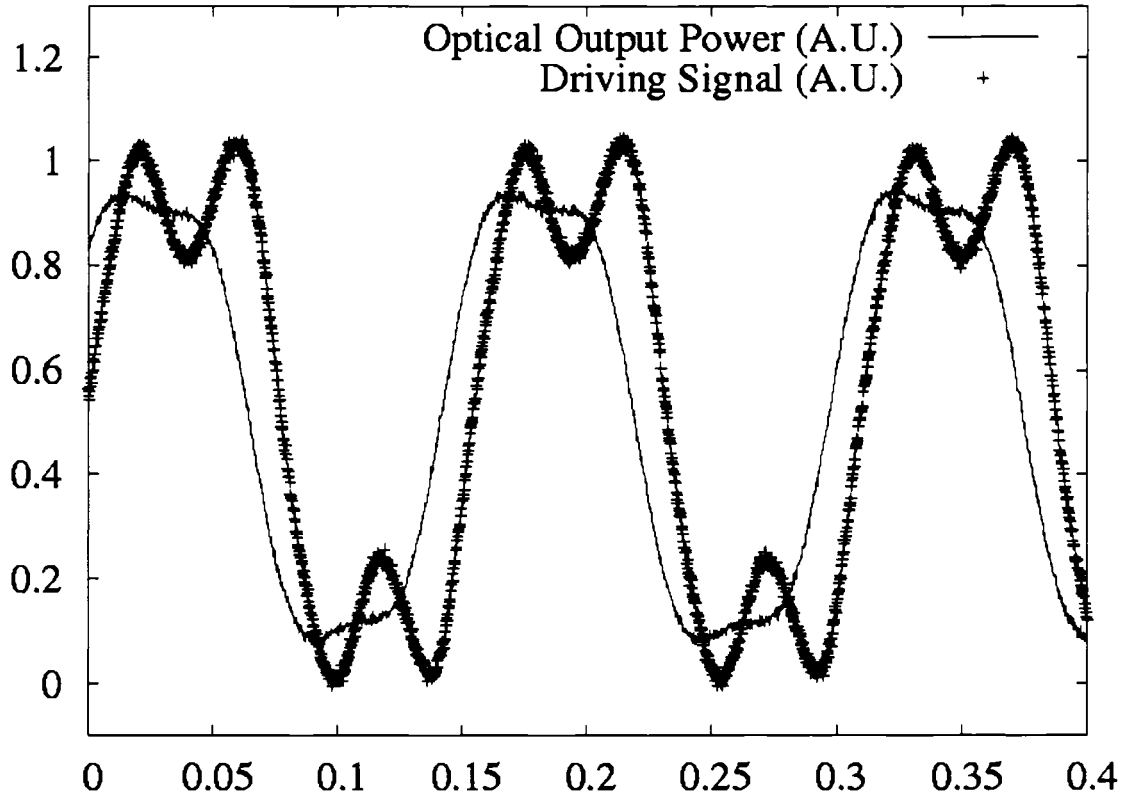

Figure 7.3: Bit pattern generated by Pockels' Effect modulation 5 dB. The vertical axis represents input voltage and output power, both in arbitrary units. Horizontal axis is time in microseconds. Voltage swing on the input signal is 20 volts..

These experiments clearly demonstrate that low-voltage electro-optic tuning and modulation can be achieved in split waveguide geometries. It should be emphasized that these devices are not optimized as modulators. By increasing the Q of the resonators to exceed 20,000, which has been demonstrated elsewhere [6], it will be possible to achieve much larger extinction values per applied voltage.

By utilizing new dendrimer-based electro-optic materials [14], we have achieved .042±.008 nm/V, or 5.2±1 GHz/V for these rings. This implies an r_{33} of 79±15 pm/V. This result is better than those obtained [12] for rings of 750 micron radius, which we believe to be the best tuning figure published to date. By contrast, our rings have radii of 40 microns. We credit our improvement over the previous results mainly to the field enhancement properties of the split waveguide geometry.

Further device performance can be seen in DC measurements shown in Figure 7.4.

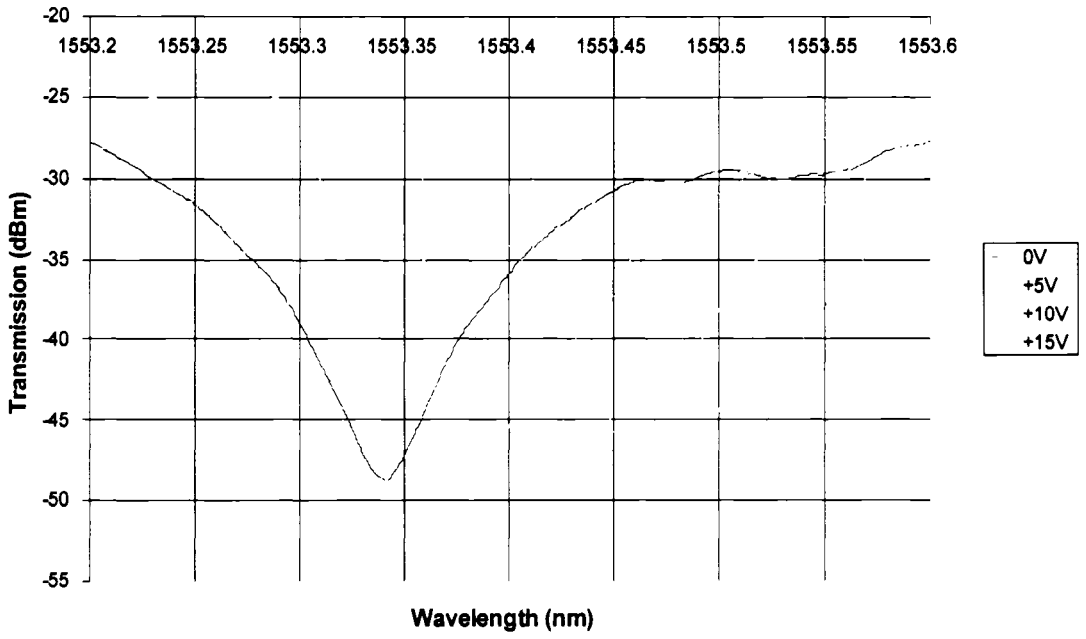

Figure 7.4: DC shifting of an improved split ring resonator device.

Section 3: Optical Rectification

Given the success of the split waveguide EO modulator devices, an attempt was made to run the experiment in reverse in order to create current from an optical signal. This would provide a route to a nanoscale photodetector that could become a vital element of future photonic integrated circuits by adding an on-chip detector.

Conceptually the experiment was simply the exact reverse of the modulator device: a modulated optical signal was passed through the resonator device and the current across the electrodes was measured. Testing was performed with single-mode polarization maintaining input and output fibers, grating coupled [16] to slotted waveguides with an insertion loss of approximately 8 dB. Optical signal was provided from an Agilent 81680a tunable laser and in some cases an erbium doped fiber amplifier from Keopsys Corporation. A continuous optical signal inserted into a poled polymer ring results in a measurable current established between the two pads, which are electrically connected through a pico-Ammeter. In the most sensitive device, a DC current of ~1.3 nA was observed, indicating an electrical output power of $\sim 10^{-9}$ of the optical input power (5×10^{-12} W of output for approximately .5 mW coupled into the chip). Control devices, in which PMMA or un-poled EO material was substituted, show no photocurrent.

The fact that there is no external bias applied to this system or indeed any energy source, other than the optical signal, demonstrates conclusively that power is

being converted from the optical signal. To establish that the conversion mechanism is actually optical rectification, we performed a number of additional experiments. First, we applied a steady bias on the chip for several minutes, as shown in Table 1A, and observed a substantial change in the photoresponse of the device. This change depends on the polarity of the bias voltage, consistent with the expected influence of repoling of the device in-place at room temperature. Specifically, if the external bias was applied opposing the original poling direction, conversion efficiency generally decreased, while an external bias in the direction of the original poling field increased conversion efficiency.

Table 7.1: Part A shows the dependence of the steady state observed current after room temperature biasing with various voltage polarities for one devices. The device was originally polled with a –12 V bias, at 110 C. With one exception, applying a voltage in the direction of the original polling voltage enhances current conversion efficiencies, while applying a voltage against the direction of the polling voltage reduces the current conversion efficiencies. It should be noted that the power coupled on-chip in these experiments was less than 1 mW due to coupler loss. Part B shows the behavior of several different devices immediately after thermal polling or cycling without voltage. Measurements were taken sequentially from top to bottom for a given device. The only anomaly is the third measurement on device 2; this was after significant testing, and the current observed was substantially less than was observed in previous tests on the same device. We suspect that the polymer was degraded by repeated testing in this case.

Part A:

Action	New Steady State Current (6 dBm input)
Initial State	-5.7 pA
+10V for 2 minutes	0 pA
-10V for 2 minutes	-7.1 pA
+10V for 2 minutes	-4.4 pA
+10V for 4 minutes	-6.1 pA
+10 V for 4 minutes	-4.5 pA
-10 V for 2 minutes	-14.8 pA

Table 7.1 (Cont.) - Part B:

Device	Action	Current Polarity of Optical Rectification
1	Positive Poling	Positive
1	Thermal Cycling to poling temperature with no voltage	Rapid fluctuation, did not settle
1	Negative Poling	Negative
2	Negative Poling	Negative
2	Thermal Cycling to Poling temperature with no voltage	None observable
2	Positive Poling	Negative
3	Negative Poling	Negative
4	Positive Poling	Positive
5	Negative Poling	Negative

To further understand the photo-conversion mechanism, 5 EO detection devices were poled with both positive and negative polarities, thus reversing the direction of the

relative χ^2 tensors. For these materials, the direction χ^2 is known to align with the polling E field direction [12] [18], and we have verified this through Pockels' effect measurements. In all but one case, we observe that the polarity of the generated potential is the same as that used in poling, and the +V terminal during poling acts as the –V terminal in spontaneous current generation, as shown in Table 1B. Furthermore, the polarity of the current is consistent with a virtual voltage source induced through optical rectification. It should be noted that these devices decay significantly over the course of testing, and that in one case the polarity of the output current was even observed to spontaneously switch after extensive testing. However, their initial behavior after polling seems largely correlated to the χ^2 direction.

A number of experiments were performed to produce negative results, and to exclude the possibility of a mistaken measurement of photocurrent. The power input to the chip was turned on and off by simply moving the fiber array away from the chip mechanically, without changing the circuit electrically, and the expected change in the electrical output signal of our detector was observed. A chip was coated in polymethylmethacrylate and tested, resulting in no observed photocurrents. Also, we tested some of the devices shown in Table 1 before any polling had been performed; no current was observed.

To establish a quantitative relationship between the laser power in the EO material and the photo-current, we used a lock-in amplifier, and achieved a noise floor of about 0.2 pA. This resulted in a reasonable dynamic range for the 10-200 pA

photocurrent readings. Figure 7.5(A) and (B) show optical transmission curves for typical devices. Figure 7.5(C) shows several traces of output current versus input laser power, and a fairly linear relationship is observed. The relationship $I = cP$, where I is the output current, P is the input laser power, and c is a proportionality constant ranging from 88 +/- 10 pA/mW at a 1 kHz lock-in measurement and when the wavelength is on resonance, changing to a lower value of 58+/-8 pA/mW off resonance for our best device. It is important to note that current was easily observed with only a pico-ammeter, or by simply connecting an oscilloscope to the output terminal and observing the voltage deflection.

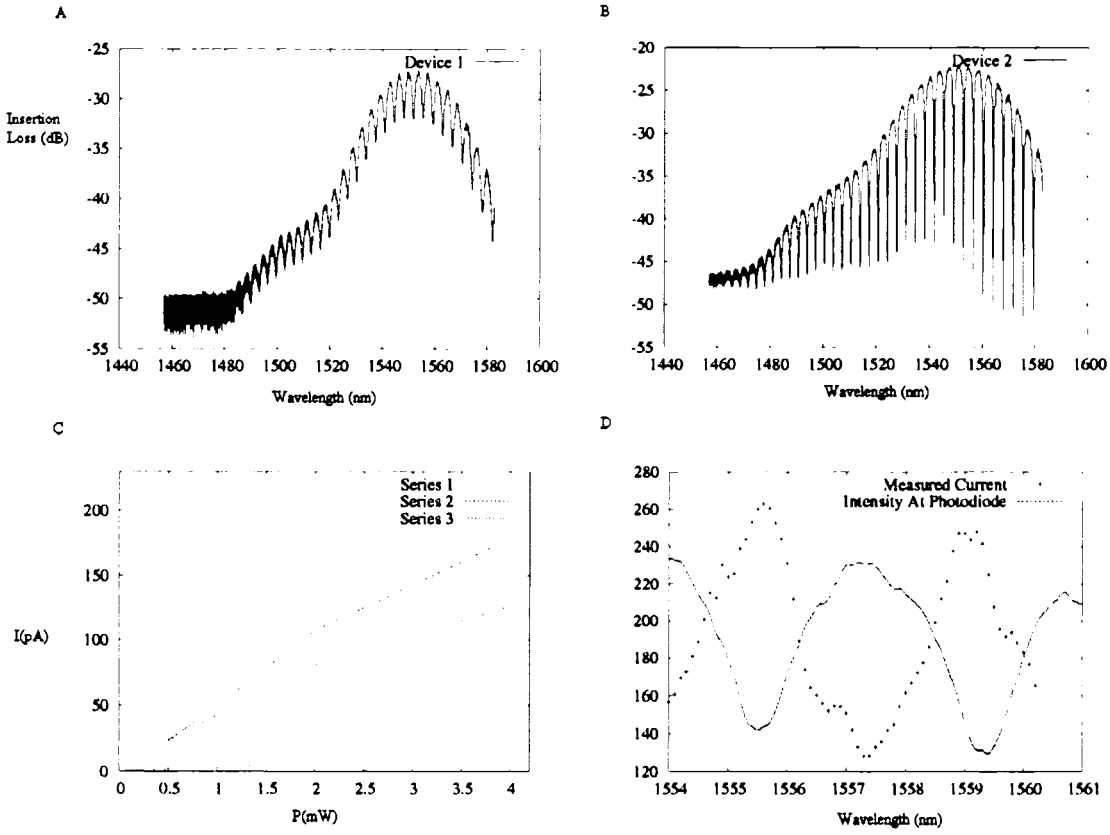

Figure 7.5: Panel A shows the transmission spectrum of detector device 1, whereas B shows detector device 2. Panel C shows several curves of current vs. power for three measurement series. Series 1 is of the first device with the wavelength at1549.26 nm, on a resonance peak. Series 2 is the first device with the wavelength at 1550.5 nm off resonance. Series 3 is for device 2, with the wavelength at 1551.3, on resonance. Finally, panel D shows the output current as a function of wavelength, overlaid with the transmission spectrum. The transmission spectrum has been arbitrarily rescaled to show the contrast.

As another demonstration of the dependence of the output current on the amount of light coupled into the resonator, we also tuned the laser frequency and measured the output current. As can be seen in Figure 7.5(D), the amount of output current increases

as the laser is tuned onto a resonance peak. This again indicates that the overlap between the EO polymer in the resonator and the optical mode is responsible for the photo-current. We have overlaid a photocurrent vs. wavelength response scan to show the resonance peaks for comparison. It should not be surprising that a small photocurrent is still measured when the laser is off resonance, since the amount of radiation in a low-Q ring resonator is non-negligible even off resonance. It is also worth noting that we have successfully observed this detector function at speeds up to 1 MHz, without significant observable roll-off. This is again consistent with optical rectification. Unfortunately, our devices could not be measured at higher speeds, due to substantial output impedance.

The conversion efficiency from our first experiments is certainly several orders of magnitude below the ultimate limit, and can be explained by the high insertion losses in our system; 75% of the input power in the fiber is not coupled onto the chip and our low-Q resonators only provide a limited path length within which light can interact with the electro-optic material. Furthermore, by design, a great deal of the light in the resonator will be dumped to an output port, and not absorbed. It is expected that with further design and higher-Q resonators, the efficiency of these devices can be greatly increased. It is, however, important to note that nothing about this effect depends on the presence of rings. The rings provide a convenient and compact device for observing these effects, but one could just as easily observe optical rectification by using a long, polymer coated, split waveguide, with each side connected to an electrical pad.

To derive the magnitude of the expected photocurrent, we assume that the χ^2 magnitude relating to the Pockels' effect is similar to that for optical rectification. A measurement of χ^2 can then be obtained from the direct observation of the electro-optic coefficient by the standard measurements described earlier. The typical measured tuning value of 2GHz/V yields approximately 50 pm/V.

In the best case, devices with 6 dBm of input power returned approximately 1.4 nA of current. With Qs ranging from 3k to 5k, and assuming approximately 7 dB of insertion loss in the input grating coupler on one of our chips, in the best case as much as 0 dBm might be circulating in a resonator on resonance. This implies a peak electric field due to the optical signal of approximately 3.1×10^6 V/m. The induced static nonlinear polarization field is then nearly 1000 V/m, which amounts to a voltage drop of 14×10^{-5} V across a 140 nm gap. If this voltage is assumed to be perfectly maintained, and the load resistance is assumed to be 5 MΩ, then 28 pA would be generated, about a factor of 100 less than is observed in the largest measurement made, but within a factor of 20 of the typical measurement of 352 pA for 6 dBm of input. Significantly, because the generated current is quadratic in E, it is clear that the current will be linearly proportional to the input intensity. This is in accordance with our observations. The best results for optical rectification were obtained with YLD/APC polymer, wheras our best Pockels' Effect results were obtained with the dendrimer materials.

Significantly, the sign of the output current matches that which would be predicted by nonlinear optical rectification. Specifically, since positive current emanates

from the positive terminal, the rectified E field has a sign reversed from the χ^2 and the polling E field. It should be noted that it is a well established fact with these materials that the χ^2 direction tends to align with the direction of the polling E field. Because of this, the rectified field acting as a voltage source will produce an effective positive terminal at the terminal that had the positive polling voltage.

We do not yet fully understand the current generation mechanism. In particular, it is not clear what provides the mechanism for charge transport across the gap. The APC material in which the nonlinear polymer is hosted is insulating, and though it does exhibit the photoconductivity effect due to visible light, it is unclear whether it can for near-infrared radiation. Photoconductivity due to second harmonic generation may play a role in this effect. It is certainly the case, however, that current flows through this gap; that is the only region in the entire system where an electromotive force exists. Also, photoconductivity alone is not adequate to explain the reversal of the current coming off of the detector devices when the poling direction is reversed, nor the conversion of the optical input into directed current in general. The only mechanism to our knowledge that adequately explains this data is optical rectification.

If we assume that it will be possible to achieve a 10x improvement in the Q's of the resonators, while still getting more than 10 dB of extinction, then the intensity circulating in such a ring would be about 13 dB up from the intensity of the input wave. By comparison, with a Q of about 1000 and high extinction, the peak circulating intensity is about the same as the intensity in the input waveguide. So it's reasonable to

expect that it will be possible to get at least 10 dB of improvement in the circulating intensity, and thus in the conversion efficiency, by fabricating higher Q rings.

Because the optical losses of the polymer and dendrimer materials could turn out to be a limiting factor for the performance of higher-Q devices, a thorough study of the optical losses of these materials is needed. Because the devices used herein were deliberately designed to have low Q's, they are not the ideal system for examining such losses. It is possible to say that an upper bound of about 10dB/cm of loss is reasonable, based on our observations that the Q's of the resonators did not change dramatically after being coated with the organic materials. However, further work is clearly required to determine whether the optical loss in these materials will prove to be a limiting factor in device performance.

Section 4: Experimental Methods

The devices described in this paper were fabricated in electronic grade silicon-on-insulator (SOI) [13] with a top layer thickness of 110 nm and an oxide thickness of 1.3 microns. The silicon layer is subsequently doped to approximately 10^{19} Phosphorous atoms/cm^3, yielding resistivities after dopant activation of ~0.025 ohm-cm. EO polymers were then spin-deposited onto the waveguide structures and subsequently poled by using a high field applied across the slot in the waveguide

Lithography was performed using a Leica EBPG 5000+ electron beam system at 100kv. Prior to lithography, the samples were manually cleaved, cleaned in acetone and isopropanol, baked for 20 minutes at 180C, coated with 2 percent HSQ resist from Dow Corning Corporation, spun for two minutes at 1000 rpm, and baked for an additional 20 minutes. The samples were exposed at 5 nm step size, at 3500 $\mu C/cm^2$. The samples were developed in AZ 300 TMAH developer for 3 minutes, and etched on an Oxford Instruments PLC Plasmalab 100 with chlorine at 80 sccm, forward power at 50 W, ICP power at 800 W, 12 mTorr pressure, and 33 seconds of etch time. The samples were then implanted with phosphorous at normal incidence, 30keV energy, and $1x10^{14}$ $ions/cm^2$ density. The sample was annealed under a vacuum at 950C in a Jipilec Jetstar rapid thermal annealer, and the samples were dipped in buffered hydrofluoric in order to remove the remnants of electron beam resist from the surface.

After initial optical testing, the samples were coated with YLD 124 electrooptic polymer, and in one case with dendrimer-based electrooptic material [14]. The samples were stored under a vacuum at all times when they were not being tested, in order to reduce the chances of any degradation.

Section 5: Conclusion

Through the use of nano-scale slotted waveguide geometry we have obtained massive enhancement of the optical field, a characteristic exploited in two types of devices that may become the building blocks of photonic integrated circuits.

Electro-optic modulators based on slotted waveguide ring resonators have produced the best figures of merit in the field to date, demonstrating modulation with less voltage, greater electro-optic effect, and in a more compact structure than those previously reported. Additionally, the SOI-based devices are significantly easier to fabricate than traditional, polymer-stack EO resonators, requiring only simple spin-coating of EO material over the resonator structure compared to the very complex multiple polymer layer, multiple photolithographic step process.

The slotted waveguide geometry has in turn enabled us to exploit nonlinear optical processes for optical rectification in the sub-mW regime that are typically only available in the kW regime. This difference is so considerable that we believe it represents a change in kind for the function of nonlinear optical devices; it may be possible to someday construct a practical, low-power detector based on nonlinear optical rectification. In addition, we expect this hybrid material system to provide a means for creating compact devices that exploit other nonlinear phenomena on-chip.

Optical rectification based detectors might have many advantages over currently available technology. In particular, such detectors would probably be able to function at a higher intrinsic rate than the typical photodiode in use, as the optical rectification process occurs at the optical frequency itself, on the order of 100 THz in WDM systems. The absence of an external bias, and the generation of a voltage rather than a change in current flow, might also prove easier to handle electronically. We also do not believe that a device based on nonlinear optical rectification would suffer from the limitation of a dark current. This in turn might mean that current WDM systems could function with lower optical power, providing numerous benefits.

We conclude by stressing the economic aspects of our development. Because our devices can be fabricated in planar, electronics grade silicon-on-Insulator, using processes compatible with advanced CMOS processing, it is likely the devices based on these principles could be built cheaply. It is our hope that electrically active slotted waveguides can someday become a platform of choice for practical linear and nonlinear integrated optics.

Notes To Chapter 7

1. R. A. Soref, J. P. Lorenzo, "All-Silicon Active and Passive Guided-Wave Components For Lambda=1.3 and 1.6 MU-M," IEEE J. Quantum Elect. **22**, 873-879 (1986).

2. A.S. Liu, R. Jones, L. Liao, D. Samara-Rubio, D. Rubin, O. Cohen, R. Nicolaescu, M. Paniccia, "A high-speed silicon optical modulator based on a metal-oxide-semiconductor capacitor," Nature **427**, 615-618 (2004)

3. A. Scherer, O. Painter, J. Vuckovic, M. Loncar, T. Yoshie, "Photonic crystals for confining, guiding and emitting light," IEEE T. Nanotechnol. **1**, 4-11 (2002).

4. A. Layadi, A. Vonsovici, R. Orobtchouk, D. Pascal, A. Koster, "Low-loss optical waveguide on standard SOI/SIMOX substrate," Opt. Commun **146**, 31-33 (1998).

5. Q. F. Xu, V. R. Almeida, R. R. Panepucci, M. Lipson, "Guiding and Confining Light in Void Nanostructures," Opt. Lett. **29**, 1206-1211 (2004).

6. T. Baehr-Jones, M. Hochberg, C. Walker, A. Scherer, "High-Q optical resonators in silicon-on-insulator-based slot waveguides," Appl. Phys. Lett. **86**, 081101 (2005).

7. M. Bass, P. A. Franken, J. F. Ward, G. Weinreich, "Optical Rectification," Phys. Rev. Lett. 9, 446 (1962).

8. L. R. Dalton, "Organic electro-optic materials," Pure Appl, Chem. **76**, 1421-1433 (2004).

9. Y. Y. Huang, G. T. Paloczi, A. Yariv, C. Zhang, L. R. Dalton, "Fabrication and replication of polymer integrated optical devices using electron-beam lithography and soft lithography," J. Phys. Chem. B. **108**, 8606-8613 (2004).

10. A. Nahata, D. H. Auston, C. J. Wu, J. T. Yardley, "Generation of Terahertz Radiation From a Poled polymer," Appl. Phys. Lett., **67**, 1358-1360 (1995).

11. F. Pockels, Lehrbuch der Kristalloptik (B. G. Teubner, Leipzig and Berlin, 1906).

12. C. Zhang, L. R. Dalton, M. C. Oh, H. Zhang, W. H. Steier, " Low V-pi electrooptic modulators from CLD-1: Chromophore design and synthesis, material processing, and characterization," Chem. Mater. **13**, 3043-3050 (2001).

13. Silicon Genesis Corporation, 61 Daggett Drive, San Jose, CA 95134.

14. Dendrimer Material results are currently in preparation

15. A. Taflove, Computational Electrodynamics, (Artech House, Boston, MA, 1995).

16. D. Taillaert, P. Bienstman, R. Baets, "Compact efficient broadband grating coupler for silicon-on-insulator waveguides," Opt. Lett. **29**, 2749-2751 (2004).

17. R. Boyd, Nonlinear Optics, Second Edition (Academic Press, New York, 2003).

18. S. Graf, H. Sigg, W. Bachtold, "High-frequency electrical pulse generation using optical rectification in bulk GaAs," Appl. Phys. Lett. 76, 2647-2649 (2000).

List of References

Albert, I. D. L.; Marks, T. J.; Ratner, M. A. *J. Am. Chem. Soc.* **1997**, 119, 6575-6582.

Baehr-Jones T, Hochberg M, Walker C, Scherer A, *Applied Physics Letters.* **2004,** *85*, 3346.

Baehr-Jones, T., M. Hochberg, C. Walker, A. Scherer, "High-Q optical resonators in silicon-on-insulator-based slot waveguides," Appl. Phys. Lett. **86**, 081101 (2005).

Bass, M., P. A. Franken, J. F. Ward, G. Weinreich, "Optical Rectification," Phys. Rev. Lett. 9, 446 (1962).

Behl, M., J. Seekamp, SS. Zankovych, C. M. S. Torres, R. Zentel, J. Ahopelto, *Adv. Mater.* **2002**, *14*, 588.

Breitung, E. M.; Shu, C. –F.; McMahon, R. J. *J. Am. Chem. Soc.* **2000**, 122, 1154-1160.

Boyd, R., Nonlinear Optics, Second Edition (Academic Press, New York, 2003).

Cedeno, C.C.; Seekamp, J.; Kam, A.P.; Hoffmann, T.; Zankovych, S.; Sotomayor Torres, C.M.; Menozzi, C.; Cavallini, M.; Murgia, M.; Ruani, G.; Biscarini, F.; Behl, M.; Zentel, R.; Ahopelto, J. *Miroelectronic Eng.* **2002**, *61*, 25.

Chen, X., M. A. Dam, K. Ono, A. Mal, H. Shen, S. R. Nutt, K. Sheran, F. Wudl, *Science* **2002**, *295*, 1698.

Chin, M. K., C. Youtsey, W. Zhao, T. Pierson, Z. Ren, S. L. Wu, L. Wang, Y. G. Zhao, and S. T. Ho, IEEE Photon. Technol. Lett. **11**, 1620 (1999).

Chou, S. Y., P. R. Krauss, P. J. Renstrom, *J. Vac. Sci. Technol. B* **1996**, *14*, 4129.

Chou, S. Y.; Krauss, P.; Renstrom, P. J. *Science* **1996**, *272*, 85.

Chu, S. T., B. E. Little, W. Pan, T. Kaneko, S. Sato, and Y. Kokubun, IEEE Photon. Technol. Lett. **11**, 691 (1999).

Colburn, M., S. Johnson, M. Stewart, S. Damle, T. Bailey, B. Choi, M. Wedlake, T. Michaelson, S. V. Sreenivasan, J. Ekerdt, C. G. Wilson, *Proc. SPIE*, Vol. 3676, **1999**, 379.

Collings, P. J., *Liquid Crystals: Nature's Delicate Phase of Matter*, 2nd ed. (Princeton University Press, Princeton, 2002), Chap. 3, pp. 33-34.

Dalton, L. R., "Organic electro-optic materials," Pure Appl, Chem. **76**, 1421-1433 (2004).

Dalton, Steier, et al., *IEEE Quant. Elect.*, **2001**, 7, 826-835.

Dalton, L. R., in *Advances in Polymer Science*, Vol. 158, Springer-Verlag, Berlin **2002**.

Dalton, L.R., A. Harper, A. Ren, F. Wang, G. Todorova, J. Chen, C. Zhang, and M. Lee, "Polymeric electro-optic modulators: from chromophore design to integration with semiconductor very large scale integration electronics and silica fiber optics," *Ind. Eng. Chem. Res., 38*, pp. 8-32, 1999

Graf, S., H. Sigg, W. Bachtold, "High-frequency electrical pulse generation using optical rectification in bulk GaAs," Appl. Phys. Lett. 76, 2647-2649 (2000).

Grote, J., J. Zetts, R. Nelson, F. Hopkins, L. Dalton, C. Zhang, W. Steier, "Effect of conductivity and dielectric constant on the modulation voltage for optoelectronic devices based on nonlinear optical polymers," *Optical Engineering, 40(11),* pp. 2464-2473, 2001

Haller, M.A., Doctoral Dissertation, Materials Science and Engineering, University of Washington 2005.

Haller, M., J. Luo, H. Li, T.-D. Kim, Y. Liao, B. H. Robinson, L. R. Dalton, A. K.-Y. Jen, *Maromolecules* **2004**, *37*, 688.

He, M. Q.; Leslie, T. M.; Sinicropi, J. A. *Chem. Mater.* **2002**, 14, 4662-4668

Heimala, P., P. Katila, J. Aarnio, and A Heinamaki, J. Lightwave Technol. **14**, 2260 (1996).

Huang, Y. Y., G. T. Paloczi, A. Yariv, C. Zhang, L. R. Dalton, "Fabrication and replication of polymer integrated optical devices using electron-beam lithography and soft lithography," J. Phys. Chem. B. **108**, 8606-8613 (2004).

Keinan, S.; Zhu, P.; Ratner, M.A.; Marks, T.J. Self-Assembled Electro-Optic Superlattices, *Chem. Mater.*, **2004**, *16*, 1848-1854.

Khang, D.-Y., H. Yoon, H. H. Lee, *Adv. Mater.* **2001**, *13*, 749.

Kuo, Y.-H.; Steier, W.H.; Dubovitsky, S.; Jalali, B. *Photon. Tech. Lett.*, 2003, *15*, 813.

Layadi, A. Vonsovici, R. Orobtchouk, D. Pascal, A. Koster, "Low-loss optical waveguide on standard SOI/SIMOX substrate," Opt. Commun **146**, 31-33 (1998).

Loeb, L.B., Electrical Coronas, University of California, Berkeley, (1965).

Little, B.E., S. T. Chu, H. A. Haus, J. Foresi, and J.–P. Laine, J. Lightwave Technol. 15, 998 (1997).

Liu, R. Jones, L. Liao, D. Samara-Rubio, D. Rubin, O. Cohen, R. Nicolaescu, M. Paniccia, Nature, 2004, 427, 615.

Liu, S., M. A. Haller, H. Ma, L. R. Dalton, S.-H. Jang, A. K.-Y. Jen, *Adv. Mater.* **2003**, *15*, 603.

Luo, J., S. Liu, M. A. Haller, J.-W. Kang, T.-D. Kim, S.-H. Jang, B. Chen, N. Tucker, H. Li, H.-Z. Tang, L. R. Dalton, Y. Liao, B. H. Robinson, A. K.-Y. Jen, *Proc. SPIE* Vol. 5351 **2004** 36.

Luo, J., M. Haller, H. Li, T.-D. Kim, A. K.-Y. Jen, *Adv. Mater.* **2003**, *15*, 1635.

Nahata, D. H. Auston, C. J. Wu, J. T. Yardley, "Generation of Terahertz Radiation From a Poled polymer," Appl. Phys. Lett., **67**, 1358-1360 (1995).

Oda, K., N. Takato, and H. Toba, J. Lightwave Technol. **9**, 728 (1991).

Paloczi, G. T.; Huang, Y.; Yariv, A.; Luo, J.; Jen, A. *Appl. Phys. Lett.* **2004**, *85*, 1662.

Pockels, F., Lehrbuch der Kristalloptik (B. G. Teubner, Leipzig and Berlin, 1906).

Rafizadeh, J. P. Hagness, A. Taflove, K. A. Stair, and S. T. Ho, Opt. Lett. **22**, 1244 (1997).

Rafizadeh, J. P. Zhang, R. C. Tiberio, and S. T. Ho, J. Lightwave Technol. **16**, 1308 (1998).

Robinson, B., L. Dalton, A. Harper, A. Ren, F. Wang, C. Zhang, G. Todorova, M. Lee, R. Aniszfeld, S. Garner, A. Chen, W. Steier, S. Houbrecht, A. Persoons, I. Ledoux, J. Zyss, A. Jen, "The molecular and supramolecular engineering of polymeric electro-optic materials", *Chemical Physics, 245,* pp. 35-50, 1999

Saleh, and M. C. Teich, *Fundamentals of Photonics*, 1st ed. (Wiley, New York, 1991), Chap. 9, pp. 314.

Scherer, A., O. Painter, J. Vuckovic, M. Loncar, T. Yoshie, "Photonic crystals for confining, guiding and emitting light," IEEE T. Nanotechnol. **1**, 4-11 (2002).

Shi, Y.; Zhang, C.; Zhang, H.; Bechtel, J. H.; Dalton, L. R.; Robinson, B. H.; Steier, W. H. *Science*, **2000**, *288*, 119.

Soref, R. A., J. P. Lorenzo, "All-Silicon Active and Passive Guided-Wave Components For Lambda=1.3 and 1.6 MU-M," IEEE J. Quantum Elect. **22**, 873-879 (1986).

Srinivasan, U.; Houston, M. R.; Howe, R. T.; Maboudian, R.J. *Microelectromech. Syst.* 1998, *7*, 252.

Sundar, V.C., J. Zaumseil, V. Podzorov, E. Menard, R. L. Wllett, T. Someya, M. E. Gershenson, J. A. Rogers, *Science*, **2004**, *303*, 1644.

Suzuki, S., Y. Hatakeyama, Y. Kokubun, and S. T. Chu, J. Lightwave Technol. **20**, 745 (2002).

Taflove, Computational Electrodynamics, (Artech House, Boston, MA, 1995).

Taillaert, D., P. Bienstman, R. Baets, "Compact efficient broadband grating coupler for silicon-on-insulator waveguides," Opt. Lett. **29**, 2749-2751 (2004).

Teng, C.C.; Man, H. T. *Appl. Phys. Lett.* **1990**, *56*, 1734.

Varanasi, P. R.; Jen, A. K-Y.; Chandrasekhar, J.; Namboothiri, I. N. N.; Rathna, A. *J. Am. Chem. Soc.* **1996**, 118, 12443-12448.

Wang, X. J., J. M. Zhao, Y. C. Zhou, Z. Z. Wang, S. T. Zhang, Y. Q. Zhan, Z. Xu, H. J. Ding, G. Y. Zhong, H. Z. Shi, Z. H. Xiong, Y. Liu, Z. J. Wang, E. G. Obbard, X. M. Ding, *J. Appl. Phys.* **2004**, *95*, 3828.

Xu, Q. F., V. R. Almeida, R. R. Panepucci, M. Lipson, "Guiding and Confining Light in Void Nanostructures," Opt. Lett. **29**, 1206-1211 (2004).

Yongqiang Shi, Cheng Zhang, Hua Zhang, James H. Bechtel, William H. Steier, Bruce Robinson, Larry R. Dalton. *Science*, *288*, **2000,** 119.

Zhang, L. R. Dalton, M.-C. Oh, H. Zhang, W. H. Steier, *Chem. Mater.* 2001, *13*, 3043.

Appendix A: Optical Rectification Theory

The general governing equation of nonlinear optics is known [17] to be:

$$D_i = \varepsilon_0(\varepsilon_r E_i + \chi_{ijk}{}^2 E_j E_k + ...) \qquad (1)$$

Our EO polymers are designed to exhibit a relatively strong χ^2 moment, ranging from 10-100 pm/V. In most χ^2 EO polymer systems, the Pockel's effect is used to allow the electric field (due to a DC or RF modulation signal) to modify the index of refraction. In such systems the modulating electric field is typically far in excess of the electric field from the optical signal and the term that produces the material birefringence is the only term of importance in the above equation.

Our waveguides, however, have a very large electric field as most of the radiation is confined to a 0.01 square micron cross section. It can be shown that the electric field is approximately uniform in the transverse direction, with a magnitude of

$$10^8\sqrt{P}\frac{V}{m} \qquad (2)$$

where P is the optical power in Watts. At large optical fields, the non-Pockels terms involved in the governing nonlinear equation cannot be neglected. For coherent input power, at a given location in the waveguide, the optical field is:

$$E_{optical}(t) = A\cos(wt + \theta) \qquad (3)$$

The term

$$E_{optical}{}^2 = \frac{A^2}{2}\cos(2(wt + \theta)) + \frac{A^2}{2} \qquad (4)$$

will therefore contain not only frequency doubled components, but also a "DC" component. This phenomenon is known as optical rectification [18]. We believe that this DC component provides a likely explanation for the photo-current that we observe. Because we have positioned electrodes (the two sides of the slot waveguide) at precisely the bounds of the induced field, the effect of optical rectification takes a small slice of the optical power and converts it into a virtual voltage source between the two arms. This in turn induces a current that we can measure and is linearly proportional to the input power $E_{optical}{}^2$.

Now let us consider the solution to Maxwell's equation in more detail. Our system can be approximated for this discussion as having two dimensions, with both the optical and DC electric field in the x direction and propagation in the z direction, for instance. Let us imagine that the χ^2 is nonzero and small for a tiny region from 0 to w in the x dimension. χ^2 is sufficiently small that the electric field due to the optical mode is still uniform. Let us imagine the system has no charge anywhere. The optical electric field can be written as $E = Ae^{ikz-iwt} + c.c.$ where c.c. indicates a complex conjugate. Let us further assume that the rectified DC field is of real amplitude C and uniformly directed in the x dimension on (0, w), and 0 elsewhere.

Other than the divergence condition, Maxwell's equations are still satisfied by this system. But at the edge of an interface on the interior, the DC frequency component of D_x, the displacement electric field, is discontinuous. At x=0, we have:

$$D_x^- = 0 \qquad (5)$$

$$D_x^+ = \varepsilon_0(\varepsilon_r C + \chi^2 C^2 + 2\chi^2 |A|^2) \quad (6)$$

We neglect χ^2 C2 because we expect the amplitude of the rectified field to be far smaller than that of the optical field. Clearly, the boundary condition of zero divergence can only be satisfied if Dx+ is 0. Then,

$$C = -\frac{2\chi^2}{\varepsilon_r}|A|^2 \qquad (7)$$

So we see that the direction of the rectified field is reversed compared to the direction of χ^2. Note that there is no particular direction associated with the optical field as it is continually oscillating. As we have seen, this rectified DC field would then, if acting as a virtual voltage source, create an effective positive terminal on the positive polling terminal.

Vita

Llewellyn Rhys Lawson was born in Sandpoint, ID and grew up in Bellingham, WA. He has earned degrees from the University of Puget Sound (B.S. Chemistry, 1999), Western Washington University (M.S. Chemistry, 2001) and the University of Washington (M.S. Chemistry, 2003; Ph.D. Chemistry and Nanotechnology, 2006; J.D. expected in 2007).